Lecture Notes in Engineering

Edited by C. A. Brebbia and S. A. Orszag

17

S. M. Baxter
C. L. Morfey

Angular Distribution Analysis in Acoustics

Springer-Verlag
Berlin Heidelberg New York Tokyo

Authors
S. M. Baxter
C. L. Morfey
Institute of Sound and Vibration Research
The University
Southhampton, SO9 5NH
U. K.

ISBN-13: 978-3-540-16220-9 e-ISBN-13: 978-3-642-82702-0
DOI: 10.1007/978-3-642-82702-0

Library of Congress Cataloging in Publication Data
Baxter, S. M.
Angular distribution analysis in acoustics.
(Lecture notes in engineering ; 17)
Includes bibliographies.
1. Acoustical engineering. 2. Wave-motion, Theory of.
I. Morfey, C. L. II. Title. III. Series.
TA365.B39 1986 620.2 85-30437

Binding: Helm, Berlin
2061/3020-543210

CONTENTS

LIST OF PRINCIPAL SYMBOLS

A	complex plane wave amplitude
A_{mn}	complex modal amplitude
a	circular duct radius
a,b	rectangular duct dimensions
B_{mn}	modal pressure spectrum
BE	backwards elimination
C	normalised CCSD
CCSD	complex cross-spectral density
c	speed of sound
E	expected value
e	exponential constant
F	F-statistic
$F(\underline{k})$, $f(\underline{r})$	spatial Fourier transform pair
FS	Forward search
f_{χ}^{q}	spherical harmonic series coefficient
H	angle-dependent plane wave weighting
I	normalised plane wave weighting
I_{χ}^{q}	spherical harmonic series coefficient
Im	imaginary part
i	$\sqrt{-1}$
J	Jacobian factor
J	mean intensity
J_m	m-th order ordinary Bessel function
j_m	m-th order spherical Bessel function
$\underline{k}$	plane wave vector
k	$\lvert \underline{k} \rvert = \omega / c_o$
m	power in cosine-power plane wave weighting model
m,n	modal co-ordinates
n,N	number of sampling positions

P_ℓ	Legendre polynomial
P_ℓ^q	associated Legendre polynomial
PSD	pressure spectral density
p	pressure
p	dimensionless wavenumber spectrum parameter
p, P	number of harmonic variables
Q	wavenumber spectrum
R	= kr
R	ordinary correlation coefficient
R_L	collinearity measure
RSS	residual sum of squares
Re	real part
$\underline{r}$	separation vector
r, θ, ϕ	spherical polar co-ordinates, $r = \lvert\underline{r}\rvert$
r	correlation vector and matrix
S	duct cross section
SPL	sound pressure level
S_N	harmonic series sum
s, ϕ, z	cylindrical polar co-ordinates
t	time
t	students' t-statistic
u,v	polar and azimuthal spherical angles
V	particle velocity
VIF	variance inflation factor
W	sound power
W_{mn}	modal sound power
w	wavenumber spectrum window factor
$\underline{x}$	position vector
x,y,z	Cartesian coordinates
x	independent variable in regression analysis
Y_ℓ^q	spherical harmonic function
y	dependent variable in regression analysis

Greek

α	dimensionless radial wavenumber
β	coefficient in regression analysis
Γ	complete gamma function
δ	delta function
δ_{mn}	Kronecker delta
ε	harmonic series mean square error
ε_m	=1 if m=0, =2 otherwise
η	sound power to PSD ratio
Λ	modal integration constant
ρ	density
τ	dimensionless axial wavenumber
ψ	real and imaginary harmonic variables
ψ	modal pressure function
ψ	$=\cos^{-1} p$, wavenumber spectrum parameter
ω	radian frequency

Superscripts

q	spherical harmonic parameter
T	matrix transpose
*	complex conjugate

Subscripts

C	circular duct
d	degrees of freedom
fw	free wave
ℓ	spherical harmonic parameter
p	sampling positions
pw	plane wave
R	rectangular duct
0	(zero) equilibrium value

CHAPTER ONE

INTRODUCTION

The purpose of this book is to present a new technique for the experimental investigation of the free wave model sound field of acoustics. The technique is based on the use of spherical harmonic functions of angle.

Acousticians frequently encounter random sound fields whose properties may be closely modelled by use of the "free wave" field. This model field is defined by two basic statistical properties: stationarity in time, and homogeneity in space. Stationarity means that any single order statistic measured by a microphone in the field will be independent of the time at which the recording is taken, while homogeneity means that the measurement will also be independent of the microphone's position in the field. Furthermore, second order statistics obtained from the measurements of two microphones will depend only on the time lapse between the two recordings, and the relative spatial separation of the microphones, and not on the microphones' absolute positions in space and time.

The free wave field may also (equivalently) be pictured as a collection of plane sound waves which approach an observation position from all angles. These are the "free waves" of the title, with no correlation between waves at different angles and frequencies, although there may exist an angle-dependant plane wave density function. This is a measure of the density of sound energy arriving from different angles.

The free wave field has proved to be a simple but remarkably powerful model. Typically a field appropriate to the free wave description may be found at high frequencies, a limit in which more conventional descriptions can become unwieldy and impractical. In the 1950's the free wave idea was put forward to model the

high frequency reverberant sound field in an enclosure, with a dauntingly large number (scores or hundreds) of room modes present. Later studies have shown both theoretically and experimentally that this description is valid within limits, and architectural acousticians have used the model to give important descriptive quantities such as reverberation time a firm theoretical foundation, as well as to establish new measures.

The present authors have used the free wave model to study sound fields in acoustic ducts at frequencies which are of practical interest, but so high that the usual mode description becomes impractical (with more than twenty propagating modes). Further, researchers into sonar techniques have used free wave ideas to model the background noise encountered in an ocean, caused by surface effects such as shipping and wave action.

A given free wave sound field may be completely described by two statistical quantities: power spectral density (PSD) which depends only on frequency, and the plane wave density function, which is a function of both frequency and angle. The PSD is readily measurable by standard techniques, but the measurement of the more unfamiliar weighting function proves the greatest obstacle to the use of the free wave idea in practice. A common challenge is to deduce weighting function information from a set of measurements taken at a small (perhaps twenty or less) number of microphone positions within a field. These positions may be arranged sparsely and irregularly in space.

This book describes an attempt to meet this challenge, with a method based on the use of spherical harmonic functions of angle. Previous applications of harmonic analysis seem to have been mostly to problems of a rather different scale, in the study of artificial satellites' orbital perturbations. This has provided information about inhomogeneities in the Earth's form, including the classic demonstration that the Earth is "pear-shaped". On a larger scale still, harmonic analysis has offered images of the structure of the magnetic fields of Jupiter and Saturn, based on sparse data from unmanned spacecraft flybys.

In the present proposal, harmonics are used to construct parametric models of a free wave field's angle-dependant plane wave weighting. Parameter values are determined from experimental data via search techniques based on regression analysis. The result is a set of images of the weighting function; these are limited in resolution but <u>not</u> by the inherent complexity of the field (i.e., by frequency).

In Chapter Two of the book, the properties of a free wave field are described in

more detail. In any given application, these properties are closely linked to those of the underlying physical field. The Chapter includes a close look at one example of this linking, and its use in practice: the sound field in an acoustic duct at high frequency.

Chapter Three is a review of various methods which are available for the experimental study of free wave fields. This review is a background to the description of the harmonic analysis technique, which is introduced in Chapter Three, and discussed in detail in Chapter Four. The application and properties of the technique are exemplified by reference to the experimental study of a duct sound field, performed by the present authors.

Finally, it should be emphasised that the duct study is meant only to illustrate the use of the harmonic analysis of free wave fields, and not to define its application exclusively. The authors believe that the analysis technique will prove of value to workers in many disparate fields.

CHAPTER TWO

THE FREE WAVE SOUND FIELD

2.1 INTRODUCTION

The purpose of this book is to present an experimental method to investigate the spatial characteristics of a certain type of complex, random wave field. A wave field qualifies as suitable for study using the new method provided it can reasonably be approximated by a "free wave" model field. The details of the investigation technique are given in later chapters. The present chapter is a description of the properties and importance of the free wave concept.

2.2 PROPERTIES OF THE FREE WAVE FIELD

2.2.1 Homogoneous sound fields in ducts

Historically, the idea of the free wave field grew out of studies of spatially complex acoustic fields such as the work of Dyer in 1958 (2.1), who studied the propagation of high frequency noise from a ducted fan. It is worthwhile as an introduction to consider Dyer's work in some detail.

The propagation of low-intensity sound in a duct, or acoustic wave guide, is traditionally (2.2) described by assuming it to obey a three-dimensional wave equation, subject to a boundary condition at the duct walls. For example, if the walls are "hard", that is totally reflecting, the boundary condition is that there should be no velocity component normal to the duct surface at a point.

Such a boundary condition forces the sound to propagate as a series of modes. Each mode has well-defined spatial characteristics, and its own speed of propagation down the duct. A mode can be pictured as a pattern of pressure maxima and minima across a duct cross section, propagating down the duct length. The total sound field consists of a sum of such modes, whose amplitudes and phases are determined by sound and duct termination characteristics.

At any frequency there are only a finite number of modes, but the number of cut-on (that is, allowed) modes progress with frequency (typically, as the square of frequency). For example, Dyer based his study on Kerka's (2.3) experimental investigation of the sound field in a 15 in. diameter circular duct, which would contain only one mode at 450 Hz (the plane wave mode, which is uniform across a

duct cross section) but 20 modes at 2 kHz. Clearly the spatial structure of a many-mode sound field is complex, increasingly so at higher frequency, and the prospect of trying to investigate a field containing many (20+) modes seems daunting.

However, the investigation of such a field proves to be practical because of a surprising fact: that the field's overall spatial structure can actually become simpler with increasing frequency.

The key is Dyer's observation that significant spatial variations of sound pressure level (SPL) in Kerka's duct were confined to a two-octave band of frequency, from about 450 Hz to 1800 Hz. At low frequencies, Dyer explained, only the plane wave mode can propagate, while at high frequencies, "because of the presence of many modes ... the transverse variations on the average are expected to be small".

Dyer's intuitive understanding seems to have been that at higher frequencies, the spatial structure of a duct sound field can become more uniform as more modes cut on and modal maxima and minima tend to cancel. At a high enough frequency, when the duct radius is large compared to a wavelength, so that a cross-section contains many modal maxima and minima, it is plausible that at least in certain regions of the duct there would be little spatial variation of (for example) SPL. Variation would still be expected however close to the duct walls (i.e. within a wavelength) because of the presence of reflections, and near to positions of symmetry such as the axis of a circular duct, because of focussing effects.

A field in which second-order statistics like SPL show no spatial variation is called "spatially homogeneous". Dyer's work showed that the sound field near a duct axis at high frequency could be modelled as a homogeneous field.

Spatial homogeneity is the central property of the "free wave" model field. Despite its simplicity of definition, the free wave model has proved to be an invaluable tool in many areas, as will become apparent from the following discussion.

2.2.2 The Free Wave Field

The properties of the free wave model have been reviewed by Waterhouse (2.4) and Jacobsen (2.5) and are summarised here. The most fundamental definition of the field is as a collection of random, uncorrelated plane waves. (In the present

discussion only waves with purely real wavenumbers will be considered.)

Taking an acoustic field as an example, the Fourier transformed pressure contributed by a single plane wave to a broadband sound field is given by

$$p_{pw}(\underline{x},\omega;\underline{k}) = A(\underline{k},\omega)\exp(i\underline{k}.\underline{x}) \tag{2.1}$$

$\underline{x}$ is the position vector of an observation point in the field, ω is radian frequency, and $\underline{k}$ is the plane wave's (purely real) vector wavenumber with $|\underline{k}| = \omega/c_o$, where c_o is the sound speed. ($i = (-1)^{\frac{1}{2}}$). A is a complex amplitude, and is regarded as a random variable whose statistics are independent of position in the field.

A complex cross-spectral density (CCSD) measurement in such a field would yield

$$\begin{aligned} CCSD_{pw}(\underline{r},\omega;\underline{k}) &= E\{p_{pw}(\underline{x},\omega;\underline{k})\, p^*_{pw}(\underline{x}',\omega;\underline{k})\} \\ &= E\{|A(\underline{k},\omega)|^2\}\exp(i\,\underline{k}.\underline{r}) \end{aligned} \tag{2.2}$$

while a pressure spectral density (PSD) measurement would yield

$$\begin{aligned} PSD_{pw}(\underline{x},\omega;\underline{k}) &= E\{|p_{pw}(\underline{x},\omega;\underline{k})|^2\} \\ &= E\{|A(\underline{k},\omega)|^2\} \end{aligned} \tag{2.3}$$

E denotes an ensemble average, ( )* denotes a complex conjugate, and $\underline{r}$ is the separation vector $\underline{x} - \underline{x}'$ between the observation points at $\underline{x}$, $\underline{x}'$.

A free wave field is made up of uncorrelated plane waves, so that the total CCSD or PSD in the field may be obtained by simply summing contributions like equations (2.2), (2.3) from all the field's component plane waves. Equation (2.3) shows that measurements of PSD are independent of position in the field (because the contribution from each plane wave is independent of position), so that the field is homogeneous. Furthermore it can be seen from equation (2.2) that two-point statistics like CCSD in a free wave field depend only on the

points' separation vector $\underline{r}$, and not on the points' absolute positions. A pair of microphones could be moved through the field and would yield the same values of CCSD everywhere, provided their relative separation was kept fixed. A homogeneous field is thus the spatial analogue of a stationary time series.

It should be noted that there is a distinction between a "homogeneous" field and an "isotropic" field. Two-point statistics like CCSD in an isotropic field depend only on the separation distance $r = |\underline{r}|$ between the two points, and not on the points' relative orientation. A free wave field is always homogeneous, but is isotropic only if it is "diffuse", that is if the statistics of the amplitude function are independent of wavenumber, so that the plane wave contributions to CCSD and PSD have a uniform weighting. (See section (2.3)).

A free wave field can alternatively be regarded as being made up of plane waves with random phase relations (2.5). The three basic properties of a free wave field (homogeneous, composed of uncorrelated waves, and composed of waves with random phase relations) are equivalent, and any one of them may be used to define the field.

2.3 SPECTRAL DENSITY MEASUREMENT IN FREE WAVE FIELDS: COOK'S THEOREM

2.3.1 Architectural acoustics

With the free wave field defined in the last section, we turn now to a theortical result of great practical significance, given first by a worker in the field of architectural acoustics.

Homogeneous fields have been extensively studied in this context. The problem of studying the many-mode sound field in an enclosure at high frequency is analogous to that of studying the many-mode sound field at high frequency in a duct, and observations dating from the time of Sabine (2.6) have indicated that such a sound field may often be considered homogeneous.

The free wave field concept has proved its value by becoming the basis of the theoretical approach to the study of reverberant sound fields in enclosures known as "geometrical acoustics" (2.2). The theory is so named by analogy with geometrical optics, and it depends on modelling the field in an enclosure by a diffuse free wave field, and assuming that the absorption properties of wall surfaces can be represented adequately by simple absorption coefficients.

Geometrical acoustic techniques have proved useful in putting the governing concepts of architectural acoustics (for example reverberation time) on a firm theoretical basis (2.7), and evidence has accumulated over the years that the two alternative models (modes and free waves) of the sound field in an enclosure are consistent. It has been shown for instance that the results of modal computations of the interference patterns at (2.8) and near (2.9) the boundaries of a rectangular hard-walled room are consistent with the results of free wave model computations (2.10). Calculations made with the two models of the spatial variance of SPL measurements in such a room have also been shown to agree (2.11, 2.4).

However, perhaps the most striking evidence of the consistency of the two models has come from the study of a quantity which proves to be of great importance: the complex cross-spectral density (CCSD) of the signals taken from two pressure microphones in a free wave field.

2.3.2 Cook's theorem for a diffuse field

Interest in CCSD measurements among architectural acousticians was stimulated by a classic paper published by Cook in 1955 (2.12). Cook was trying to find a "criterion of diffuseness", an observable quantity which would give some indication of whether a given sound field could be regarded as truly diffuse (i.e. isotropic).

To this end Cook presented an argument equivalent to the following. Consider the CCSD between the sound pressures observed by two microphones at points $\underline{x}$, $\underline{x}'$ in a broadband free wave sound field. (In fact, Cook considered zero-time correlation coefficients in a stationary single-frequency free wave field, but Cook's method of proof and results about the spatial structure of correlation are equivalent to those below about the spatial structure of CCSD. In the following discussion, all results about the spatial structure of correlation as studied by previous workers will be assumed to refer also to broadband field CCSD, which is the principal quantity considered in the present work.) Let a plane wave's wavenumber vector $\underline{k}$ be specified by polar and azimuthal spherical angles (v,u) relative to some coordinate system, so that $\underline{k}$ has Cartesian coordinates

$$\underline{k} = (k \sin v \cos u, k \sin v \sin u, k \cos v) \qquad (2.4)$$

$\underline{k}$ is purely real, so the angles (v,u) take only real values. The range of v is 0 to π, and the range of u is 0 to 2π. Let the observation point separation vector be specified by spherical polar coordinates (r, θ, ϕ) so that it has Caresian coordinates.

$$\underline{r} = (r \sin \theta \cos \phi, r \sin \theta \sin \phi, r \cos \theta) \tag{2.5}$$

Then the contribution of a single plane wave to the CCSD can be written (from equation (2.2))

$$\begin{aligned} CCSD_{pw}(\underline{r}, \omega; \underline{k}) &= \{ |E\{|A(\underline{k}, \omega)|^2\} \\ &\times \exp(ikr \cos\theta \cos v + ikr \sin\theta \sin v \cos(\phi - u)) \end{aligned} \tag{2.6}$$

The amplitude factor may be removed by defining a normalised CCSD

$$C(\underline{r}, \omega) = CCSD(\underline{r}, \omega) / \{PSD(\underline{x}, \omega) PSD(\underline{x}', \omega)\}^{\frac{1}{2}} \tag{2.7}$$

so that the plane wave's contribution becomes

$$C_{pw}(\underline{r}, \omega; k) = \exp(ikr \cos\theta \cos v + ikr \sin\theta \sin v \cos(\phi - u)) \tag{2.8}$$

If and only if the field is diffuse, the normalised CCSD for the complete field may be obtained by averaging equation (2.8) with a uniform weighting over every direction from which the uncorrelated plane waves can come:

$$C(\underline{r}, \omega) = (1/4\pi) \int_0^{\pi} dv \sin v \int_0^{2\pi} du \; C_{pw}(\underline{r}, \omega; k) \tag{2.9}$$

Because of the symmetric nature of the sound field, the value of this integral has to be independent of the orientation of the axes, and so independent of the values of θ, ϕ. For convenience, let the axes be chosen so that the z-axis is

parallel to the line joining the microphones, so that $\theta = 0$:

$$C(\underline{r}, \omega) = (1/4\pi) \int dv \sin v \int du \exp (ikr \cos v) \qquad (2.10)$$

Evaluation of the integral gives a surprisingly simple final result:

$$C(\underline{r}, \omega) = \sin (kr)/kr \qquad (2.11)$$

Note that this quantity depends only (apart from on frequency) on r, demonstrating that a diffuse field is isotropic as well as homogeneous.

Having derived this elegant result, Cook went on to measure correlation coefficients in a reverberation chamber. Diffuseness was promoted by using frequency modulation and loudspeakers mounted on large rotating vaners, and a good agreement was demonstrated between prediction (equation (2.11)) and measurement.

Architectural acousticians were later to find Cook's result useful not only as a means of assessing diffuseness, but also as evidence that their two competing theoretical models of the sound fields in rooms (modes and free waves) were consistent.

The first deduction of Cook's results using a mode model of a rectangular room sound field was given by Lyon and Maidanik in 1962 (2.13). Similar proofs were also given by Morrow (2.14), Chu (2.15, 2.16) and Chien and Soroka (2.17).

2.3.3 Cook's Theorem and Ocean acoustics

Cook's impressive derivation of equation (2.11), "plucked out of the air containing all those flying waves" (2.4) "with a simple elegance reminiscent of Sabine's theory" (2.14) created a great deal of interest in the properties of CCSD in a diffuse field, but Cook's presentation (3.10) of the result was not the first. Cook and Edelman had given the result at an Acoustical Society of America meeting in 1950 (2.18), and the result was implicit in the work of Eckart published in 1953 (2.19). Furthermore, workers in the field of ocean acoustics were also studying the properties of correlation in random noise fields, and were

independently deriving Cook's results, generally by rather different methods. (Cron and Sherman (2.20) did however credit Marsh (2.21) with a free wave field derivation dating from 1950.)

Correlation is important in the study of the signal-to-noise gain behaviour of a hydrophone array in an ocean containing background noise (2.22). Ambient sea noise is mainly generated by surface wave motion, contributing high frequency noise, and by distant shipping, contributing low frequency noise, and can be modelled by distributions of uncorrelated sources. By 1960 Freeman (2.23) had shown that if an ensemble of identical point sources were distributed throughout a large sphere, Cook's correlation function, equation (2.11), would be observed near the centre of the sphere. The same result was given independently by Cron and Sherman (2.20) and Liggett and Jacobson (2.24) went on to show that the result would still hold even if the medium in which the sources were embedded had a small attenuating viscosity. Jacobson (2.25) also studied correlation in the sound field of an ensemble of point sources spread over the surface of a large sphere. Once again, Cook's result followed for measurements made near the centre of the sphere.

2.4 EXTENSION OF COOK'S THEOREM FOR ANISOTROPIC FIELDS

2.4.1 Anisotropic fields

Cook's result, equation (2.11), is thus not only satisfyingly simple and elegant, but also robust in that it can be derived using a variety of theoretical models of isotropic fields. It is however limited to the special case of a diffuse field, and would not be expected to describe CCSD in more general, anisotropic free wave fields.

Duct sound fields and ambient sea noise fields are examples of anisotropic free wave fields, because of their anisotropic energy flows. Cook's theorem can be extended to fields of this type - fields which are homogeneous, but no longer necessarily isotropic. This extension proves to be of great practical significance, as will be seen.

To derive equation (2.11), Cook averaged the CCSD contributed by a single plane wave over all wavenumber angles (v, u) with a uniform weighting. However a more general average can be written down:

$$CCSD\ (\underline{r}, \omega) = \int_0^{\pi} dv \sin v \int_0^{2\pi} du\ H\ (v, u, \omega)\ \exp\ (i\underline{k}.\underline{r}) \qquad (2.12)$$

This is an expression for CCSD in a free wave field with an arbitrary angle-dependent plane wave weighting function H. A representation for the PSD is obtained when $\underline{r}$ is set to zero:

$$PSD\ (\underline{x}, \omega) = \int dv \sin v \int du\ H\ (v, u, \omega) \qquad (2.13)$$

The CCSD function may be normalised following Cook's example by applying equation (2.7). The function C has an integral representation

$$C\ (\underline{r}, \omega) = (1/2\pi) \int dv \sin v \int du\ I\ (v, u, \omega)\ \exp\ (i\underline{k}.\underline{r}) \qquad (2.14)$$

where the normalised weighting I is given by

$$I\ (v, u, \omega) = 2\pi\ H\ (v, u, \omega)/PSD \qquad (2.15)$$

The factor $(1/2\pi)$ is included so that in the important special case of azimuthally symmetric fields, the normalisation takes the simple form

$$1 = \int_0^{\pi} dv \sin v\ I\ (v, \omega) \qquad (2.16)$$

A knowledge of the plane wave weighting function amounts to a complete description of the free wave field. As will be seen, in a given application the plane wave weighting function is intimately linked to the physical properties of the underlying field to which the free wave field is an approximation. Equations (2.12), (2.14), which provide the connections between the weighting function and the <u>observable</u> quantity CCSD, are therefore of great practical significance, and are the focal point of the present study.

Much of the rest of the book is concerned with the means whereby equations

(2.12), (2.14) may be used to yield weighting information from CCSD data. Before proceeding further, however, we will look more closely at the properties and interpreation of the plane wave weighting function, and consider in detail one example of how it can be connected to the underlying physical field.

2.4.2 Interpretation of the Plane Wave Weighting Function: Energy Flow

Continuing to take acoustics as our example of the application of the free wave concept, the plane wave function H is to be interpreted as the mean square pressure density associated with a bundle of waves coming through an element of solid angle sin v dv du in the direction (v, u); it is real, always positive, and has the dimensions (pressure)^2 (frequency)$^{-1}$ (solid angle)$^{-1}$. The dimensions of the normalised function I are (solid angle)$^{-1}$.

The mean intensity in any given direction, for example the positive x-direction, can be written down in terms of H. Using the linearised fluid momentum equation

$$\rho_o \ \partial V_z/\partial t \ = \ -\partial p/\partial z \tag{2.17}$$

between z-direction particle velocity and pressure, and the fact that the mean z-direction intensity of a plane wave is given by

$$J \ = \ E \ \{\tfrac{1}{2} \ \mathrm{Re} \ (pV_z^*)\} \tag{2.18}$$

(2.26) (where Re denotes the real part, and ρ_o is equilibrium density), the mean free wave field z-direction intensity can be written as

$$J \ = \ (1/2 \ \ \rho_o c_o) \int dv \sin v \int du \cos v \ H \ (v, u, \omega) \tag{2.19}$$

The values of mean intensity in other directions can be derived from the function H in a similar fashion. These values will not be the same unless H is a constant over angle, in which case the field is diffuse. In a general free wave field, the function H (and also the normalised weighting I) is thus associated with the non-uniform energy flow in the field.

Note that the RHS of equation (2.13) contains no x-dependence. The field is not isotropic but it is still homogeneous, with PSD values the same everywhere. These results were considered as long ago as 1953 by Eckart (2.19) and were studied in detail by Cox (2.22), who worked on the problem of ambient sea noise with arbitrary directionality.

2.4.3 Application to Duct Acoustics

In any application of this work, it is necessary to show that the free wave model is a valid approximation to the given physical field. The techniques used for this proof will depend on the particular application.

The motivation for the present study came from a need to investigate the distribution of sound power among the modes in an acoustic duct at high frequency (2.27, 2.28, 2.29, 2.30). Appendix A is an account of how the validity of the free wave approximation for this example may be demonstrated, together with a detailed description of the interpretation of the plane wave weighting function, which proves to be connected in a simple way to the duct's modal power distribution.

Finally, from duct acoustics can be drawn a concluding example of a practical problem in which a knowledge of the plane wave weighting function is valuable: the derivation of a simple relation by which the total sound power in an acoustic duct field may be determined from a single measurement of PSD. This problem has been of considerable interest to researchers into the acoustics of fan ducts (2.1).

The ratio of power to PSD in a field composed of one plane wave mode is

$$\eta_{pw} = S/2\rho_o c_o \qquad (2.20)$$

where S is the duct's cross section. In a general many-mode sound field there is no such simple relation, with the ratio depending on position in the duct.

However, if the field may be modelled as free wave, it is straightforward to show from equations (2.15, 2.19) for z-direction intensity that the ratio of total power in the z-direction to PSD is

$$\eta_{fw} = JS/PSD \tag{2.21}$$

$$= (S/4\pi\rho_o c_o) \int_0^{2\pi} du \int_0^{\pi} dv \sin v \cos v \, I(v,u,\omega) \tag{2.22}$$

(In this example, the z-direction is the axis of the duct.)

Thus the free wave prediction differs from the plane wave prediction for a given value of PSD by a factor

$$\eta_{fw}/\eta_{pw} = (1/2\pi) \iint du\, dv \sin v \cos v \, I(v,u,\omega) \tag{2.23}$$

In a semidiffuse field (see the Appendix), this factor takes the value 1/2. In a "cosine-power" free wave field (see Chapter 3), whose plane wave weighting is given by

$$I(v,u,\omega) = (m+1)\cos^m v \quad 0 \leq v \leq \pi/2$$

$$= 0 \text{ otherwise} \tag{2.24}$$

the factor is (m+1)/(m+2). When $m \to \infty$ this model field approaches a plane wave, and the plane wave PSD prediction is recovered.

2.5 SUMMARY

The main ideas presented in this chapter may now be summarised.

In a wide variety of circumstances, spatially complex random fields may be described by use of the free wave model field. This field is composed of uncorrelated plane waves, and is spatially homogenous (though not necessarily isotropic).

Associated with a free wave field is a plane wave weighting function, a knowledge of which is sufficient to describe the field completely, and which is closely

linked to the physical properties of the underlying random field. An example of this linking is presented in some detail in Appendix A, where it is shown that the plane wave weighting function for a free wave field in an acoustic duct is based on the distribution of power among the duct's propagating modes.

If the plane wave function is known, such quantities of practical importance as the flow of energy in any direction in the free wave field may be determined in a straightforward fashion. The experimental estimation of the weighting function from spectral density measurements is therefore the key step in the practical use of the free wave concept, and in the rest of the book the means by which this estimation may be made is described.

REFERENCES

2.1 DYER, I., Journal of the Acoustic Society of America 30, 833-841 (1958). Measurement of noise source in ducts.

2.2 MORSE, P.M. and INGARD, K.U., Theoretical Acoustics. McGraw-Hill, New York (1969).

2.3 KERKA, W.F., Heating, Piping and Air Conditioning 29, 139-146 (1957). Evaluation of four methods for determing sound-power output of ducted fans.

2.4 WATERHOUSE, R.V., Journal of the Acoustic Society of America 54, 931-934 (1973). Noise measurement in reverberant rooms.

2.5 JACOBSON, F., The Acoustics Laboratory, Technical University of Denmark, Report No. 27 (1979). Statistical considerations concerning the reverberant field in the steady state.

2.6 LINDSAY, R.B. (ed.), Acoustics: Historical and Philosophical Development. Dowden, Hutchinson and Ross, Inc., Pennsylvania (1972).

2.7 JOYCE, W.B., Journal of the Acoustical Society of America 64, 1429-1436 (1978). Exact effect of surface roughness on the revereration time of a uniformly absorbing spherical enclosure.

2.8 WATERHOUSE, R.V. and COOK, R.K., Journal of the Acoustical Society of America 59, 576-581 (1976). Diffuse sound fields: eigenmode and free-wave models.

2.9 CHU, W.T., Journal of the Acoustical Society of America 68, 184-190 (1980). Eigenmode analysis of the interference patterns in reverberant sound fields.

2.10 WATERHOUSE, R.V., Journal of the Acoustical Society of America 27, 247-258 (1955). Interference patterns in reverberant sound fields.

2.11 WATERHOUSE, R.V. and van WULFFTEN PALTHE, D.W., Journal of the Acoustical Society of America 62, 211-213 (1977). Space variance for rectangular modes.

2.12 COOK, R., WATERHOUSE, R., BERENDT, R., EDELMAN, S. and THOMPSON, M., Journal of the Acoustical Society of America 27 1072-1077 (1955). Measurement of correlation coefficients in reverberant sound fields.

2.13 LYON, R.H. and MAIDANIK, G., Journal of the Acoustical Society of America 34, 623-639 (1962). Power flow between linearly coupled oscillators.

2.14 MORROW, C.T., Journal of Sound and Vibration 16, 29-42 (1971). Point-to-point correlation of sound pressures in reverberation chambers.

2.15 CHU, W.T., Journal of the Acoustical Society of America 69, 1710-1715 (1981). Comments on the coherent and incoherent nature of a reverberant sound field.

2.16 CHU, W.T., Journal of Sound and Vibration 62, 309-311 (1979). Spatial cross-correlation of reverberant sound fields.

2.17 CHIEN, C.F. and SOROKA, W.W., Journal of Sound and Vibration 48, 235-242 (1976). Spatial cross-correlation of pressures in steady and decaying reverberant sound fields.

2.18 COOK, R. AND EDELMAN, S., Journal of the Acoustical Society of America 22, 678 (1950). Correlation coefficients as criteria for randomness of reverberant sound fields.

2.19 ECKART, C., Journal of the Acoustical Society of America 25, 195-199 (1953). The theory of noise in continuous media.

2.20 CRON, B.F. and SHERMAN, C.H., Journal of the Acoustical Society of America 34, 1732-1736 (1962). Spatial-correlation functions for various noise models.

2.21 MARSH, H.W., U.S. Navy Underwater Sound Laboratory Quarterly Report, March 1950. Correlation in wave fields.

2.22 COX, H., Journal of the Acoustical Society of America 54, 1289-1301 (1973). Spatial correlation in arbitrary noise fields with application to ambient sea noise.

2.23 FREEMAN, J.J., Journal of the Acoustical Society of America 32, 1025-1027 (1960). A systematic error in underwater acoustic direction finding.

2.24 LIGGETT, W.S. and JACOBSON, M.J., Journal of the Acoustic Society of America 36, 1183-1194 (1964). Covariance of noise in attenuating media.

2.25 JACOBSON, M.J., Journal of the Acoustical Society of America 34, 971-978 (1962). Space-time correlation in spherical and circular noise fields.

2.26 KINSLER, L.E. and FREY, A.R., Fundamentals of Acoustics. John Wiley, New York (1962).

2.27 BAXTER, S.M. Acoustic Modal Power Distribution in a Duct at High Frequencies. I.S.V.R., Southampton University, Technical Report No. 111.

2.28 BAXTER, S.M. and MORFEY, C.L., A.I.A.A. Journal 21, 74-80 (1983). Modal power distribution in ducts at high frequencies.

2.29 BAXTER, S.M. and MORFEY, C.L. A.I.A.A. Journal (To be published). Experimental investigation of the modal power distribution in a duct at high frequencies.

2.30 BAXTER, S.M. Modal Power Distribution in a Duct at High Frequency. PhD Thesis, Institute of Sound and Vibration Research, Southampton University (1983).

2.31 ABRAMOWITZ, M. and STEGUN, I.A., Handbook of Mathematical Functions. Dover Publications, New York (1972).

2.32 ROE, G.M., Journal of the Acoustical Society of America 13, 1-7 (1941). Frequency distribution of normal modes.

2.33 RICE, E.J. NASA Technical Memorandum TM X-73539 (1976). Modal density function and number of propagating modes in ducts.

2.34 OLVER, F.W.J. (ed.), Royal Society Mathematical Tables, Volume VII. Cambridge University Press, London (1960).

2.35 RICE, E.J. and HEIDELBERG, L.J., Journal of Aircraft 18, 810-817 (1981). Comparison of inlet suppressor data with approximate theory based on cut-off ratio.

2.36 MORSE, P.M. and FESHBACK, H., Methods of Theoretical Physics, McGraw-Hill, New York (1953).

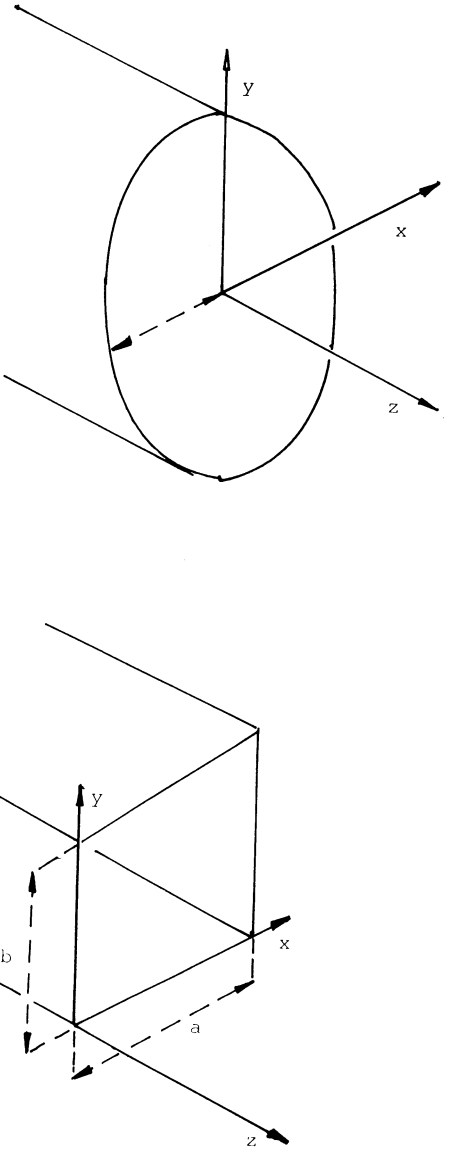

Figure 2.1 Geometry and coordinate system for circular and rectangular ducts.

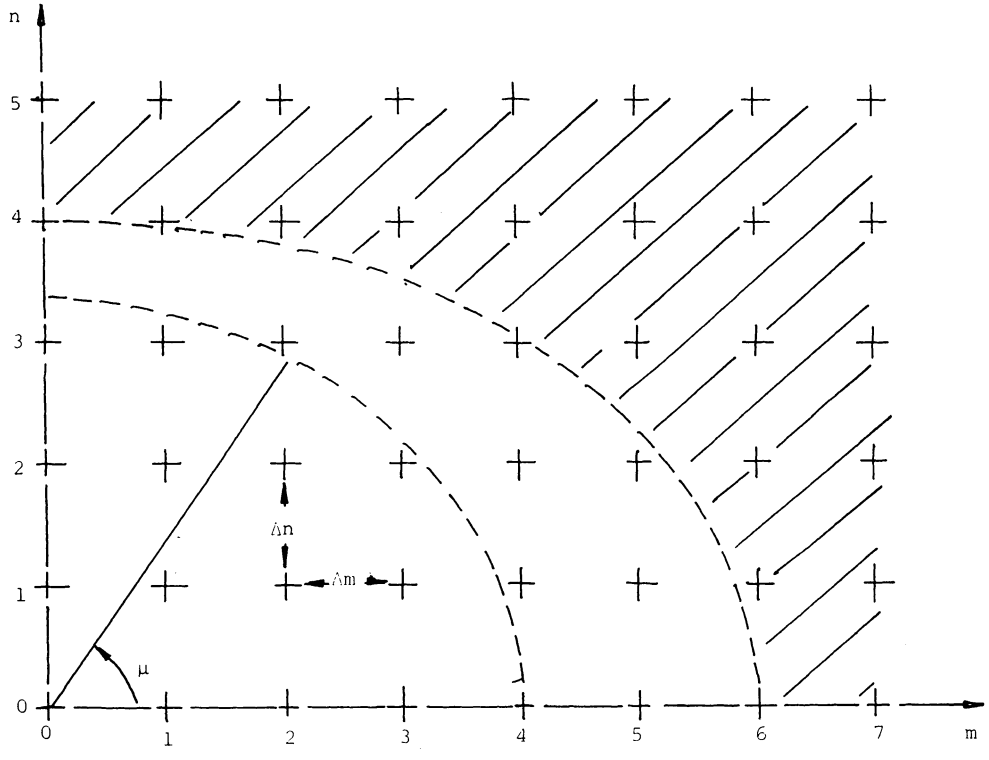

Figure 2.2 The (m,n) plane. Broken lines are contours of constant axial wavenumber τ. + = mode. The outermost contour is $\tau = 0$; the modes in the shaded region are cut-off.

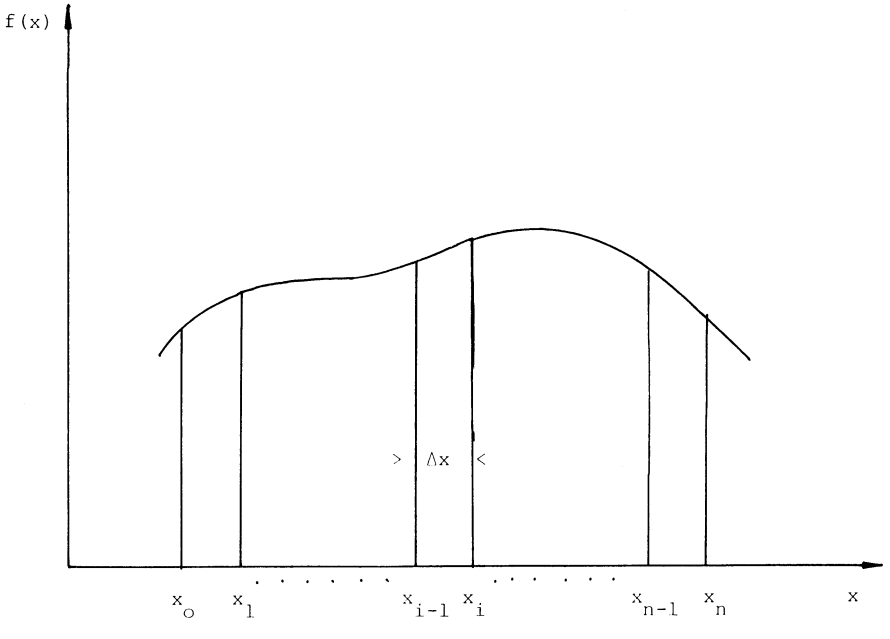

Figure 2.3 Evaluation of the area under the graph of a function. The i-th strip has approximate area $f(x_{i-1})\ \Delta x$.

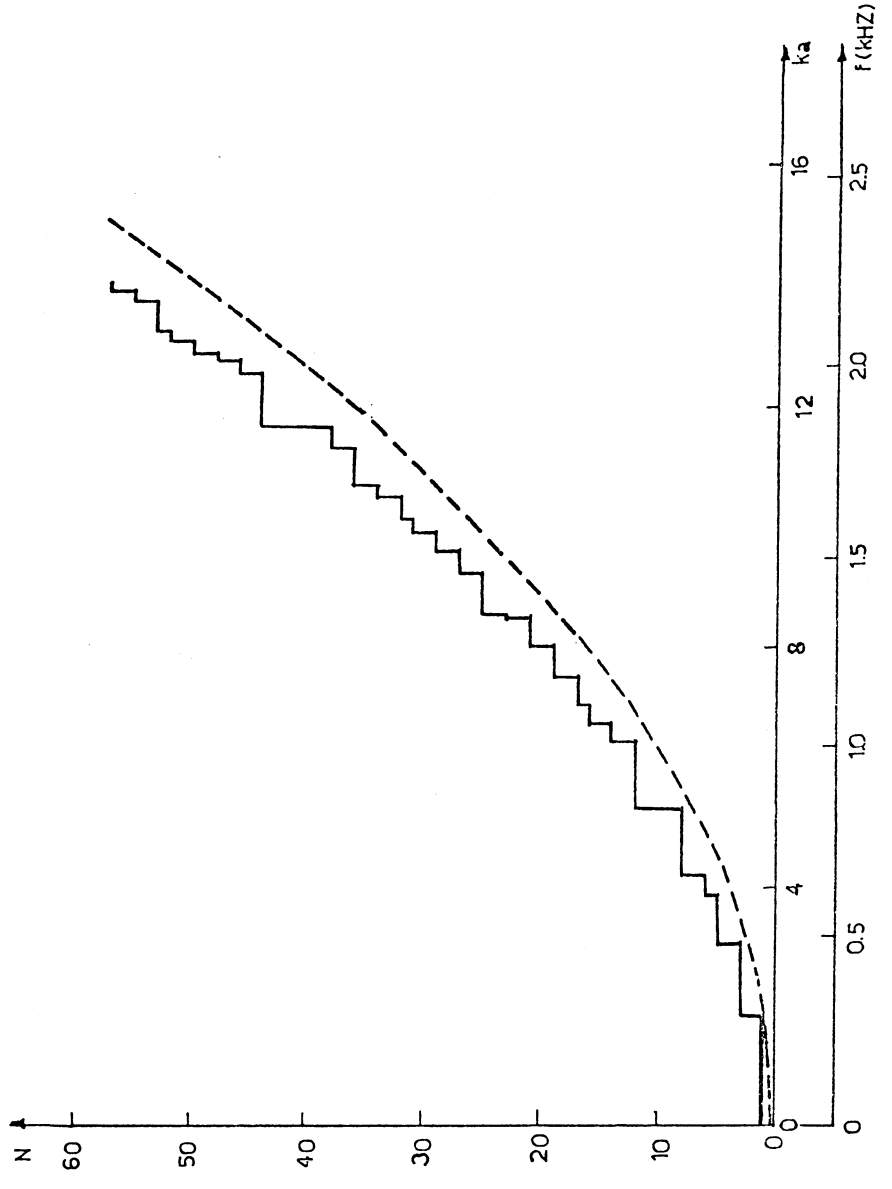

Figure 2.4 Number of cut on modes in a circular duct. Frequency scale is for duct radius a = 34.29 cm. Solid line is exact count; broken line is $k^2S/4\pi$.

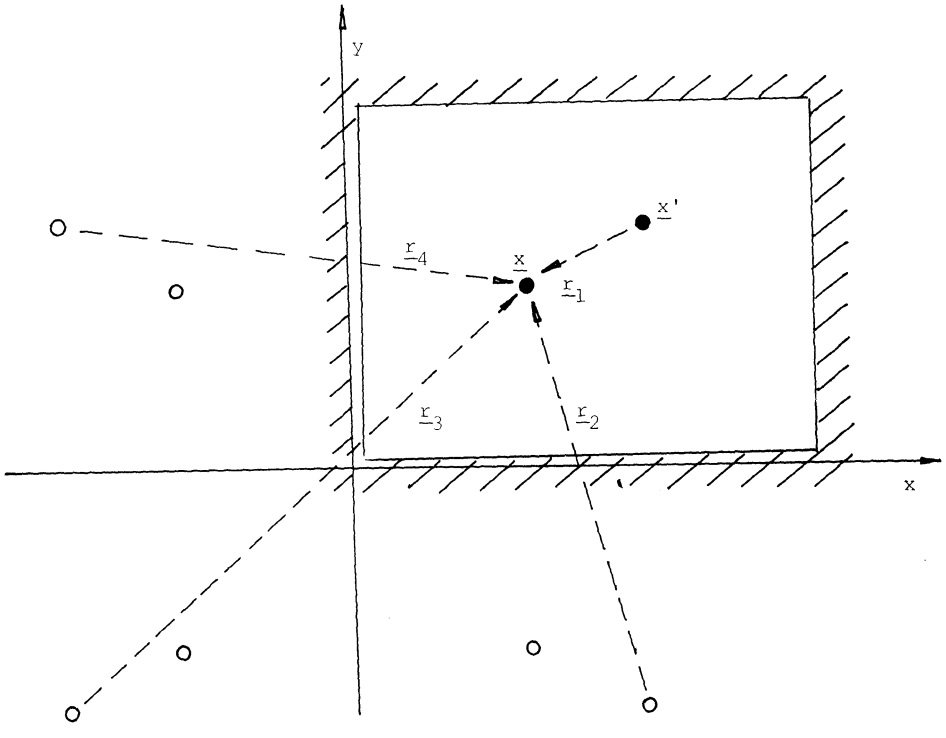

Figure 2.5 Microphone image pairs contributing to CCSD in a rectangular duct. ● = microphone diaphragm; o = image of diaphragm.

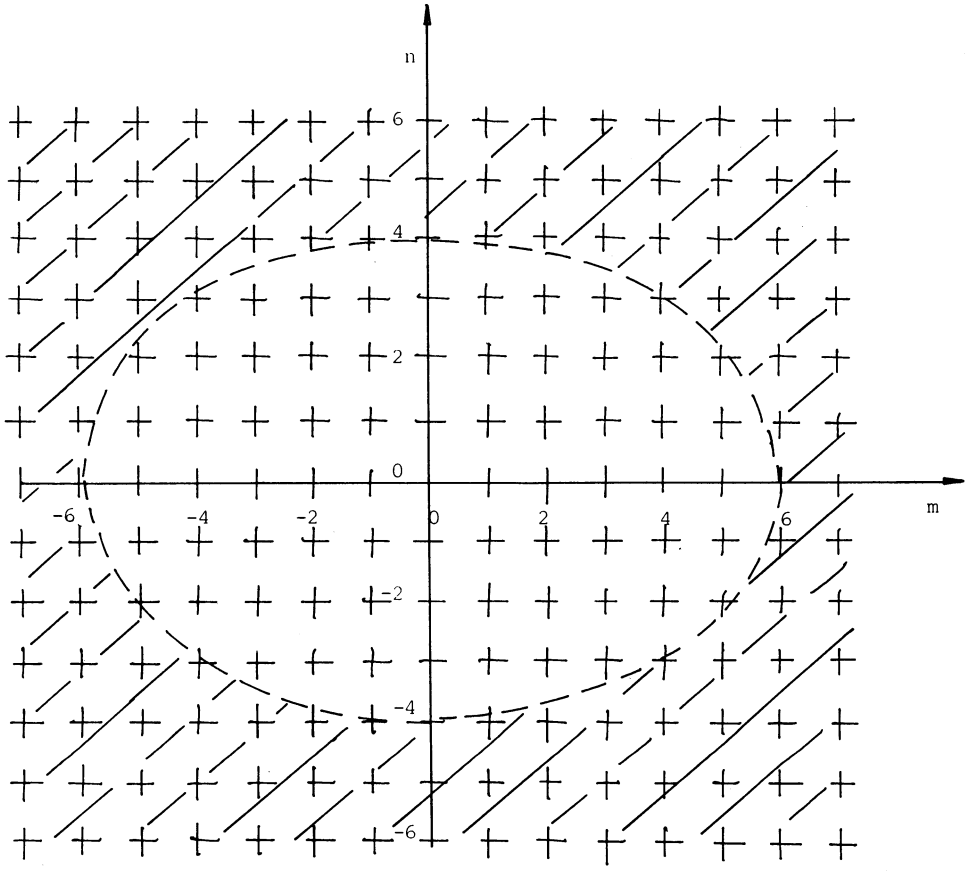

Figure 2.6 The extended (m,n) plane. The summation of equation (A53) is over all the points in the unshaded area.

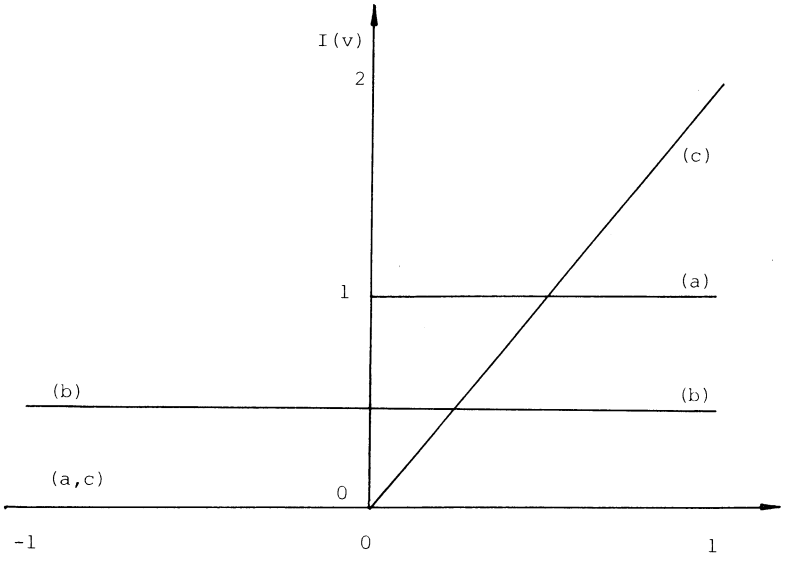

Figure 2.7 Plane wave weighting functions. Graph (a): semidiffuse field. Graph (b): diffuse field. Graph (c): modal power proportional to modal axial wavenumber.

CHAPTER THREE
INFERENCE OF THE PLANE WAVE WEIGHTING FUNCTION FROM SPECTRAL DENSITY MEASUREMENTS

3.1 INTRODUCTION

The last chapter was a description of the free wave idea. In whatever context a free wave field is encountered, it will always have certain general characteristics: in particular, the complex cross-spatial density (CCSD) taken between two observation points in the field may always be expressed as a weighted integral of uncorrelated plane wave contributions. The plane wave weighting function occurring in this integral completely characterises the field, and its interpretation was outlined in Chapter Two.

A means to obtain an estimate of the plane wave weighting function in an anisotropic free wave field is therefore a key part of any free wave analysis. The weighting is not directly observable, however, it must be preferred from measurements of the observable quantity CCSD. The present chapter and the next are a description of the practical development of a weighting inference method.

The framework of this chapter is a review of a variety of methods developed by previous workers for studying anisotropic free wave fields in various contexts. The earliest methods used Cook's diffuse field result as the basis of simple criteria of the non-diffuseness of sound fields. Later more precise analyses were made of the anisotropy of sound fields with the inductive comparison of measured CCSD with predictions based on assumed forms of plane wave weighting. Finally came the development of completely general methods involving the direct analysis of CCSD data with no (or very unrestrictive) assumptions about the underlying weighting. One such direct method is chosen for further development in the next chapter.

The discussion, which is couched in general terms, as illustrated by the consideration of specific model examples of anisotropic free wave fields, taken from various contexts. Some results derived about the example fields are of interest in themselves and may be of value to future workers.

The scope of this chapter is the fundamental properties of each analysis method. The details of the practical implementation of one method, including its sensitivity to data limitations (such as the available number of sampling positions, and the presence of spectral density estimation error) are given in

the next chapter.

3.2 COOK'S THEOREM AND NONDIFFUSE FIELDS

3.2.1 Applications of Cook's Theorem

The simple expression (equation 2.11)) derived by Cook (2.12) for CCSD in a diffuse free wave field created great interest among architectural acousticians, who put the result to extensive practical use. For example, valuable results were derived about the use of spatial averaging of measurements of acoustical parameters of diffuse fields to improve the accuracy of estimates of such quantities as sound pressure level (SPL). It was shown (3.1, 3.2, 3.3) that averaging over several properly chosen discrete positions could yield statistically better estimates than averaging over a continuous line (3.4, 3.5), despite the comparative simplicity of the discrete technique. This is because much of the extra information obtained from a continuous traverse comes from the oversampling of well-correlated values. Similarly, it was shown that a continuous average taken over the perimeter of a disc could be statistically bettter than a continuous average over the disc's surface (3.5), and that an average over the surface of a sphere could be better than an average throughout the sphere's volume (3.6).

Another economising application of correlation results was made by Broadhurst (3.7, 3.8, 3.9) who described the use of an acoustic telescope in the context of architectural acoustics. An acoustic telescope as developed in the study of jet noise sources can be "focussed" on the sound coming from a given source by the careful processing of the signals from an array of microphones. Broadhurst used correlation results to show that a 5 x 5 x 5 cubical array of microphone positions could be reduced to a 52-point array without the telescope suffereing a significant loss of statistical reliability.

3.2.2 Criteria of Diffuseness

Cook's result was thus proven useful in a variety of ways. However the motivation for Cook's original work had been the need to develop a "criterion of diffuseness" which could be used to establish experimentally whether a given enclosure's sound field was truly diffuse.

An assumption of diffuseness played an important role in the theory behind many of the most useful quantities in architectural acoustics (3.10). For example, a diffuseness assumption was necessary for the analysis of wall absorption

measurements, because of the definition of mean free path used in the derivation of the decay rate of sound; for the study of transmission loss through partitions; for definitions of the total absorption of a room; and for deductions of the total power output of a source from the measurement of space-averaged pressure. A way to determine the diffuseness or nondiffuseness of an enclosure's sound field was thus clearly important.

Qualitative investigations of the anisotropy of sound fields using Cook's result were made by Balachandran and Robinson (3.11), who compared correlation measurements with Cook's prediction to study the diffuseness of steady and decaying fields in a reverberation chamber, and by Pisarevskii (3.12) who plotted contours of isocorrelation in a room sound field. The contours in a truly diffuse field would be concentric circles, while those in a field consisting of a single plane wave would be straight lines parallel to the plane wave's wavefronts. The form of the contours could be used to study energy flow in a nondiffuse field.

More precise quantitative investigations of nondiffuseness were based on the definition of indices to show the overall nondiffuseness of a field, involving the mean-square deviation of correlation measurements from Cook's prediction. Such investigations were made by Balachandran (3.13) and by Bodlund (3.14), who described a similar study by Koyasu (3.15) in the course of which it was shown that the behaviour of such diffuseness criterion is consistent with the variation of estimates of absorption coefficients made in the presence of nondiffuse fields.

3.3 INDUCTIVE WEIGHTING ANALYSIS: PARAMETRIC MODELS

An index of diffuseness such as described in subsection (3.2.2) is both quantitative and comparative, in that it can be used to show which of two given sound fields is the "less diffuse". However, it can yield no information about the precise way in which a sound field differs from the perfectly diffuse: that is, about the nature of an arbitrary free wave field's plane wave weighting function. The first attempts to use correlation measurements to study anisotropic plane wave weightings seem to have been based on induction methods developed by workers in ocean acoustics.

3.3.1 Inductive Weighting Analysis: Sea Noise

As mentioned in the last chapter, the generation of sea noise by wave action on

an ocean surface can be modelled with a plane distribution of identical sources. Each source is assumed to have the same unknown directivity. Several workers have approached this problem inductively, by supposing the directivity to belong to a well-defined parametric family. The small number of adjustable parameters (generally one) could be chosen by comparing the resulting CCSD predictions with measurements made of real sea noise.

For example, Cron and Sherman (2.20) studied a source distribution which produced in deep water a free wave field with a plane wave weighting function given by

$$I(v) \quad \alpha \quad \cos^m v, \quad 0 \leq v \leq \pi/2$$

$$= \quad 0, \quad \pi/2 < v \leq \pi \qquad (3.1)$$

with m an odd integer, and polar angle v measured away from the downward normal to the ocean surface (see Figure 3.1)). Cron, Hassel and Keltonic (3.16) showed good agreement of theory and measurement when a dipole surface source model (m=1) was used. Rein (3.17) later showed that Cron and Sherman's deep water correlation results for their surface noise model also applied to correlation in regions near to the surface. Linnette and Thompson (3.18) independently made a similar theoretical and experimental study.

Kuryanov (3.19) suggested a different approach to the surface noise problem involving the correlation produced in deep water beneath a surface distribution of independent sources with a specified plane correlation. Liggett and Jacobson (3.20) showed that such an approach was consistent with the methods of Cron and Sherman, etc. and studied the case of a Gaussian surface correlation producing a deep water plane wave weighting function

$$I(v) \quad \alpha \quad \cos v \exp(-\sin^2 v/4\gamma), \quad 0 \leq v \leq \pi/2$$

$$= \quad 0, \quad \pi/2 < v \leq \pi \qquad (3.2)$$

with γ an adjustable parameter.

Other ocean noise models based on simple anisotropic plane wave weighting functions were suggested by Liggett and Jacobson (3.2.1), who studied the family

of weightings

$$I(v) \alpha \exp(A \cos v), \quad 0 \leq v \leq \pi/2$$

$$= 0, \quad \pi/2 < v \leq \pi \tag{3.3}$$

and by Talham (3.22), who proposed a weighting proportional to the radius vector of an oblate spheroid:

$$I(v) \alpha (1 - e^2 + e^2 \sin^2 v)^{-\frac{1}{2}}, \quad 0 \leq v \leq \pi/2$$

$$= 0, \quad \pi/2 < v \leq \pi \tag{3.4}$$

A,e are adjustable parameters.

3.3.2 Inductive Weighting Analysis: Fan Noise

Piersol (3.23) made an interesting inductive attempt to model fan noise in a wind tunnel with a diffuse field produced by a volume distribution of sources close to the observation point, together with a single distant source to represent the fan. The relative output power of the fan source was chosen by fitting the resulting predicted correlation function to observations made in a wind tunnel.

3.3.3 Inductive Weighting Analysis: Room Fields

Architectural acousticians have also used inductive methods to study simple nondiffuse fields in enclosures. A straightforward generalisation of a diffuse field is the "partially reverberant" field. The plane wave weighting function in a diffuse field is constant over all angles; in a partially reverberant field it is constant over a restricted range of angles:

$$I(v) = \text{constant}, \quad v_1 \leq v \leq v_2, \quad u_1 \leq u \leq u_2$$

$$= 0 \text{ otherwise} \tag{3.5}$$

v_1, v_2, u_1, u_2 are constants. The field is azimuthally symmetric if the range of u is 0 to 2π. One special case is that of the semidiffuse field ($v_1 = 0$, $v_2 = \pi/2$, $u_1 = 0$, $u_2 = 2\pi$) which was mentioned in Chapter 2 as a simple model of the sound field in a duct with an anechoic termination at high frequency.

Partially reverberant fields were studied theoretically by Blake and Waterhouse (3.24). Earlier, Dammig (3.25) had found good agreement between predicted and measured correlation in a partially reverberant field stimulated by an array of loudspeakers which formed an octant of a sphere.

3.3.4 The Use of Parametric Weighting Families

The inductive analysis methods described above depended on the theoretical study of CCSD in a free wave field with a plane wave weighting belonging to a parametric family. The main theme of the rest of this chapter is a discussion of a series of direct analysis methods. However the further consideration of two sets of model free wave fields with simple parametric weightings proves to be a useful counterpoint to this theme. The model fields' main use here is to illustrate points made about the properties of the direct methods, and so to provide an intuitive background to the theoretical results presented below. Moreover some of the new results obtained (especially those concerning the computation of CCSD in fields with arbitrary plane wave weightings, subsection (3.3.7)), are of interest in themselves.

The rest of this section of the chapter is an introduction to the two parametric families of weightings. The choice of these families for study has been inspired by the models considered by earlier workers, as described above. The weightings are all azimuthally symmetric (I independent of u). Each family includes weightings with a wide variety of forms, characterised by a small number of parameters, but each includes as a special case the semidiffuse field weighting, which as noted in Chapter 2 corresponds (for example) to a uniform modal power distribution in a duct with an anechoic termination.

An important preliminary result is that the general free wave integral representation for CCSD (equation (2.14)) in an azimuthally symmetric field may be simplified by using the standard Bessel function integral result (2.31, Chapter 2):

$$J_o(x) = (1/2\pi) \int_0^{2\pi} \exp(ix \cos \phi)\, d\phi \qquad (3.6)$$

to perform the u-integration, leaving

$$C(\omega,r,\theta) = \int_0^{\pi} dv \sin v\, I(\omega,v) \exp(ikr \cos\theta \cos v) \times J_0(kr \sin\theta \sin v) \qquad (3.7)$$

3.3.5 Cosine-Power Weighting

The first family is of "cosine-power" plane wave weightings:

$$I(v) = (m+1)\cos^m v, \quad 0 < v < \pi/2$$
$$= 0 \qquad \pi/2 < v \leq \pi \qquad (3.8)$$

The parameter m need not be an integer, and its range is

$$-1 < m < \infty \qquad (3.9)$$

The lower limit ensures that the weighting is integrable; the weighting is square integrable if $m > -\frac{1}{2}$. (See subsection (3.7.1) for a discussion of the importance of integrability properties.) Members of this family were studied by Cron and Sherman (2.20) et al. in the context of ocean acoustics.

Despite its analytic simplicity, the cosine-power family encompasses a wide range of fields, from the semidiffuse field to a field composed of a single plane wave. Some members of the family are shown in Figure (3.2). The case m = 0 is the semidiffuse weighting. In the limit $m \to \infty$, the weighting approaches a delta function with its peak at cos v = 1; this represents a field composed of a single plane wave with its wavenumber vector parallel to the z-axis of coordinates. The expected normalised CCSD in such a field is

$$C(\omega,r,\theta) = \exp(ikr\cos\theta) \qquad (3.10)$$

(see equation (2.8)).

It may be shown (2.30) that the CCSD function in such a field can be expressed in terms of standard functions in the special cases $\theta = 0, \pi/2$. The case $\theta = 0$ describes an "axial" CCSD, while the case $\theta = \pi/2$ describes a "cross-sectional" CCSD. Plots of axial and cross-sectional CCSD for a range of m values are given in Figure (3.3).

The axial CCSD may be computed easily in certain cases by using an iterative formula. Writing C_m for the axial CCSD in an m-th order cosine-power field, it follows from integrating the right hand side of equation (3.7) by parts that for $m > -1$,

$$C_m = \exp(ikr) - (ikr/m+2)\ C_{m+1} \tag{3.11}$$

In the semidiffuse field case $m = 0$,

$$C_0 = \sin(kr)/kr + (i/kr)(1-\cos(kr)) \tag{3.12}$$

When m is $-\frac{1}{2}$, the integral for CCSD may be expressed in terms of the standard Fresnel integrals

$$\begin{Bmatrix} C_F \\ S_F \end{Bmatrix} (x) = \int_0^x dt \begin{Bmatrix} \cos \\ \sin \end{Bmatrix} (\pi t^2/2) \tag{3.13}$$

to give

$$C_{-\frac{1}{2}} = (C_F(x) + i\ S_F(x))/x,\ x = (2kr/\pi)^{\frac{1}{2}} \tag{3.14}$$

Equations (3.11-3.14) may be used to compute the value of C_m by iteration on m for any integer or half-integer m.

Another consequence of equation (3.11) is that as $m \to \infty$,

$$C_m \to \exp(ikr) \tag{3.15}$$

since $|C_m| \leq 1$ for all values of m. This is the plane wave limit of equation (3.10).

When $\theta = \pi/2$, the standard Bessel function result

$$\int_0^{\pi/2} dv\, J_o(z \sin v) \sin v \cos^{2p+1} v = 2^p \Gamma(p+1) \times J_{p+1}(z)/z^{p+1} \qquad (3.16)$$

(2.31) may be used to show that

$$C(r,\pi/2) = (2/kr)^{\frac{m+1}{2}} J_{\frac{m+1}{2}}(kr)\, \Gamma\left(\frac{m+3}{2}\right) \qquad (3.17)$$

Γ is the complete gamma function (2.31)

Special cases occur when m is an odd integer:

$$C = n!\, J_n(kr)(2/kr)^n \qquad (3.18)$$

where $m = 2n-1$, $n = 1, 2, \ldots,$ and when m is an even integer:

$$C = (2n+1)!\, j_n(kr)/n! \qquad (3.19)$$

where $m = 2n$, $n = 0, 1, 2, \ldots$. These results are given by Cox (2.22).

In the semidiffuse case m=0, equation (3.19) reduces to

$$C = j_o(kr) \qquad (3.20)$$

In the limit in $m \to \infty$, the asymptotic expansions

$$J_n(z) \sim (ez/zn)^n (2\pi n)^{-\frac{1}{2}} \tag{3.21}$$

and

$$\Gamma(n) \sim (n/e)^n (2\pi/n)^{\frac{1}{2}} \tag{3.22}$$

(2.31) may be used to show that $C_m \to 1$, agreeing with equation (3.10).

Equations (3.12, 3.20) were first given by Blake and Waterhouse (3.24).

3.3.6 Strip Function Weightings

The second family of model weightings is of "strip function" weightings:

$$I(v) = I_j \text{ for } v_{j-1} < v < v_j,\ j = 0, n-1 \tag{3.23}$$

I_j, v_j are constant with $v_o = 0$, $v_n = \pi$ (see Figure 3.4)). The normalisation of the weighting (equation (2.16)) leads to the constraint

$$1 = \sum_{j=1}^{n} I_j (\cos(v_{j-1}) - \cos(v_j)) \tag{3.24}$$

This model family includes the partially reverberant field family described in subsection (3.3.3). The semidiffuse weighting is the special case n = 2, $v_1 = \pi/2$, $I_1 = 1$, $I_2 = 0$, while a more general partially reverberant field is the special case n = 3, $I_1 = I_3 = 0$, $I_2 = (\cos v_1 - \cos v_2)^{-1}$ (see Figure (3.4)).

The main value of this weighting family is as the basis of a highly efficient procedure to compute CCSD in an arbitrary free wave field, as described in subsection (3.3.7). However, the family also affords a useful introduction to a practically significant property of the relation between CCSD and plane wave weighting as described by equation (3.7).

The shape of a weighting function I(v) could be described by a series of moments:

$$\mu_1 = \int_{-1}^{1} dc\ c\ I(c) \tag{3.25}$$

$$\mu_2 = \int_{-1}^{1} dc\ (c - \mu_1)^2\ I(c) \tag{3.26}$$

$$\mu_3 = \int_{-1}^{1} dc\ (c - \mu_1)^3\ I(c) \tag{3.27}$$

.....

where $c = \cos v$. These moments may be called the mean, variance, skewness etc. of the weighting, by analogy with the moments of a probability distribution. If the weighting is dominated by a single peak, μ_1 describes the position of the peak, μ_2 describes its width, and so on. The more moments are known, the more detail of the weighting is specified.

If the field is partially reverberant, the first two moments are

$$\mu_1 = \tfrac{1}{2}(\cos v_1 + \cos v_2) = \cos \bar{v} \cos \Delta v \tag{3.28}$$

$$\mu_2 = (1/12)(\cos v_1 - \cos v_2)^2 = (1/3)(\sin \bar{v} \sin \Delta v)^2 \tag{3.29}$$

where $\bar{v} = (v_1 + v_2)/2$, $\Delta v = (v_2 - v_1)/2$. The significance of these moments for the form of CCSD is illustrated by a consideration of the axial CCSD in a partially reverberant field. Substitution of the strip field weighting into equation (3.7) yields

$$C(\omega,r,0) = (1/ikr) \sum_{j=1}^{n} I_j(\exp(ikr \cos(v_{j-1}))-\exp(ikr \cos(v_j))) \tag{3.30}$$

If the field is partially reverberant, $C(\omega,r,0)$ takes the form

$$C(\omega,r,0) = (1/ikr)\ I_2\ (\exp(ikr \cos v_1)-\exp(ikr \cos v_2)) \tag{3.31}$$

$$= \frac{\sin(kr \sin \bar{v} \sin \Delta v)}{kr \sin \bar{v} \sin \Delta v} \exp(ikr \cos \bar{v} \cos \Delta v) \qquad (3.32)$$

- a result first given by Blake and Waterhouse (3.24). It follows that the slope of the phase of C at the origin (kr = 0) is

$$\mathrm{Im}(dC/d(kr)) = \cos \bar{v} \cos \Delta v = \mu_1 \qquad (3.33)$$

while the first zero of the modulus of C occurs when

$$kr \sin \bar{v} \sin \Delta v = \pi \qquad (3.34)$$

i.e. when

$$kr = \pi/(3\,\mu_2)^{\frac{1}{2}} \qquad (3.35)$$

Thus the lowest-order moments of the plane wave weighting are reflected in the low-kr range of CCSD, so that if only a limited range of kr values were available, only the lowest-order features of the plane wave weighting could be observed. This point will be considered in more detail in subsection (3.7.3).

3.3.7 Computational Applications of Strip Weightings

The computational usefulness of a strip field comes from the fact that one of the derivatives of a strip weighting can be expressed exactly as a summation. It may be shown (2.30) that for every value of r,θ,

$$\frac{dC}{d\theta}(\omega,r,\theta) = i \sum_{j=1}^{n} I_j \,(f(v_{j-1}) - f(v_j)) \qquad (3.36)$$

where

$$f(v) = \exp(ikr \cos\theta \cos v)\, J_1(kr \sin\theta \sin v) \tag{3.37}$$

The value for C for any r, θ can thus be computed from

$$C(\omega,r,\theta) = C(\omega,r,0) + \int_0^{\theta} d\theta \, \frac{dC}{d\theta} \tag{3.38}$$

with $C(\omega,r,0)$ given by equation (3.30). For example, for a semiduffuse field,

$$\frac{dC}{dr}(\omega,r,\theta) = -i\, J_1(kr \sin\theta) \tag{3.39}$$

so that

$$C(\omega,r,\theta) = C(\omega,r,0) - i \int_0^{\theta} d\theta \; J_1(kr \sin\theta) \tag{3.40}$$

Equations (3.36- 3.38) may be used to compute $C(\omega,r,\theta)$ over, say, a grid of values $\{r_k, \theta_\ell : k = 1, M;\ \ell = 1, N\}$, with only M integrations needing to be performed: one integration over θ for each fixed value of r. If the original formula of equation (3.7) were used to compute C over the same grid, an integration for each of the grid's M x N points would need to be performed. Thus the use of equations (3.36 - 3.38) would result in an N-fold improvement in computational efficiency, with a corresponding reduction in computer time.

These ideas may be used to estimate efficiently $C(\omega,r,\theta)$ for an arbitrary (azimuthally symmetric) plane wave weighting, by approximating the weighting by a strip field. This is especially suited to computing the low-kr range of C, since (as noted in subsection (3.3.6)) this range is dominated by the gross features of the weighting, rather than the fine detail.

The results of a computer program based on these ideas are given in Figures (3.5 - 3.9). Each Figure includes a graph of the associated strip field weighting, and graphs of $C(\omega,r,\theta)$ in modulus and phase form as functions of frequency over the range 0 - 5 kHz for the three cases r = 12 cm, θ = 0; r = 12 cm, $\theta = \pi/2$; r = 11.4 cm, θ = 1.1 rad.

Figure (3.5) illustrates C in a semidiffuse field. Figures (3.6 - 3.9) illustrate the convergence of C estimates obtained with quite coarse strip models of plane wave weightings. Figures (3.6, 3.7) were obtained using 6-strip and 11 strip approximations of the m = 1 cosine-power plane wave weighting, and Figures (3.8, 3.9) were obtained using 6-strip and 11-strip approximations of the m = -0.9 cosine-power weighting.

These results show that the method provides an efficient way to produce CCSD predictions from an azimuthally symmetric plane wave weighting function. The function should be approximated by a strip function, and equations (3.36 - 3.38) used to evaluate the CCSD as required. A significant reduction in computer time is to be expected.

3.4 DIRECT WEIGHTING ANALYSIS: THEORETICAL INVERSE

In this section the main thread of the chapter is resumed, with the beginning of a discussion of direct plane wave weighting methods, illustrated by reference to the weighting families described above.

A direct weighting analysis method involves the deduction of information about plane wave weighting from CCSD measurements, with no (or very unrestrictive) assumptions about the nature of the final answer. This is in contrast to the inductive methods described in subsections (3.3.1 - 3.3.4), in which the weighting was assumed to be of a specified form dependent on the value of adjustable parameters, which may be determined by a fitting to experimental data.

The analysis methods described here are all single-frequency techniques (except for the spatial Fourier Transform technique described in this section), and for convenience the frequency dependence of CCSD and weighting functions will be regarded as implicit for the rest of the chapter. The methods discussed all depend on the sampling of a field with an omnidirectional receiver, such as a standard microphone.

The choice of a method of weighting analysis appropriate for a given case is determined by the nature of the available CCSD data set. Samples of CCSD may be available throughout a volume, or over a restricted but well-ordered set of points such as a straight line through the field, or - more commonly - over a restricted and disordered set of points scattered through a volume. In the following discussion methods appropriate to each of these cases will be reviewed in turn, and one method will be developed in practical detail later.

3.4.1 Use of Theoretical Inverse

If samples of CCSD are available throughout a volume, the theoretical inverse of equation (2.14) may be used to deduce information about the plane weave weighting. This depends on the three-dimensional spatial Fourier Transform pair:

$$f(\underline{r}) = f(r,\theta,\phi) = \int_0^{\pi} dv \int_0^{2\pi} du \int_0^{\infty} dk\, k^2 \sin v\, F(\underline{k}) \exp(i\underline{k}.\underline{r}) \tag{3.41}$$

$$F(\underline{k}) = F(k,v,u) = (1/2\pi)^3 \int_0^{\pi} d\theta \int_0^{2\pi} d\phi \int_0^{\infty} dr\ r^2 \sin\theta f(\underline{r}) \times \exp(-i\underline{k}.\underline{r}) \tag{3.42}$$

The integrals are volume integrals taken over the whole of physical space ($\underline{r}$) and wavenumber space ($\underline{k}$).

The theoretical inverse of the C-I equation (2.14) is available in two forms, the choice between these being determined by the assumed availability of information on the frequency dependence of CCSD. If C is known at all frequencies, a function of position may be defined by integrating C over frequency (that is, over k):

$$f(\underline{r}) = 2\pi \int_0^{\infty} dk\, k^2\, C(\omega,\underline{r}) \tag{3.43}$$

$$= \iiint dv\, du\, dk\, k^2 \sin v\, I(\omega,v,u) \exp(i\underline{k}.\underline{r}) \tag{3.44}$$

The function I may now be found by using the inversion equation (3.42):

$$I(\omega,v,u) = \left(\frac{1}{2\pi}\right)^2 \iiint dr\, d\theta\, d\phi\, r^2 \sin\theta\, e^{-i\underline{k}.\underline{r}} \int k_1^2\, dk_1\, C(\omega_1,\underline{r}) \tag{3.45}$$

Alternatively, if C is known at only one frequency, say ω', a delta-function may be introduced into equation (2.14) (with $k' = \omega' c_o$):

$$C(\omega',\underline{r}) = (1/2\pi) \iiint dv\, du\, dk\, k^2 \sin v\, I(\omega,v,u)\ \ \delta(k-k')/k'^2 \tag{3.46}$$

and I determined using equation (3.42):

$$(1/2\pi)^3 \; I(\omega,v,u) \; \delta(k-k')/k'^2 = (1/2\pi)^3 \iiint dr \, d\theta \, d\phi \, r^2 \sin\theta \times C(\omega,\underline{r}) \exp(-i\underline{k}.\underline{r}) \qquad (3.47)$$

This form of the theoretical inverse depends only on a knowledge of C as a function of position; it will yield a function defined throughout wavenumber space which will be non-zero only on the sphere with radius $|\underline{k}| = k'$.

A practical application of the theoretical inverse of the C-I equation would involve an array of samples of C - perhaps an n x n x n cubical array of points. Fourier inversion would yield an n x n x n array of samples in wavenumber space. The rapid growth of such arrays with n is one disadvantage of the method. Another is the fact that, as noted above, either an integration of CCSD over frequency (as well as over space) must be performed to obtain a weighting estimate at each frequency of interest, or, if the inversion is performed at one frequency only, the n x n x n array in wavenumber space will consist mostly of zeroes. The only non-zero samples will be those lying on or near a sphere of radius k'.

3.4.2 Practical Application

A reverberation chamber free wave field analysis method using the theoretical inverse was developed by Freudenstein and Ebeling (3.26). A digitally generated, exactly repeatable narrow band signal was used to excite the chamber; a single microphone was traversed successively to each point in a 16 x 16 x 16 (= 4096 points) cubical array of positions to give the equivalent of a simultaneous sampling by 4096 microphones. The procedure was automated and took several hours; nevertheless the method was proven to work. The method was later (3.27) applied to the assessment of the diffuseness of the sound field in a reverberation chamber under various conditions.

3.5 DIRECT WEIGHTING ANALYSIS: WAVENUMBER SPECTRA

In most practical instances, only much more restricted sets of CCSD data will be available than is necessary for the use of the theoretical inverse technique

described in section (3.4). Suppose, for example, that samples of CCSD are available only along a single straight line passing through the field, so that the data set is

$$\{C(r, \theta, \phi): \theta, \phi \text{ fixed}, \quad 0 \leq r < \infty\} \tag{3.48}$$

In practical cases, a truncated and discretely sampled version of this will be available. What information can be derived about the field's plane wave weighting from this data?

This question was studied by Cox (2.22) who in the course of his ocean acoustic work proposed the use of a "wavenumber spectrum", involving a Fourier-type integral of CCSD with respect to distance. Cox found that the wavenumber spectrum method was powerful enough to give complete information about plane wave weighting in certain cases, despite the restricted nature of the input data set. The properties of wavenumber spectra are the subject of this section.

3.5.1 Fundamental Properties

Consider an azimuthally symmetric free wave field extending to infinite distance. The wavenumber spectrum as studied by Cox can be defined by

$$Q(p, \theta) = (1/2\pi) \int_{-\infty}^{\infty} dR \; C(R, \theta) \exp(-ipR) \tag{3.49}$$

(C,Q are also functions of frequency implicitly). The integration variable is the normalised distance

$$R = kr \tag{3.50}$$

$Q(p, \theta)$ depends only on the straight line data set, equation (3.48).

The integral has been extended to negative R values by defining

$$C(-R,\theta) = C^*(R,\theta) \tag{3.51}$$

This range of integration has been chosen for analytic simplicity. It ensures that Q is a real function of the real parameter p.

However Q contains information about both real and imaginary parts of C, as can be seen from the inverse of equation (3.49):

$$C(R,\theta) = \int_{-\infty}^{\infty} dp\ Q(p,\theta)\ \exp(ipR) \tag{3.52}$$

The dimensionless parameter p can be interpreted as a normalised plane wave flight time, as will be discussed below.

Q can be expressed in terms of plane wave weighting by substituting equation (3.7) into equation (3.49). If the order of integration is changed, the result is

$$Q(p,\theta) = \int_{0}^{\pi} dv\ \sin v\ w(p,v,\theta)\ I(v) \tag{3.53}$$

where

$$w(p,v,\theta) = (1/2\pi) \int_{-\infty}^{\infty} dR\ \exp(iR\cos\theta\ \cos v - ipR)\ J_o\ (R\sin\theta\ \sin v) \tag{3.54}$$

Equation (3.53) can alternatively be written in terms of the variable c = cos v:

$$Q(p,\theta) = \int_{1}^{1} dc\ w(p,c,\theta)\ I(c) \tag{3.55}$$

An important special case is that of an "axial" spectrum, $\theta = 0$, which depends only on axial CCSD data. When $\theta = 0$, the window factor w becomes

$$w(p,c,0) = (1/2\pi) \int dR \exp(iR(c-p))$$

$$= \delta(c-p) \qquad (3.56)$$

so that

$$Q(p,0) = I(p) \qquad (3.57)$$

(The $(1/2\pi)$ normalisation factor and the sign of p in equation (3.49) were chosen with this result in mind.) This somewhat surprising fact, that a wavenumber spectrum can yield complete information about a plane wave weighting despite the comparatively limited nature of the data on which it is based, was noted by Cox (2.22).

For $\theta \neq 0$, Q as expressed by equation (3.53) is in general a weighted integral over plane wave angle. It may be shown (2.30) using standard Bessel Function results (2.31, Chapter 11) that

$$w(p,v,\theta) = (1/\pi) \{(\sin\theta \sin v)^2 - (\cos\theta \cos(v-p))^2\}^{-\frac{1}{2}} \qquad (3.58)$$

This result holds provided the expression in curly brackets is positive; w is zero otherwise.

The window factor w is sketched as a function of cos v in Figure (3.10). It has the property that the area under its graph as a function of cos v is 1, independently of the value of p.

To interpret the properties of the window function, let an angle ψ be defined by

$$p = \cos\psi \qquad (3.59)$$

so that Q may be written $Q(\psi,\theta)$. Then it may be shown that w is non-zero only when the ψ, v, θ satisfy the condition

$$\cos\cdot(\psi+\theta) \leq \cos v \leq \cos(\psi-\theta) \tag{3.60}$$

Thus the limits in the integral of equation (3.53) representing Q must be replaced by cos $(\psi+\theta)$, cos $(\psi-\theta)$, since w is zero outside this interval, so that only waves from a restricted range of angles contribute to Q. (The range will be further restricted if the plane wave weighting is also non-zero only within a restricted band of angle, for example if the field is partially reverberant.)

A further interpretation of this is that the contributing range of angles decreases as p approaches the value 1 (that is, $\psi \to 0$). In the limit, the spectrum once again becomes a copy of the plane wave weighting. This follows because as p approaches 1 the range of contributing angles (equation (3.60)) shrinks to a narrow band around θ, so that the only contributing plane waves make up a thin bundle with their wavenumber vectors almost parallel to the line on which the basic CCSD data has been taken. Finally, in the limit,

$$Q(1,\theta) = I(\theta) \tag{3.61}$$

This result has a physical interpretation in terms of the flight time of waves between two microphones in the sound field. Consider Figures (3.11, 3.12). It is straightforward to show (see the Figure captions) that the time taken for a wave characterised by wavenumber angle v passing from a microphone at $\underline{x}'$ to a microphone at $\underline{x}$ is

$$\tau = (r/c_o) \left|\cos(v-\theta)\right| \tag{3.62}$$

and the flight time of a wave passing from $\underline{x}$ to $\underline{x}'$ is

$$\tau = (r/c_o) \left|\cos(v+\theta)\right| \tag{3.63}$$

The range is thus 0 to r/c_o. Waves with wavenumbers almost perpendicular to the line joining the microphones have very short flight times; while the more nearly parallel a wave's wavenumber is to the microphone axis, the longer its flight time, up to the limit r/c_o. It may be shown from equation (3.60) that the only

waves contributing to $Q(p,\theta)$ are those satisfying one of the conditions

$$|\cos(v-\theta)| \geq |p|, \quad |\cos(v+\theta)| \geq |p| \tag{3.64}$$

- that is, waves with flight times satisfying

$$|p|r/c_o \leq \tau \leq r/c_o \tag{3.65}$$

As p approaches 1, this contributing set grows smaller, until finally only that plane wave with a wavenumber vector parallel to the microphone axis can contribute to Q. The same argument holds for every microphone separation distance r, and so equation (3.61) follows.

The dimensionless parameter p can thus be interpreted as normalised delay time, which specifies the set of free waves which can contribute to the spectrum Q.

In summary, the wavenumber spectrum $Q(p, \theta)$ is a copy of the plane wave weighting in the two limits $p = 1$, $\theta = 0$. Otherwise it is a convolution of the weighting with a window factor w.

3.5.2 Wavenumber Spectra for Parametric Model Weighting

Closed-form expressions are available (2.30) for wavenumber spectra in a free wave field whose plane wave weighting belongs to one of the model families introduced in section (3.3). This may be useful in future applications, since closed form expressions for CCSD are not in general available.

An example is the wavenumber spectrum in a semidiffuse field. The spectrum takes different forms in different regions of the (θ,ψ) plane (Figure (3.13)). In region (i), defined in the figure, $Q(\psi,\theta)$ is zero.

In region (ii), $Q(\psi,\theta)$ is unity. In region (iii),

$$Q(\psi,\theta) = \tfrac{1}{2}+(1/\pi)\sin^{-1}(\cot\theta\cot\psi) \tag{3.66}$$

3.5.3 Truncation Effects

The definition of wavenumber spectrum Q (equation (3.49)) was in terms of an integral with respect to distance. The integral was taken out to infinity; however an important limitation on spectra computed in practice is that the available CCSD data will always be truncated at some finite value, say R = R'.

To see the consequence of this, consider the example of a truncated estimate of the axial wavenumber spectrum Q(p,0) in a semidiffuse field:

$$Q'(p;R') = (1/2\pi) \int_{-R'}^{R'} dR\ C(R,0)\ \exp(-ipR) \tag{3.67}$$

Substitution of equation (3.12) for the CCSD in this case into equation (3.67) allows Q' to be expressed in terms of the standard sine integral function (2.31, chapter 5):

$$S_i(x) = \int_0^x \sin x/x\ dx \tag{3.68}$$

so that

$$\pi Q'(p-R') = S_i((1-p)R') - S_i(pR') \tag{3.69}$$

Since the spectrum is axial, in the limit $R' \to \infty$ this should reduce to a copy of the plane wave weighting function. This follows from the fact that

$$\lim_{x\to\infty} S_i(x) = \pi/2, \quad \lim_{x\to\infty} S_i(x) = -\pi/2 \tag{3.70}$$

so that as $R' \to \infty$

$$S_i((1-p)R') \to \pi/2 \text{ if } p > 1, \to -\pi/2 \text{ if } p < 1 \tag{3.71}$$

and

$$S_i(pR') \rightarrow \pi/2 \text{ if } p > 0, \rightarrow -\pi/2 \text{ if } p < 0 \tag{3.72}$$

These results combine to give as $R' \rightarrow \infty$

$$Q'(p;R') \rightarrow 1 \text{ if } 0 < p < 1, \rightarrow 0 \text{ otherwise} \tag{3.73}$$

which as expected is a copy of the semidiffuse weighting.

Q' is plotted for various R' in Figure (3.14), to show the distortion suffered by Q' as a result of truncation of the integral. Note the presence of Gibb's phenomenon fringes to either side of the discontinuities, which will persist even at large R'. The Figure suggests that R' should be at least as large as 4π before truncation effects can be neglected; this corresponds to a maximum sampling separation of 13.6 cm at a frequency of 5 kHz, and 34 cm at 2 kHz.

3.5.4 Practical Applications

The practical application of wavenumber spectral analysis to the study of free wave fields has been quite limited. Tohyama (3.28, 3.29) studied wavenumber spectra in a room field but concentrated on low frequencies with few modes present whose amplitudes could be found from the spectra.

In a comparable study, Gorskaya (3.30), working in ocean acoustics, investigated the field in an acoustic waveguide by means of a wavenumber spectrum. Again, attention was restricted to low frequencies with few modes present.

Lubman (3.31) adapted wavenumber spectrum ideas to the analysis of the signal from a single microphone. Traversing the microphone produced a record of the spatial variation of a sound field in the form of a time series. Fourier transforming the time series was then equivalent to taking a wavenumber spectrum. Lubman used a circular tranverse, and obtained spectra with the expected band-limited shape. Lubman suggested that such transforms performed in three perpendicular directions could be sufficient to assess the directivity of the field.

3.6 DIRECT WEIGHTING ANALYSIS: STATIONARY PHASE APPROXIMATION

The wavenumber spectrum method described above is powerful enough to yield in certain cases complete information about plane wave weightings even if the available CCSD data is quite limited compared to that necessary for the theoretical inverse technique described in section (3.4). However the data set was assumed to be well ordered, with samples of the field taken along a straight line.

The subject of this subsection is a direct data analysis method with which plane wave weighting information can be deduced from an even more limited CCSD data set: a sparse, irregular array of sampling positions. Provided only that the points are well separated compared to a wavelength, an asymptotic form of the basic C-I relation (equation 2.14)) may be used to obtain weighting information relatively easily.

The method of stationary phase (3.32) is a standard method of estimating integrals of the form

$$\int dt\ q(t)\ \exp(ix\ p(t)) \tag{3.74}$$

where x is a large parameter, and p,q are differentiable functions. The method is based on the fact that the main contribution to the integral comes from those points in the range of integration where the phase is stationary, i.e. p' (=dp/dt) is zero. The contribution from such a point t_o in the interior of the range is, when x is large,

$$(2\pi/xp''(t_o))^{\frac{1}{2}}\ q(t_o)\ \exp(ix\ p(t_o) + i\pi/4) \tag{3.75}$$

The method can be applied to the integral of the basic C-I relation, equation (2.14).

The main conclusion is that when the normalised distance R = kr between a pair of sampling positions is large, the principal contribution to C comes from those plane waves with wavenumber vectors parallel to the separation vector. When $\theta \neq 0$, so that the sampling positions are not both on the z-axis.

$$C(R,\theta,\phi) \sim (1/iR)(\exp(iR)\ I(\theta,\phi) - \exp(-iR)\ I(\pi-\theta,\phi\pm\pi)) \qquad (3.76)$$

(The choice of sign in the second term depends on whether ϕ is greater or less than π.) A similar result holds for positions on the axis, but with the I terms replaced by azimuthal averages of I.

Weighting estimates could thus be taken directly from an arbitrary set of CCSD measurements, provided R is large enough for equation (3.76) to be a valid approximation. The relative error is O(1/R), suggesting that R should be at least 10, giving r = 11 cm at 5 kHz, and 27 cm at 2 kHz.

3.7 DIRECT WEIGHTING ANALYSIS: SPHERICAL HARMONIC EXPANSIONS

Only one restriction - large sampling position separations - was made on the CCSD data set necessary for the stationary phase analysis method described in the last section. Suppose now that the data set is still more limited, to a sparse irregular array of points which cannot be assumed to be far apart. An analysis method which will work even under these conditions is based on the spherical harmonic expansion of CCSD and weighting, and is discussed in this section.

The first part of the discussion is a review of some of the basic properties of spherical harmonic series.

3.7.1 Fundamental Properties

Spherical harmonic functions (3.33) are a set of standard functions of the spherical polar angles v,u. Each harmonic Y_ℓ^q is a complex combination of trigonometric functions of v (with maximum order ℓ) and u (with maximum order q). ℓ takes integer values 0 to ∞, and for each ℓ, q takes integer values from $-\ell$ to ℓ.

$Y_\ell^q(v,u)$ is proportional to the product of the associated Legendre polynomial P_ℓ^q with exp(iqu):

$$Y_\ell^q(v,u) \propto P_\ell^q(v)\exp(iqu) \qquad (3.77)$$

The harmonics with q = 0 are azimuthally symmetric:

$$Y_{\ell}^{q}(v,u) \quad \alpha \quad P_{\ell}^{q}(v) = P_{\ell}(\cos v) \tag{3.78}$$

where P_{ℓ} is the Legendre polynomial of order ℓ.

Spherical harmonics are "orthonormal"; that is, they are orthogonal and normalised in the sense that

$$\int_{0}^{\pi} dv \sin \int_{0}^{2\pi} du \; Y_{\ell}^{q}(v,u) \; Y_{\ell'}^{q'*}(v,u) = \delta_{\ell\ell'} \, \delta_{qq'} \tag{3.79}$$

The first few associated Legendre polynomials are listed in Ref. (3.32), page 639.

The usefulness of spherical harmonics comes from the ability of a harmonic series to approximate to almost any function f (v,u) of angle:

$$f(v,u) \cong S_{N}^{f} = \sum_{\ell=0}^{N} \sum_{q=-\ell}^{\ell} f_{\ell}^{q} \, Y_{\ell}^{q}(v,u) \tag{3.80}$$

A spherical harmonic series is to a function of angle what a Fourier series is to a periodic time series. An azimuthally symmetric function would be approximated by a sum of harmonics with q = 0:

$$f(v) \cong S_{N}^{f} = \sum_{\ell=0}^{N} f_{\ell}^{o} Y_{\ell}^{o}(v) \tag{3.81}$$

If the coefficients f_{ℓ}^{q} are chosen properly, then most functions can be approximated arbitrarily closely by a large enough series. This fact depends on a property of harmonics called "completeness", and to understand this properly some properties of functions of angle must be introduced.

A function of angle is called "integrable" if the integral

$$\int_0^{\pi} dv \sin v \int_0^{\pi} du\, f(v,u) \tag{3.82}$$

exists, and "square integrable" if

$$\int_0^{\pi} dv \sin v \int_0^{2\pi} du\, |f(v,u)|^2 \tag{3.83}$$

exists. A square integrable function is always integrable as well, but the converse is not necessarily true. For example, all partially reverberant weightins are both integrable and square integrable. All cosine-power weightings are integrable for $m > -1$, but only square integrable for $m > -\frac{1}{2}$. (This is easily seen by evaluating the integrals in equations (3.82, 3.83) for the general cosine-power weighting given by equation (3.8). The integral result becomes infinite as m approaches -1, as does the square integral result as m approaches $-\frac{1}{2}$.) A function composed of delta-functions would be integrable but not square integrable. Integrability and square integrability are thus associated with the presence and strength of singularities in the function f. All plane wave weightings encountered in practice would be expected to be square integrable.

A reasonable way to choose the coefficients f_{ℓ}^{q} for the series S_N^f (equation (3.80)) for a given N would be to minimise the mean square error

$$R_N = \int\int dv\, du \sin v \; | f(v,u) - S_N^f |^2 \tag{3.84}$$

with respect to the values of the coefficients. Expansion of the square and the use of the orthogonality of harmonics may be used (3.33) to show that the minimising coefficients are given by

$$f_{\ell}^{q} = \int\int dv\, du \sin v\, f(v,u)\, Y_{\ell}^{q*}(v,u) \tag{3.85}$$

The "completeness" of the harmonics means that as $N \to \infty$ then $R_N \to 0$ for any square integrable f. The approximatipn S_N^f is said to be "convergent in the mean to f". An arbitrarily good harmonic approximation of f may be obtained by taking a large enough series, and it is valid to write down an exact harmonic representation of f:

$$f(v,u) = \sum_{\ell=0}^{\infty} \sum_{q=-\ell}^{\infty} f_\ell^q \, Y_\ell^q(v,u) \qquad (3.86)$$

If the function f contains a discontinuity, Gibbs' phenomenon fringes are found to occur, because of the inability of a finite series of continuous functions to fit the infinite slope required at a discontinuity. This point is discussed further in Appendix B.

Another subtlety of harmonics is that the harmonic approximation of a function still has some meaning and usefulness even if the function is not square integrable. The coefficients f_ℓ^q as given by equation (3.85) still exist provided only that f is integrable, and the series S_N^f of equation (3.80) may still be written down. However, the series no longer converges in the mean, but only point by point - and will not converge at, for example, singularities of the function. It is thus no longer valid to write down the exact equation (3.86). Nevertheless S_N^f is still a useful approximation to f, as will be illustrated in Appendix B.

No harmonic expansion exists for functions which are not integrable, because the coefficients are not defined.

3.7.2 Harmonic Expansions of CCSD, Weighting

Spherical harmonic theory provides a new light in which to consider again the problem of the extraction of information from the basic C-I relation (equation (2.14)) between CCSD and plane wave weighting in a free wave field.

The plane wave function $\exp(i\underline{k}.\underline{r})$ is a square integrable function of v,u (and also of θ,ϕ) and has a standard harmonic representation (3.33)

$$\exp(i\underline{k}.\underline{r}) = \sum_{\ell=0}^{\infty} \sum_{q=-\ell}^{\ell} 4\pi i^\ell \, j_\ell(kr) \, Y_\ell^q(\theta,\phi) \, Y_\ell^{q*}(v,u) \qquad (3.87)$$

j_ℓ is the spherical Bessel function of order ℓ.

Suppose that a plane wave weighting I at a given frequency is modelled by a finite sum of N spherical harmonics:

$$I(v,u) \cong S_N^I = \sum_{\ell}^{N} \sum_{q} I_{\ell}^{q} Y_{\ell}^{q}(v,u) \tag{3.88}$$

Substitution of equations (3.87, 3.88) into the C-I relation gives a harmonic expression for C:

$$C(\underline{r}) \simeq S_N^C = \sum_{\ell}^{N} \sum_{q} 2\, I_{\ell}^{q}\, i^{\ell} \cdot j_{\ell}(kr)\, Y_{\ell}^{q}(\theta,\phi) \tag{3.89}$$

Reference (2.30) contains a rigorous statement of some theoretical results about the convergence of the series in equation (3.89). The main conclusion is that provided only that I is integrable (not necessarily square integrable) then C may be approximated by a series of this form, with coefficients given by an integral of the form of equation (3.85). The C series is convergent at every value of kr, and may thus be extended to $N \to \infty$, to an exact representation of C, even when the same is not true of the corresponding I series. The series is thus a very robust representation of C, and is in a sense "more convergent" than the corresponding I series.

A simple special case is that of a diffuse field, whose weighting series has only one non-zero coefficient

$$I_0^0 = \pi^{\frac{1}{2}} \tag{3.90}$$

so that the C series becomes

$$C(\underline{r}) = j_0(kr) = \sin(kr)/kr \tag{3.91}$$

which is Cook's result, equation (2.11).

The pair of equations (3.88,3.89) is basic to the development of a plane wave weighting analysis method. Suppose the weighting I is modelled by a series of the form of equation (3.88) with a fixed set of harmonics and unknown coefficients. Then equation (3.89) gives a prediction for C at any position as a function of the unknown coefficients. The coefficients can then be determined

by comparing the predictions with experimental data on CCSD, and an estimate of I may be constructed.

This basic procedure can be refined by introducing least-square fit methods, and by searching through different sets of harmonics to see which produces the "best" models for a given number of terms. The procedure is flexible because of the great variety of weighting shapes which can be approximated with a small number of harmonics. The procedure is also convergent, because a large enough CCSD data set could yield an arbitrarily large set of estimated coefficients, and so as well converged an approximation to the weighting as desired.

The procedure places no restrictions on the form of the input data set; it will produce results no matter how sparse or irregular the array of sampling positions, though the quality of the results will depend on the nature of the array.

Strictly speaking, this technique is an inductive analysis method, since each fit depends on the adjustment of the values of a small number of parameters in a weighting model of a specified form. However the flexibility introduced by the search procedure and the ability of the technique in principle to produce an arbitrarily good image of any plane wave weighting justified its classification as a "direct" deductive method.

3.7.3 Fundamental Limitations

The power and general applicability of the harmonic analysis technique will make it the focus of attention for the rest of this study. However, the technique does suffer from some fundamental limitations, which stem from the fact that CCSD and weighting must be represented by finite harmonic series, and it is wothwhile to consider these limitations as a background to the application of the technique.

Appendix B is a detailed discussion of some convergence properties of the two series, equations (3.88,3.89). The emphasis of the discussion is on the consequences of limited convergence for a practical harmonic analysis algorithm.

There are three main conclusions. First, the presence of discontinuities and singularities in the plane wave weighting has (as might be anticipated) an adverse effect on convergence. Second, the low-frequency (i.e. low -kr) range of CCSD contains information only about the lowest-order moments of the underlying

weighting, and not about finer details. (This recalls the discussion in subsection (3.3.6).)

Finally, if the rates of convergence of the CCSD and weighting series are compared, it emerges that a weighting series with a given number of terms is in general a worse representation of the true weighting than is the corresponding series for CCSD with the same number of terms. All these results have important practical consequences.

Typical experimental data for CCSD will be restricted to low values of kr because of frequency sampling considerations, and will be subject to a certain amount of statistical estimation error. The fact that the low-kr range of CCSD contains information only about the lowest order harmonic coefficients - even in the absence of measurement errors - means that a harmonic series analysis method could be expected to yield only low order harmonic models of plane wave weightings showing only gross features. Furthermore, a C series tends to be better converged than an I series of a comparable size, so that the variation of estimated harmonic coefficients due to the presence of even a small experimental error in CCSD measurements may have a marked effect on the variance of the resulting weighting models. Well-resolved data will be needed to obtain even a moderately good approximation of the weighting.

3.7.4 Practical Applications

In common with many of the important results considered in this chapter, the basic pair of harmonic series for C,I were given by Cox (2.22). Cox applied the results inductively to show that CCSD functions related to low order harmonic series models of plane wave weightings could be made to fit to measurements made of ambient sea noise fields at various frequencies.

Spherical harmonic expansions were used in the course of the proof by Cron and Sherman (2.20) that the sound field at the centre of a large sphere filled with sources is diffuse. Pierce (3.34) suggested the use of harmonic series to define an index of diffuseness for anisotropic fields. A similar idea was put forward by Ebeling and Freudenstein (3.27).

Bart (3.35) suggested the modelling of an anisotropic free wave field with simple combinations of harmonics, whose coefficients could be determined by measuring correlations with various microphone orientations. The results were used to measure the energy flow towards and away from a piece of carpet; the estimates

of absorption coefficient that Bart thus obtained were consistent with reverberation time measurement results. Makita and Fujiwara (3.36) used Bart's idea in the discussion of the precision of measurements of absorption coefficients in the presence of anisotropic fields.

The application of harmonic series to problems encountered by workers in other fields, such as the study of the angular dependence of planetary magnetic fields, will be described in Chapter 4.

3.8 CONCLUSIONS

The framework of this chapter has been a review of methods to obtain information about the plane wave weighting of a free wave field from CCSD measurements made in the field. A series of methods requiring progressively less restrictions on the quality of the input data was presented, finishing with the harmonic series method which is capable of extracting weighting information from input data limited to a sparse, irregular array of sampling positions.

Of all the methods reviewed, the harmonic series method is the least demanding in terms of the quality of its input data, and would therefore be expected to be the most widely applicable. In the next chapter, we will focus our attention on a harmonic series free wave field analysis method, and develop the ideas presented in this chapter into a practical algorithm.

REFERENCES

3.1 LUBMAN, D., Journal of the Acoustical Society of America 46, 532-534 (1969). Spatial averaging in a diffuse sound field.

3.2 WATERHOUSE, R. and LUBMAN, D., Journal of the Acoustical Society of America 48, 1-5 (1970). Discrete versus continuous space averaging in a reverberant sound field.

3.3 WATERHOUSE, R., Journal of the Acoustical Society of America 43, 1436-1443 (1968). Statistical properties of reverberant sound fields.

3.4 SCHROEDER, M., Journal of the Acoustical Society of America 46, 277-283 (1969). Effect of frequency and space averaging on the transmission responses of multimode media.

3.5 LUBMAN, D., WATERHOUSE, R. and CHIEN, C.-S., Journal of the Acoustical Society of America 53, 650-659 (1973). Effectiveness of continuous spatial averaging in a diffuse sound field.

3.6 CHIEN, C.-S., WATERHOUSE, W. and LUBMAN, D., Journal of the Acoustical Society of America 57, 972-975 (1975). Spherical averaging in a diffuse sound field.

3.7 BROADHURST, A.D., Acustica 43, 188-196 (1979). The application of the acoustic telescope in architectural acoustics.

3.8 BROADHURST, A.D., Acustica 46, 299-310 (1980). An acoustic telescope for architectural acoustic measurements.

3.9 BROADHURST, A.D., Acustica 50, 33-38 (1982). Sparse volume array for architectural acoustic measurements.

3.10 SCHULTZ, T.J., Journal of Sound and Vibration 16, 17-28 (1971). Diffusion in reverberation rooms.

3.11 BALACHANDRAN, C.G. and ROBINSON, D.W., Acustica 19, 245-257 (1968). Diffusion of the decaying sound field.

3.12 PISAREVSKII, N.N., Soviet Physics-Acoustics 10, 323-325. Isocorrelation curves as characteristics of the sound field in reverberation chambers.

3.13 BALACHANDRAN, C.G., Journal of the Acoustical Society of America 31, 1319-1321 (1959). Random sound field in reverberation chambers.

3.14 BODLUND, R., Journal of Sound and Vibration 44, 191-207 (1976). A new quantity for comparative measurements concerning the diffusion of stationary sound fields.

3.15 KOYASU, M. and YAMASHTA, M., Acoustical Journal of Japan 26, 132-143 (1971). Evaluation of the degree of diffuseness in reverberation chambers by spatial correlation techniques. (In Japanese.)

3.16 CRON, B.F., HASSELL, B.C. and KELTONIC, F.J., Journal of the Acoustical Society of America 37, 523-529 (1965). Comparison of theoretical and experimental values of spatial correlation.

3.17 REIN, C.R., Journal of the Acoustical Society of America 50, 321-325 (1971). Vertical cross-correlation of noise from a horizontal surface.

3.18 LINNETTE, H.M. and THOMPSON, R.J., Journal of the Acoustical Society of America 36, 1788-1794 (1964). Directivity study of the noise field in the ocean, employing a correlative dipole.

3.19 KURYANOV, B.F., Soviet Physics-Acoustics 9, 360-364 (1964). Spatial correlation of fields emitted by random sources on a plane.

3.20 LIGGETT, W.S. and JACOBSON, M.J., Journal of the Acoustical Society of America 38, 303-312 (1965). Covariance of surface-generated noise in a deep ocean.

3.21 LIGGETT, W.S. and JACOBSON, M.J., Journal of the Acoustical Society of America 39, 280-288 (1966). Noise covariance and vertical directivity in a deep ocean.

3.22 TALHAM, R.J., Journal of the Acoustical Society of America 69, 213-215 (1981). Noise correlation functions for anisotropic noise fields.

3.23 PIERSOL, A.G., Journal of Sound and Vibration 56, 215-228 (1978). Use of coherence and phase data between two receivers in evaluation of noise environments.

3.24 BLAKE, W.R. and WATERHOUSE, R., Journal of Sound and Vibration 54, 589-599 (1977). The use of cross-spectral density measurements in partially reverberant sound fields.

3.25 DAMMIG, P., Acustica 7, 387-398 (1957). Zur messung der diffusitat von schallfeldern durch korrelation.

3.26 FREUDENSTEIN, K. and EBELING, K.J., "Fortschritte der Akustik, FASE/DAGA '82" 199 (1982). Messung von schallrichtungsverteilungen und absorptionsgradbestimmung im hallraum.

3.27 EBELING, K.J. and FREUDENSTEIN, K., "Fortschritte der Akustik, FASE/DATA '82", 203 (1982). Determination of spatial diffusivity of sound fields in rooms.

3.28 TOHYAMA, M., SUZUKI, A. and YOSHIKAWA, S., Acustica 39, S1-S3 (1977). Correlation coefficients in a rectangular reverberant room.

3.29 TOHYAMA, M., SUZUKI, A. and YOSHIKAWA, S., Acustica 42, 184-186 (1979). Correlation coefficients in a rectangular reverberant room - experimental results.

3.30 GORSKAYA, N.V., KUSTOV, L.M., NIKOLAEV, G.N., and SALIN, B.M., Soviet Physics - Acoustics 27, 52-54 (1981). A method of investigating the mode structure of the field of an acoustic waveguide in model situations.

3.31 LUBMAN, D., Journal of the Acoustical Society of America 56, 1302-1304 (1974). Traversing microphone spectroscopy as a means of assessing diffusion.

3.32 JEFFREYS, H. and JEFFREYS, B., Methods of Mathematical Physics. Cambridge University Press, London (1972).

3.33 WYLD, H.W., Mathematical Methods for Physics. Benjamin, Inc., Mass. (1976).

3.34 PIERCE, A.D., Journal of the Acoustical Society of America 56, 1304-1305 (1974). Concept of a directional spectral energy density in room acoustics.

3.35 BART, G.C.J., Acustica 28, 45-49 (1973). Spatial cross-correlation in anisotropic sound fields.

3.36 MAKITA, Y. and FUJIWARA, K., Acustica 39, 331-335 (1978). Effects on precision of a reverberant absorption coefficient of a plane absorber due to anisotropy of sound energy flow in a reverberant room.

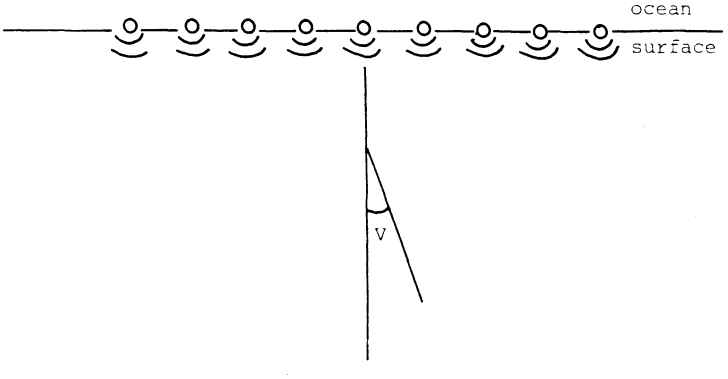

Figure 3.1 Generation of ambient sea noise by a surface distribution of sources.

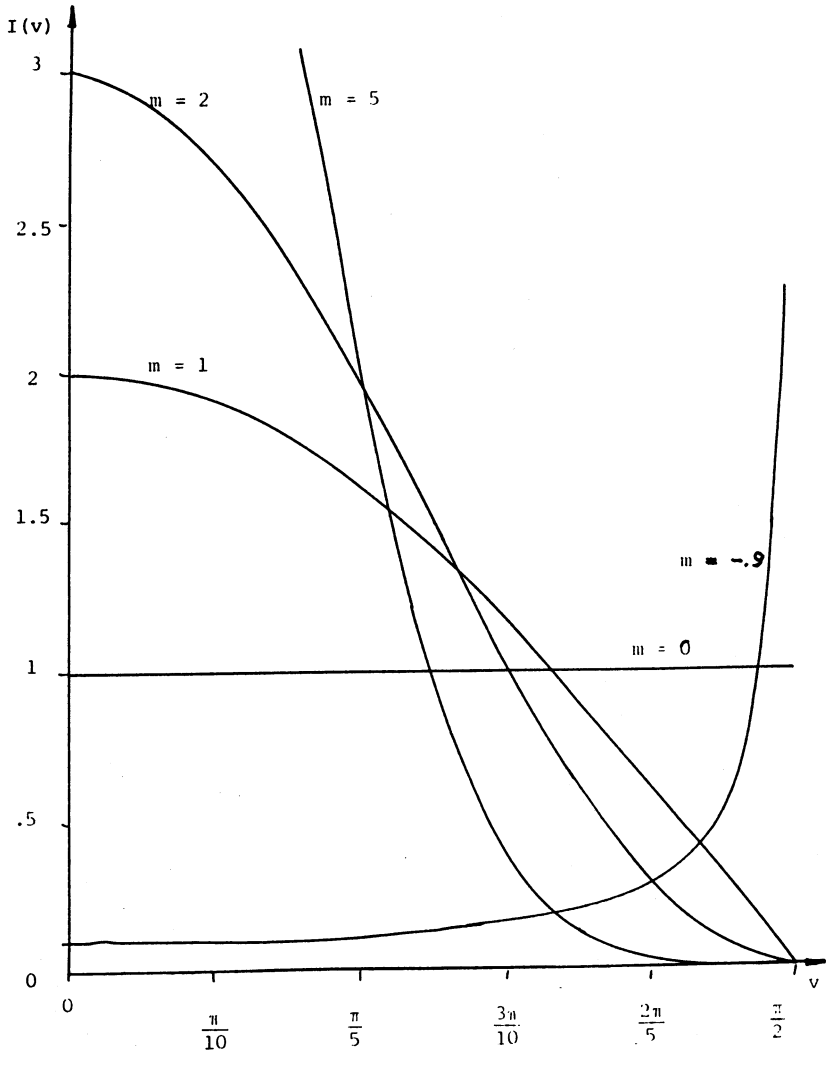

Figure 3.2 Members of the cosine-power family of plane wave weightings. $I(v) = (m+1)\cos^m v$, $0 \leq v \leq \pi/2$.

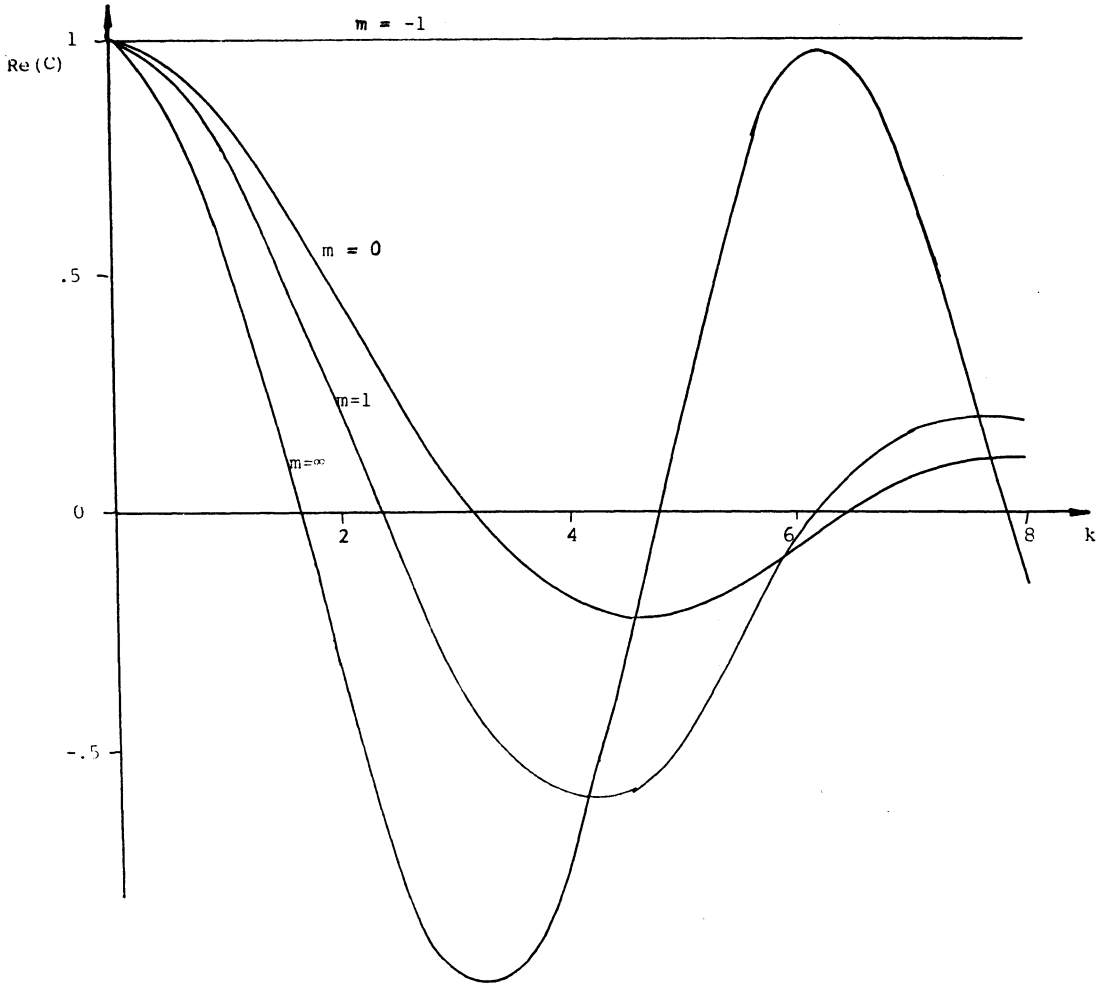

Figure 3.3(a) Axial CCSD for cosine-power fields (real part).

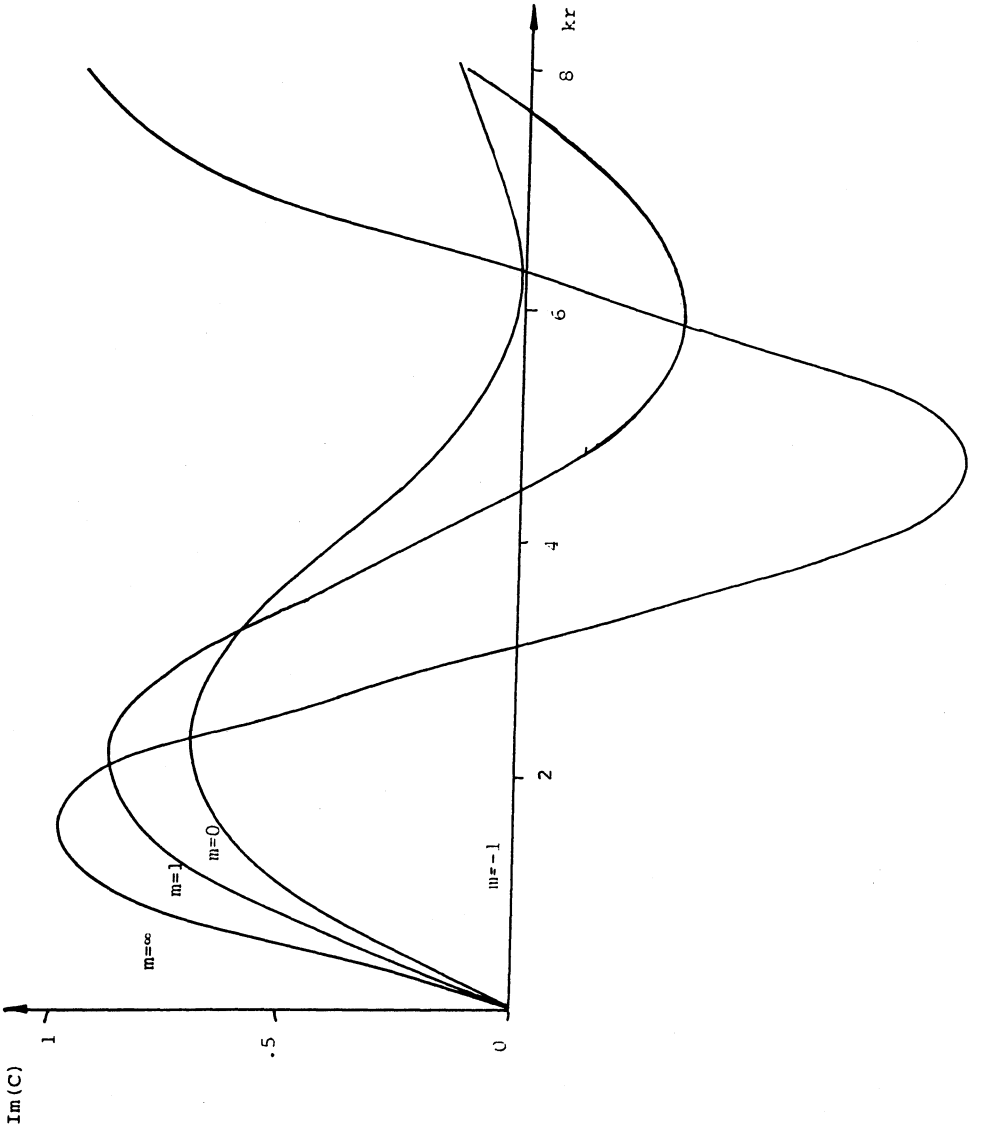

Figure 3.3(b) Axial CCSD for cosine-power fields. (Imaginary part).

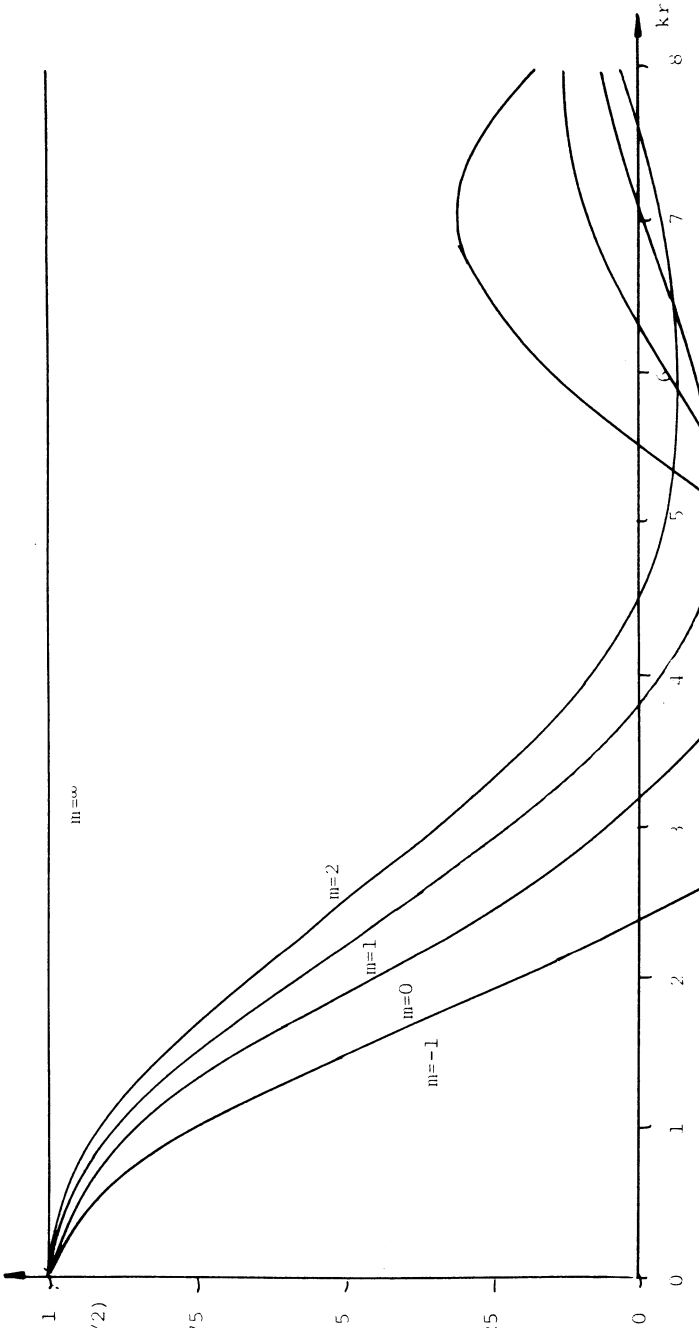

Figure 3.3(c) Cross-sectional CCSD in cosine-power fields. (In this case the QCSD is purely real).

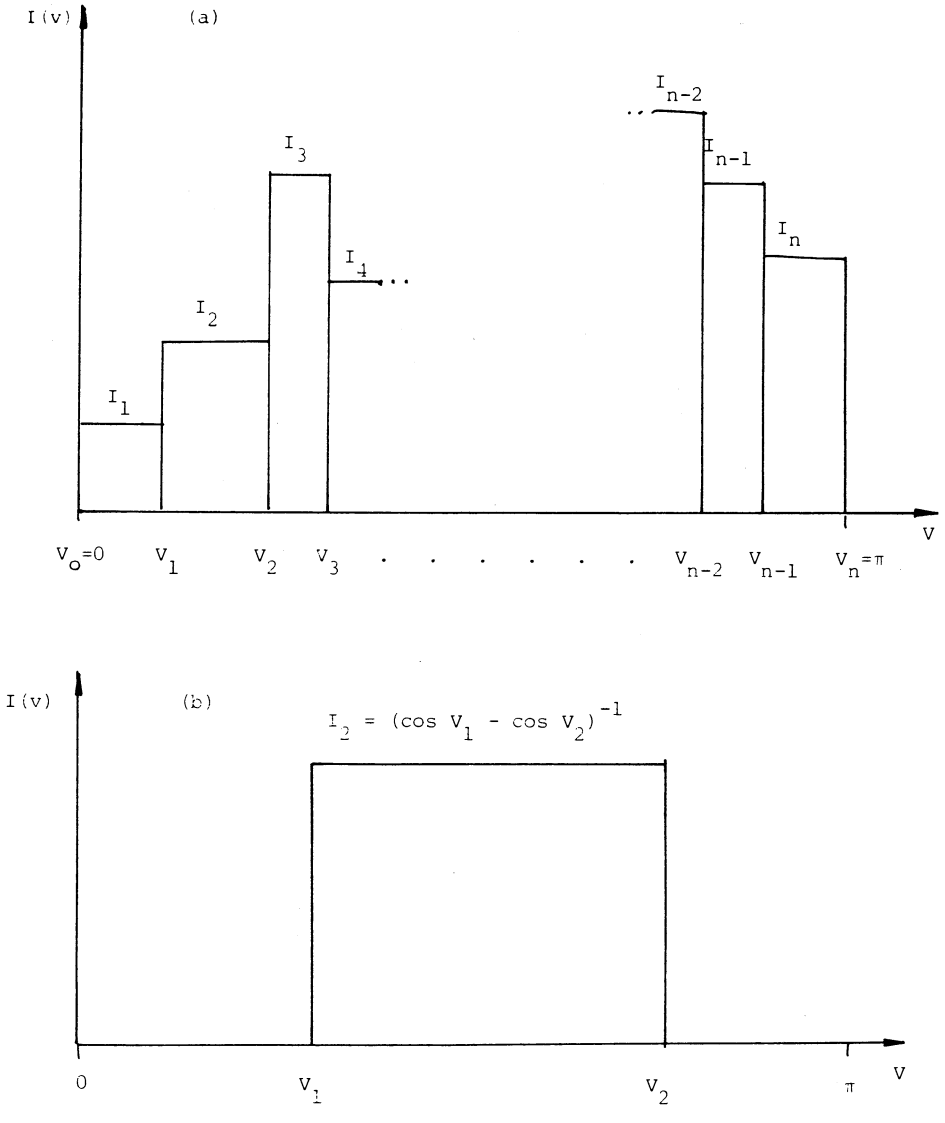

Figure 3.4 Strip function plane wave weighting. (a) General weighting. (b) Partially reverberant field weighting.

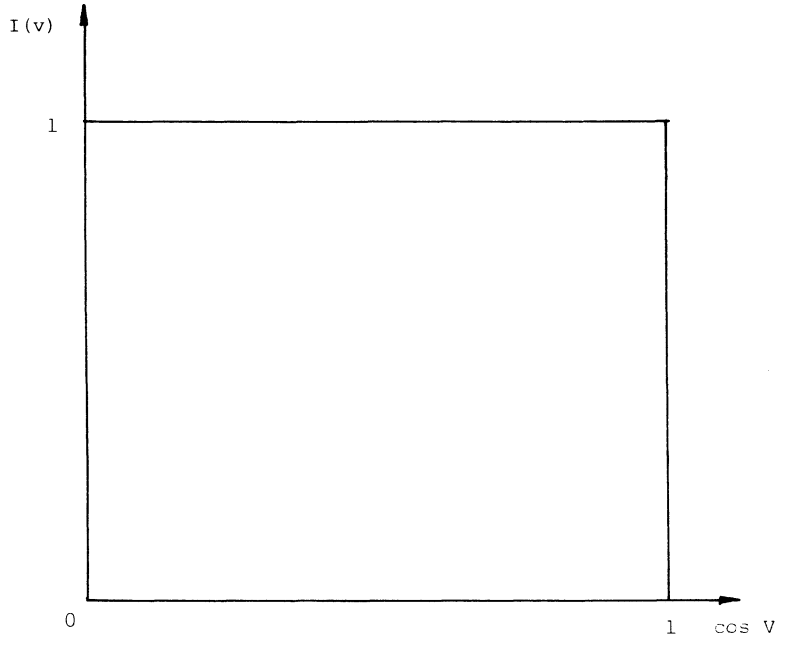

Figure 3.5(a) Strip function weighting:semidiffuse field.

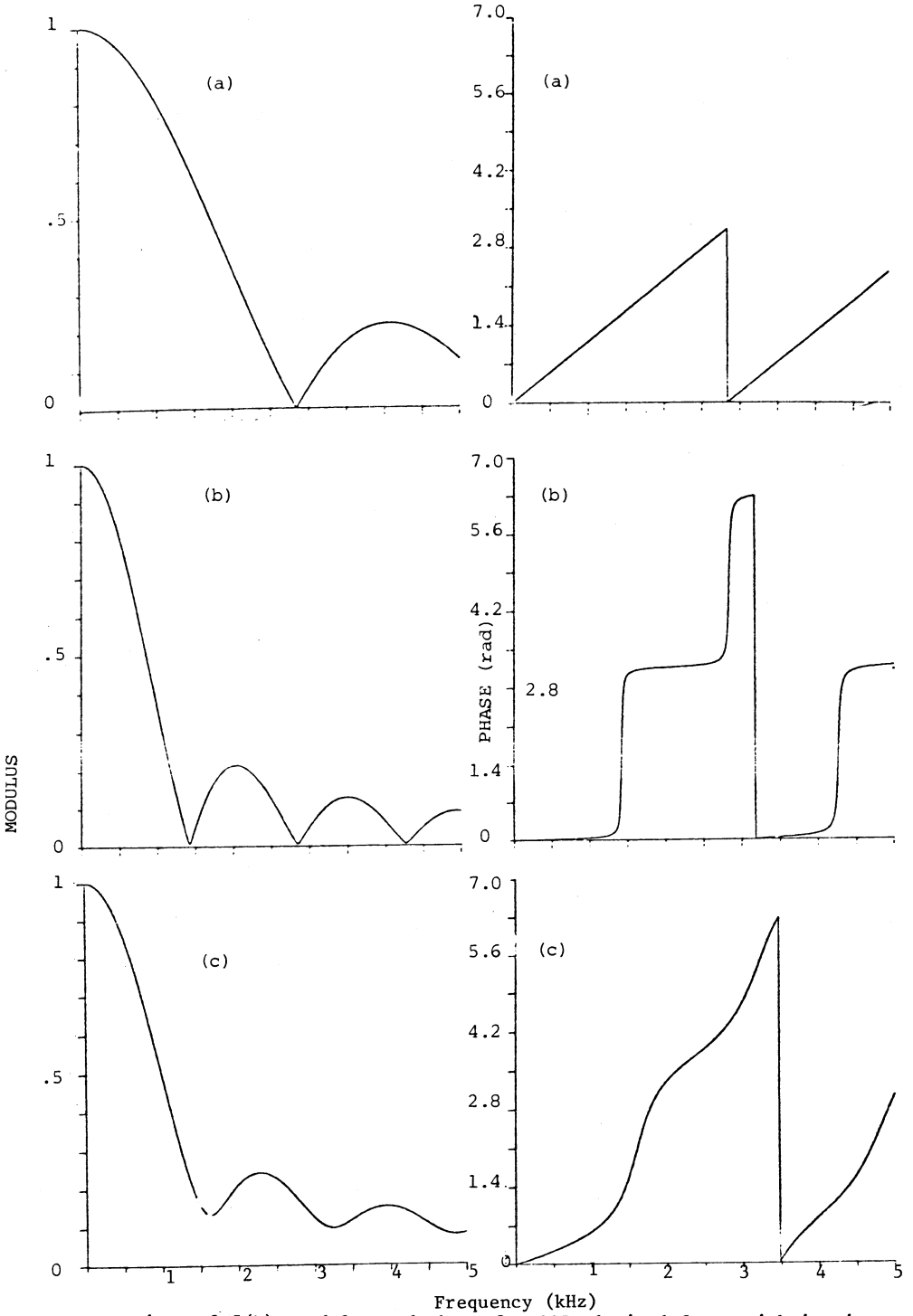

Figure 3.5(b) Modulus and phase for CCSD derived from weighting in Figure 4.5(a); CCSD taken at (a) r = 12 cm, θ = 0; (b) r = 12 cm, θ = $\pi/2$; (c) r = 11.4 cm, θ = 1.1.

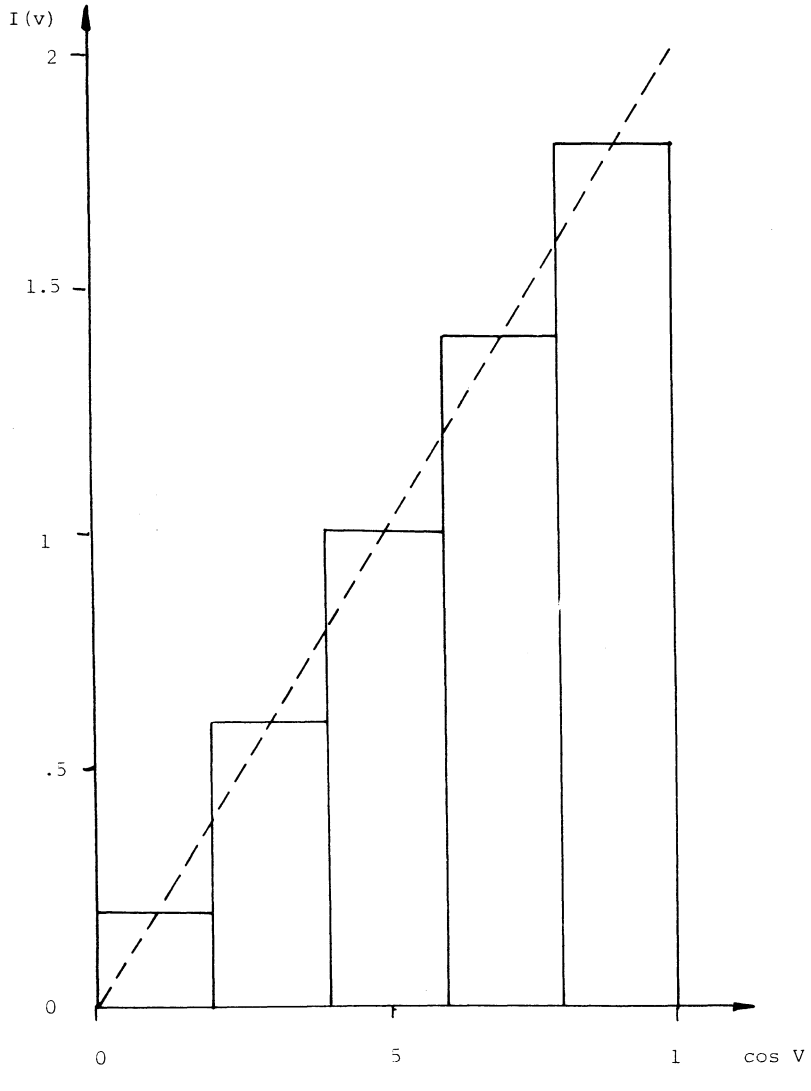

Figure 3.6(a) Strip function weighting: 6-strip model of linear weighting (- - -).

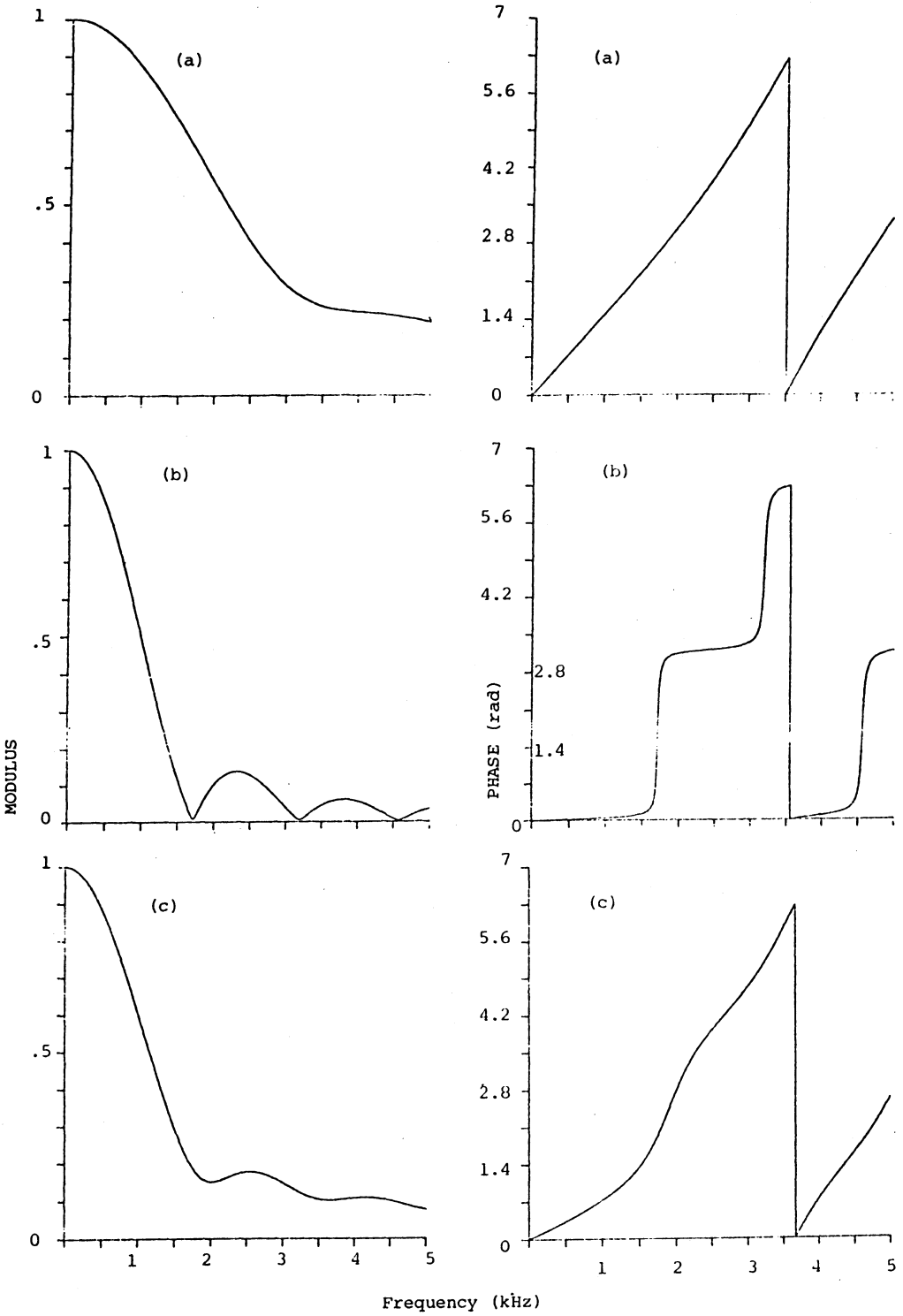

Figure 3.6(b) CCSD. See caption Figure 3.5(b)

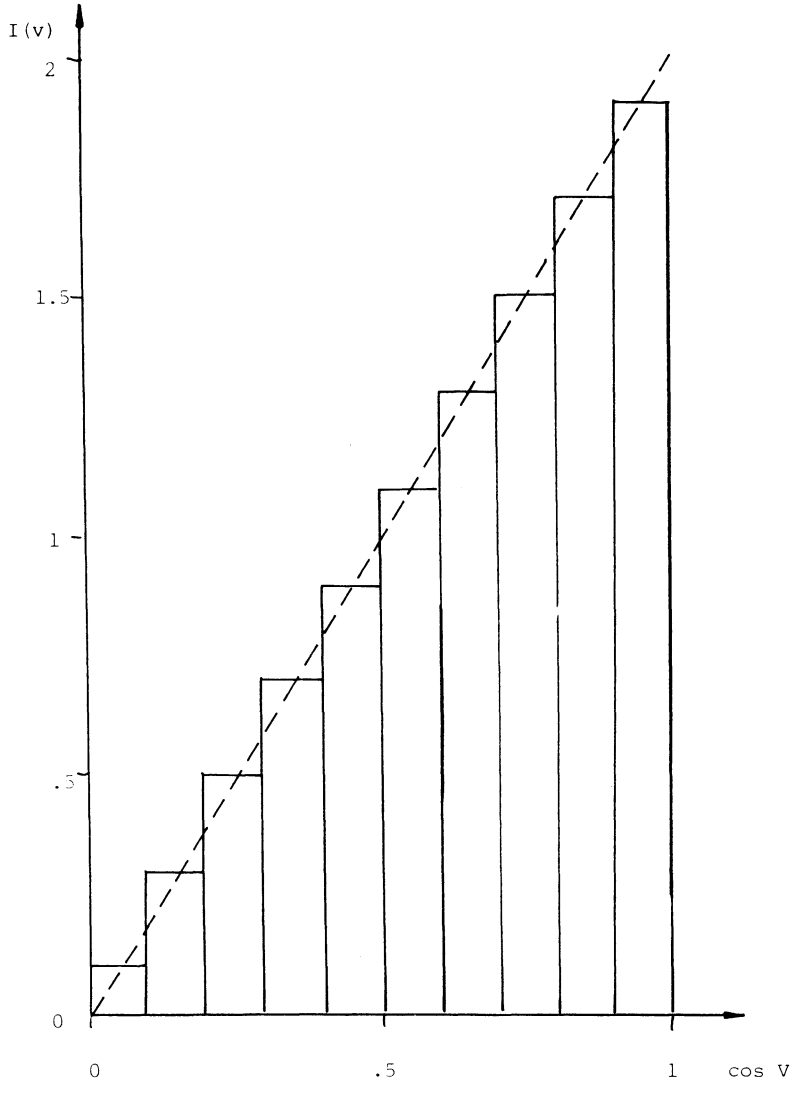

Figure 3.7(a) Strip function weighting: 11-strip model of linear weighting (- - -).

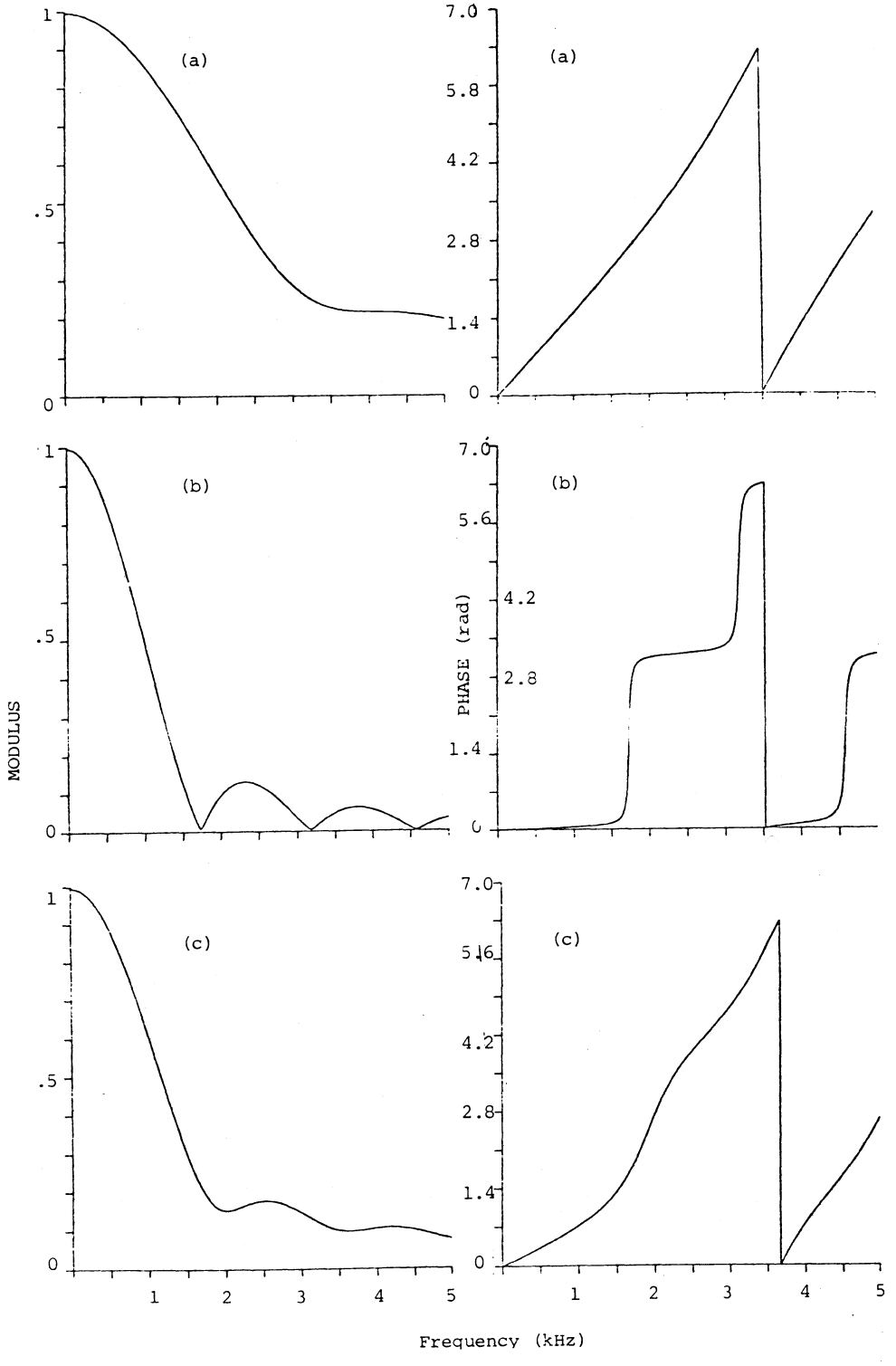

Figure 3.7(b) CCSD. See caption for Figure 3.5(b).

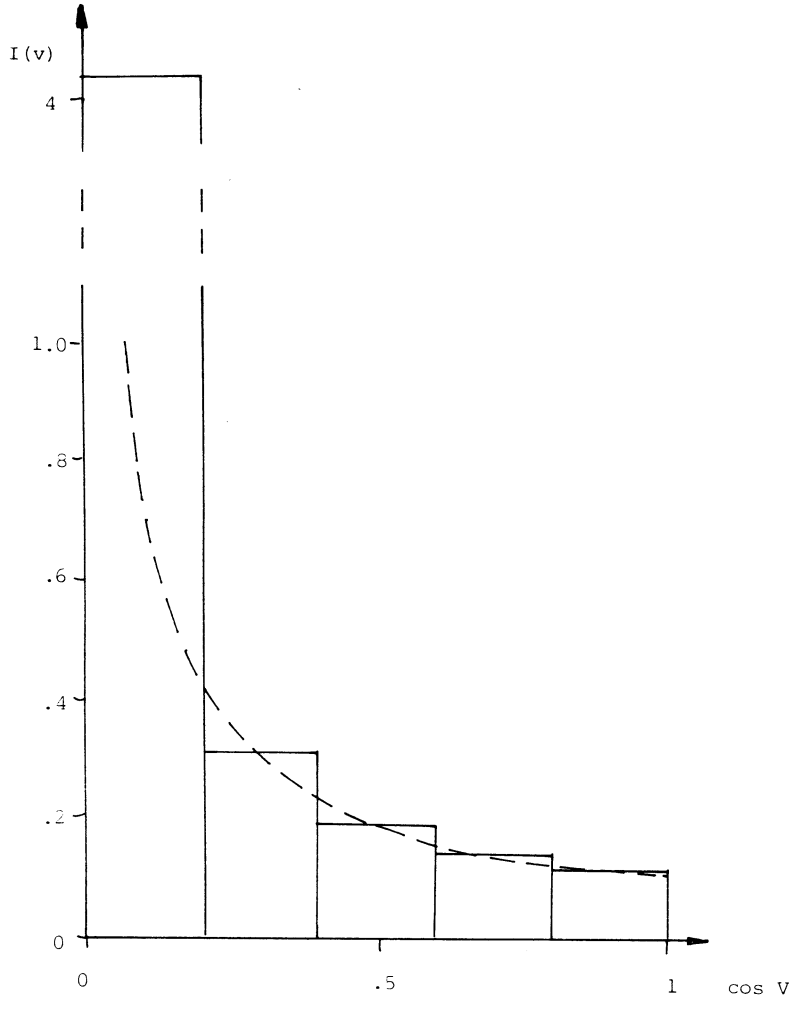

Figure 3.8(a) Strip function weighting: 6-strip model of cosine-power weighting, m = -0.9 (- - -).

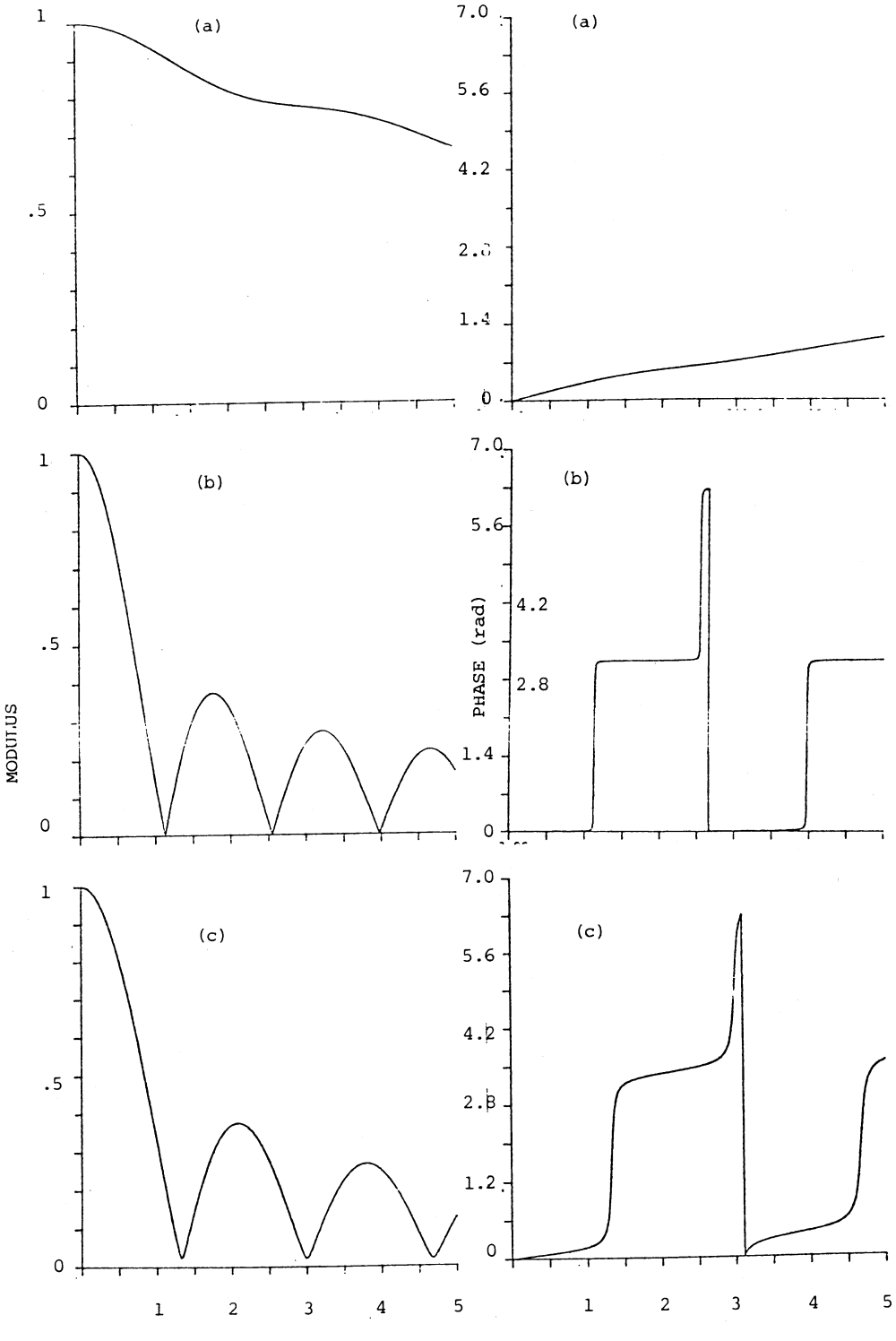

Figure 3.8(b) CCSD. See caption for Figure 3.5(b).

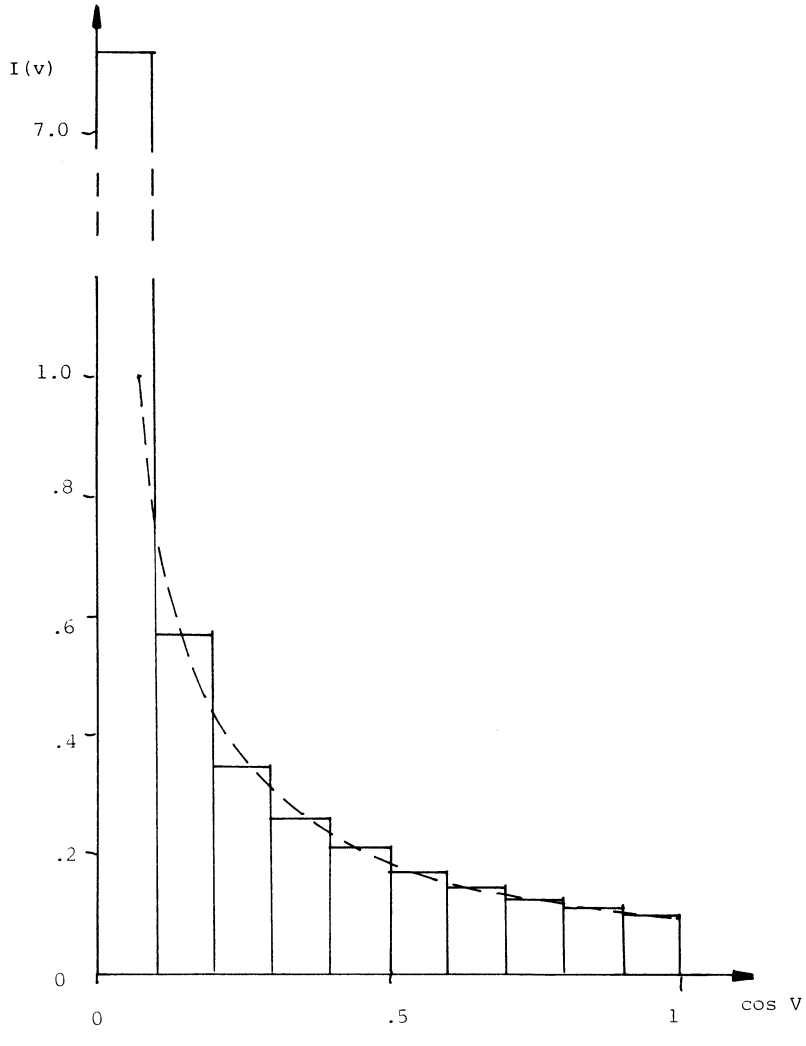

Figure 3.9(a) Strip function weighting: 11-strip model of cosine-power weighting, m = -0.9 (- - -).

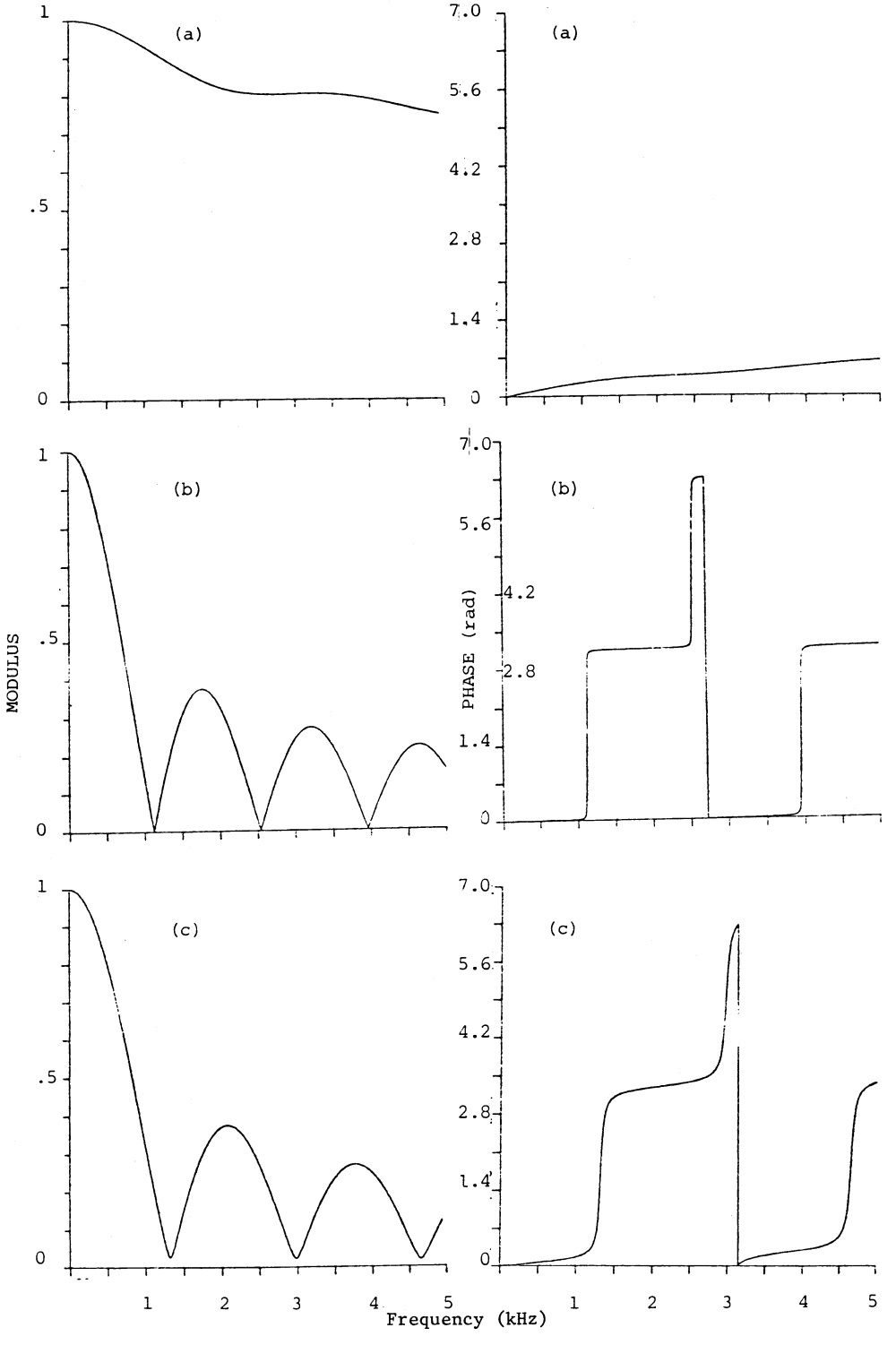

Figure 3.9(b) CCSD. See caption for Figure (3.5(b).

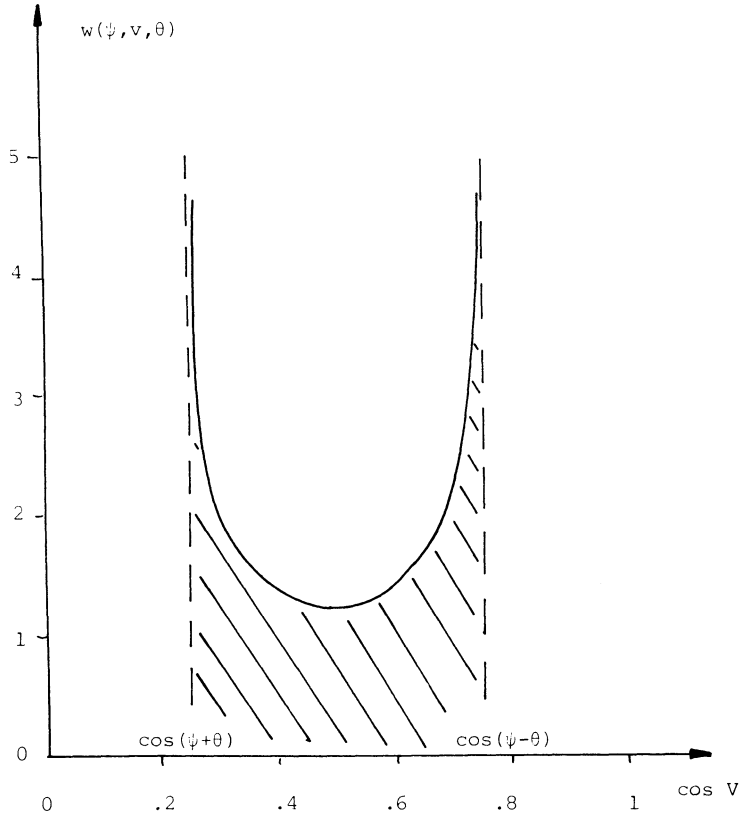

Figure 3.10 Window factor $w(\psi,v,\theta)$. The shaded area is unit for all ψ, θ.

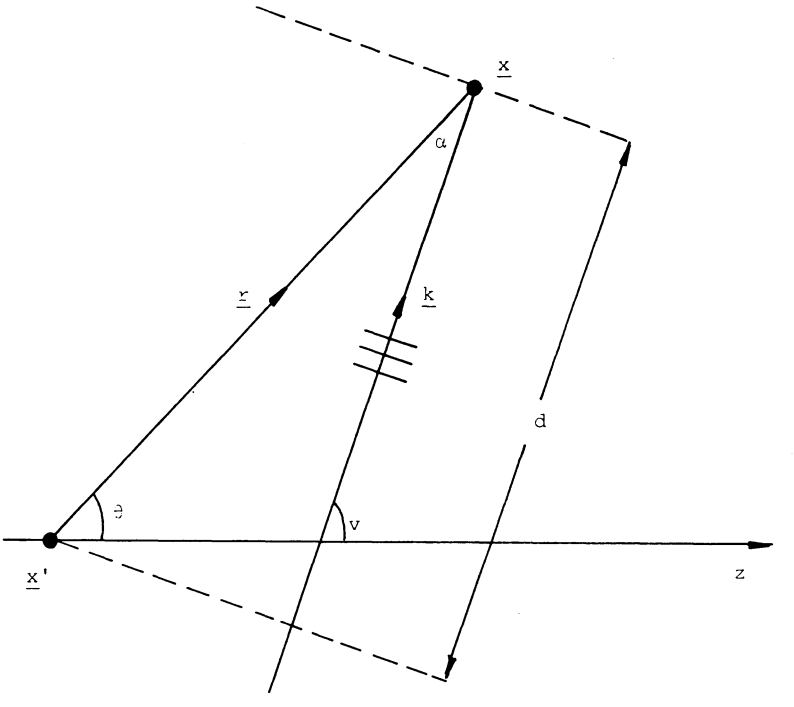

Figure 3.11 The figure shows wavefronts (- - -) travelling from microphone $\underline{x}'$ to microphone $\underline{x}$. Angle α is $v - \theta$. The distance travelled by the wavefronts is $d = |r \cos \alpha| = r|\cos (v - \theta)|$.

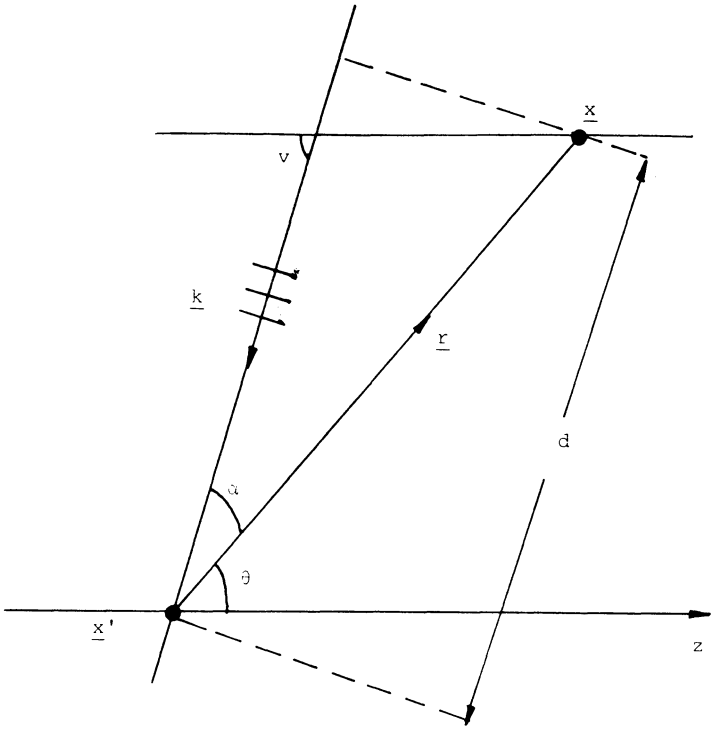

Figure 3.12 This figure shows wavefronts travelling from $\underline{x}$ to $\underline{x}'$; angle α is $\pi-v-\theta$, so the distance travelled by the wavefronts is $d = |r \cos \alpha| = r|\cos(\pi-v-\theta)| = r|\cos(v+\theta)|$.

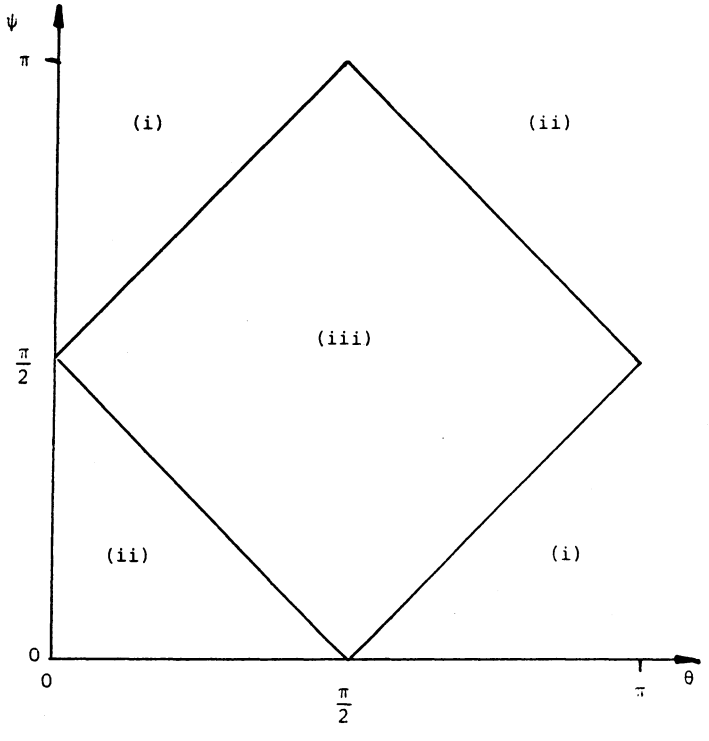

Figure 3.13 The (θ,ψ) plane used to define wavenumber spectra in a semidiffuse field.

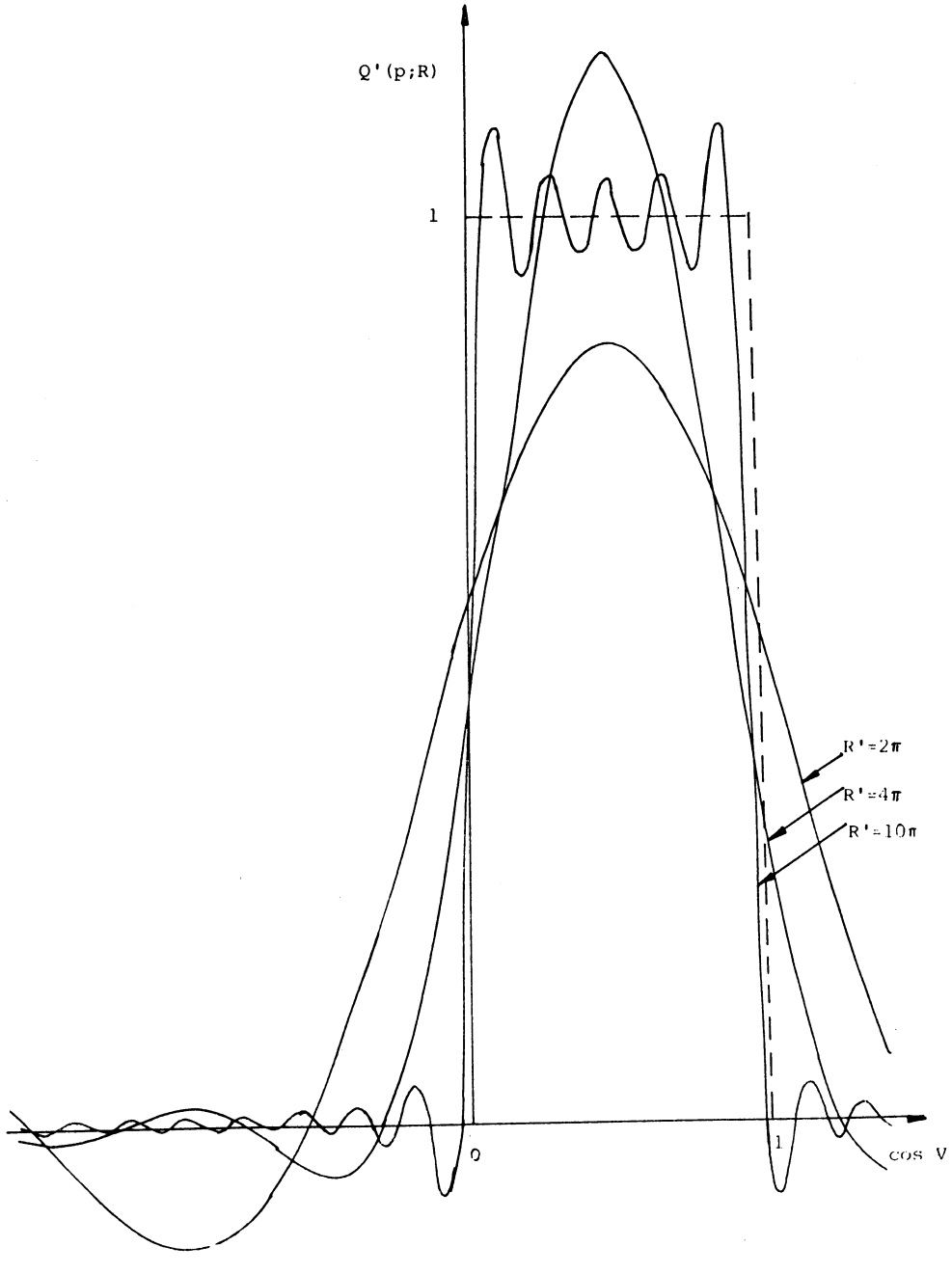

Figure 3.14 Truncated estimates of axial wavenumber spectrum Q'(p,R) in semidiffuse field. - - - true weighting.

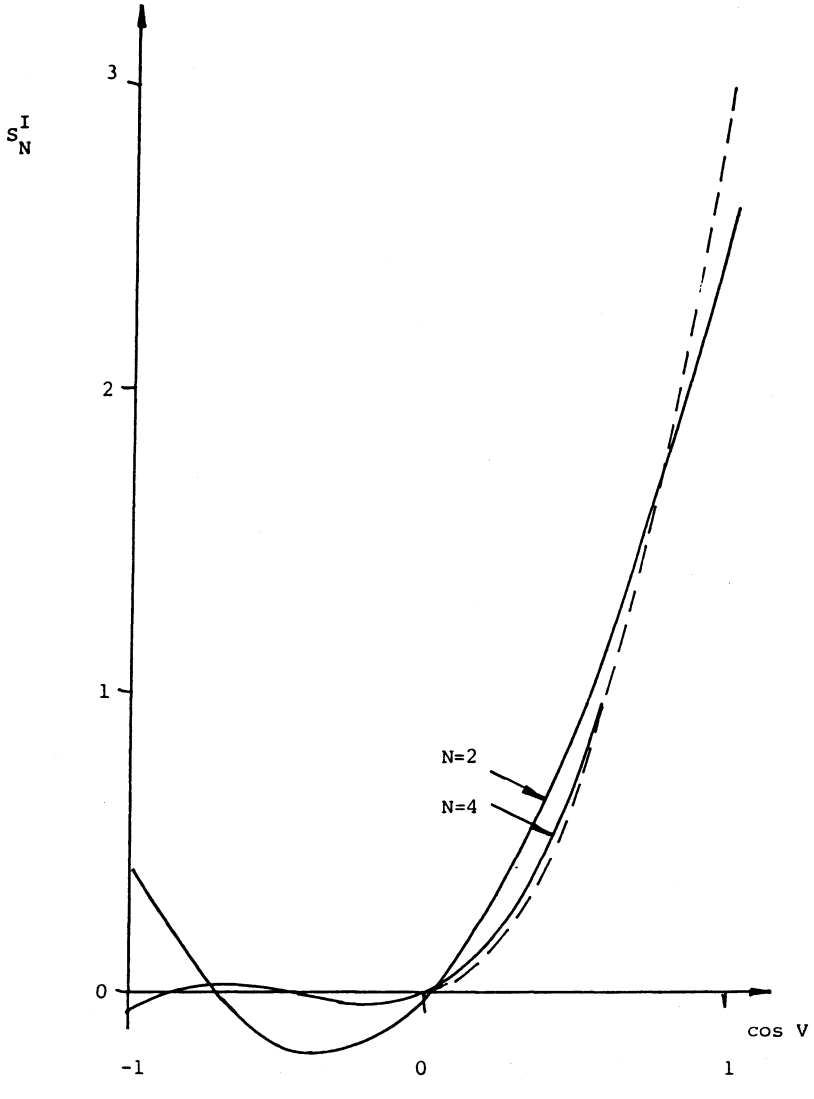

Figure 3.15 Spherical harmonic approximation to cosine-power weighting, m = 2. - - - true weighting.

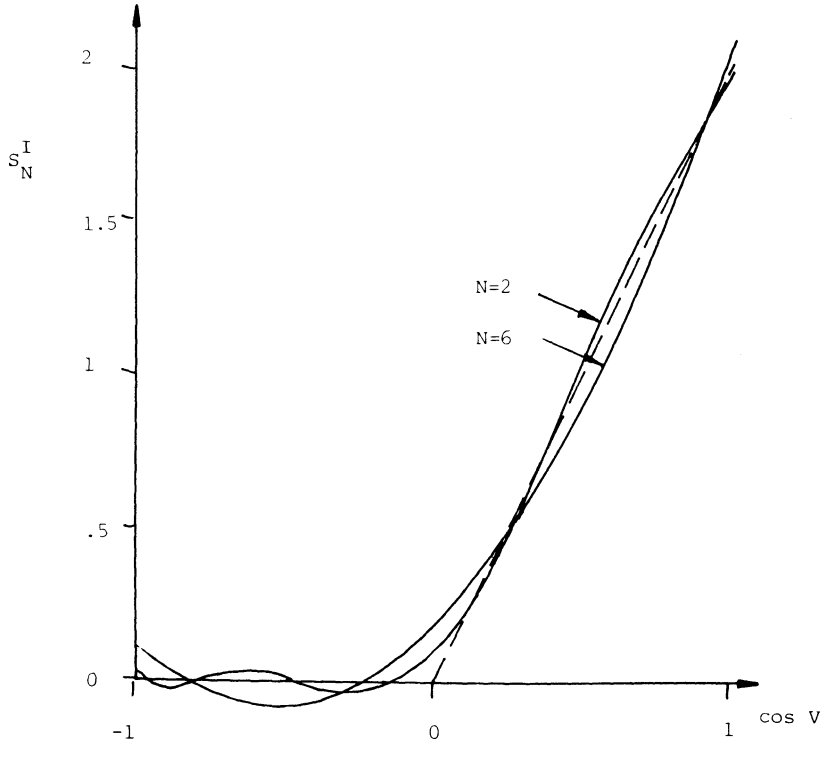

Figure 3.16 Spherical harmonic approximation to cosine-power weighting, m = 1. - - - true weighting.

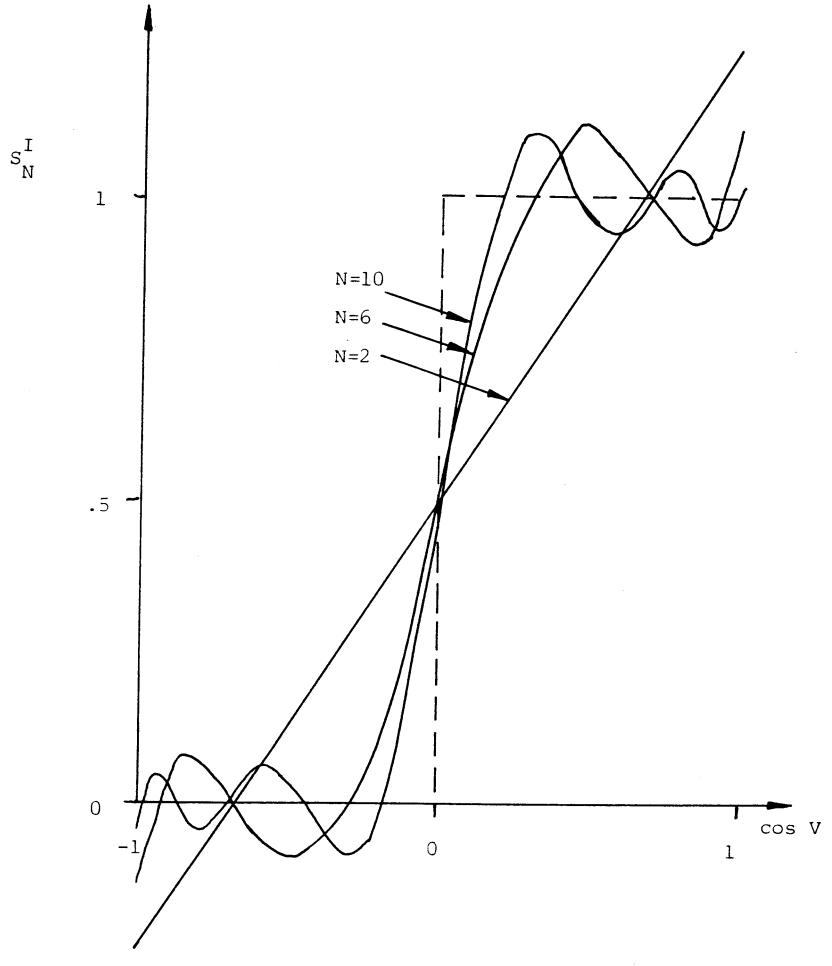

Figure 3.17 Spherical harmonic approximation to semidiffuse field weighting. - - - true weighting.

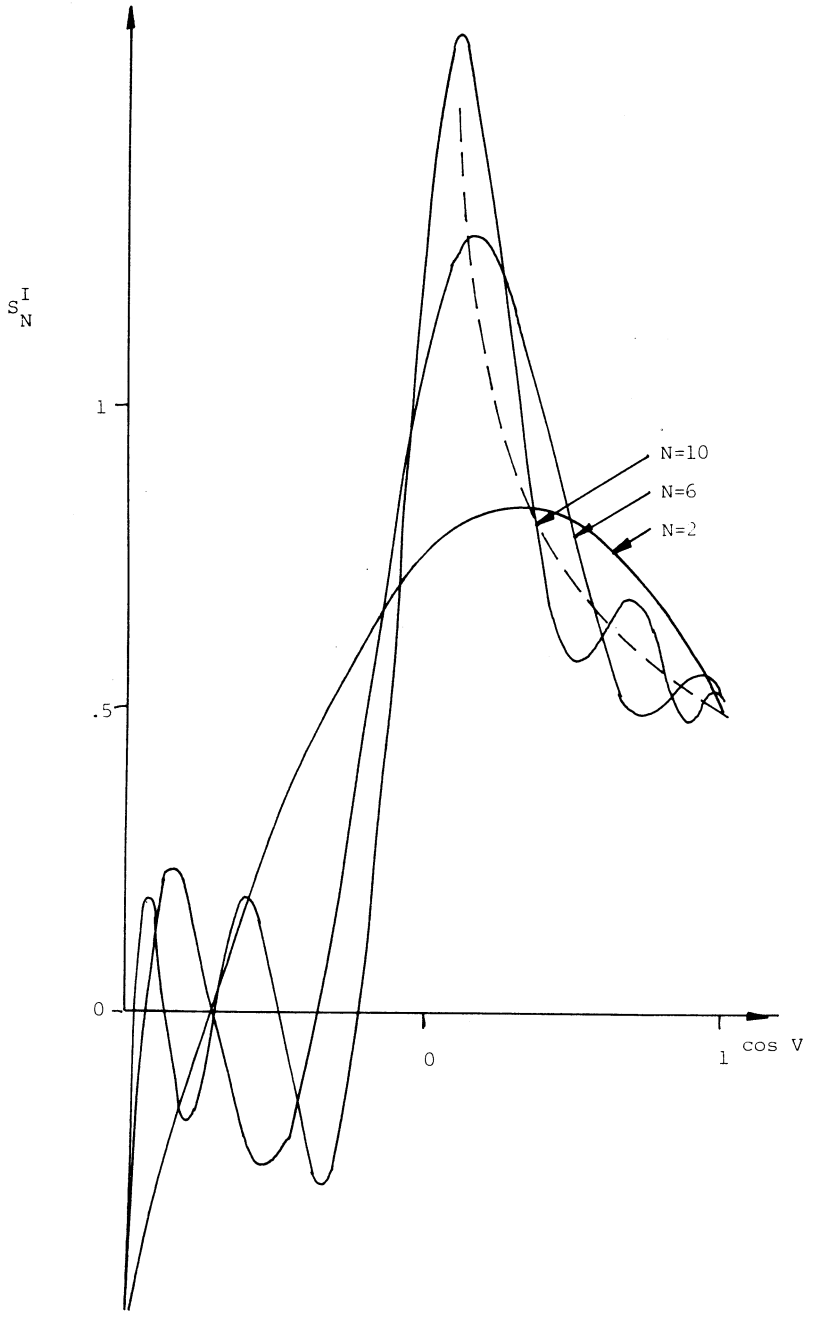

Figure 3.18 Spherical harmonic approximation to cosine-power weighting, m = $-\frac{1}{2}$. - - - true weighting.

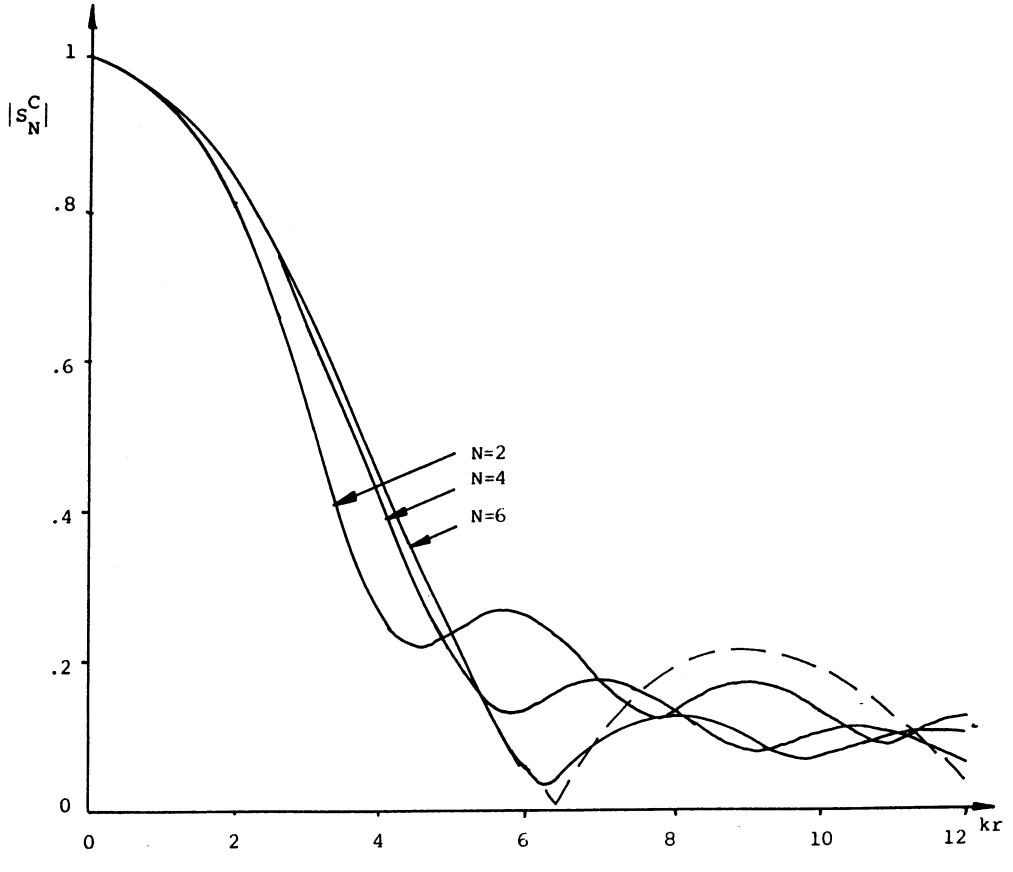

Figure 3.19(a) Spherical harmonic approximation to axial CCSD in semidiffuse field (modulus). - - - true weighting.

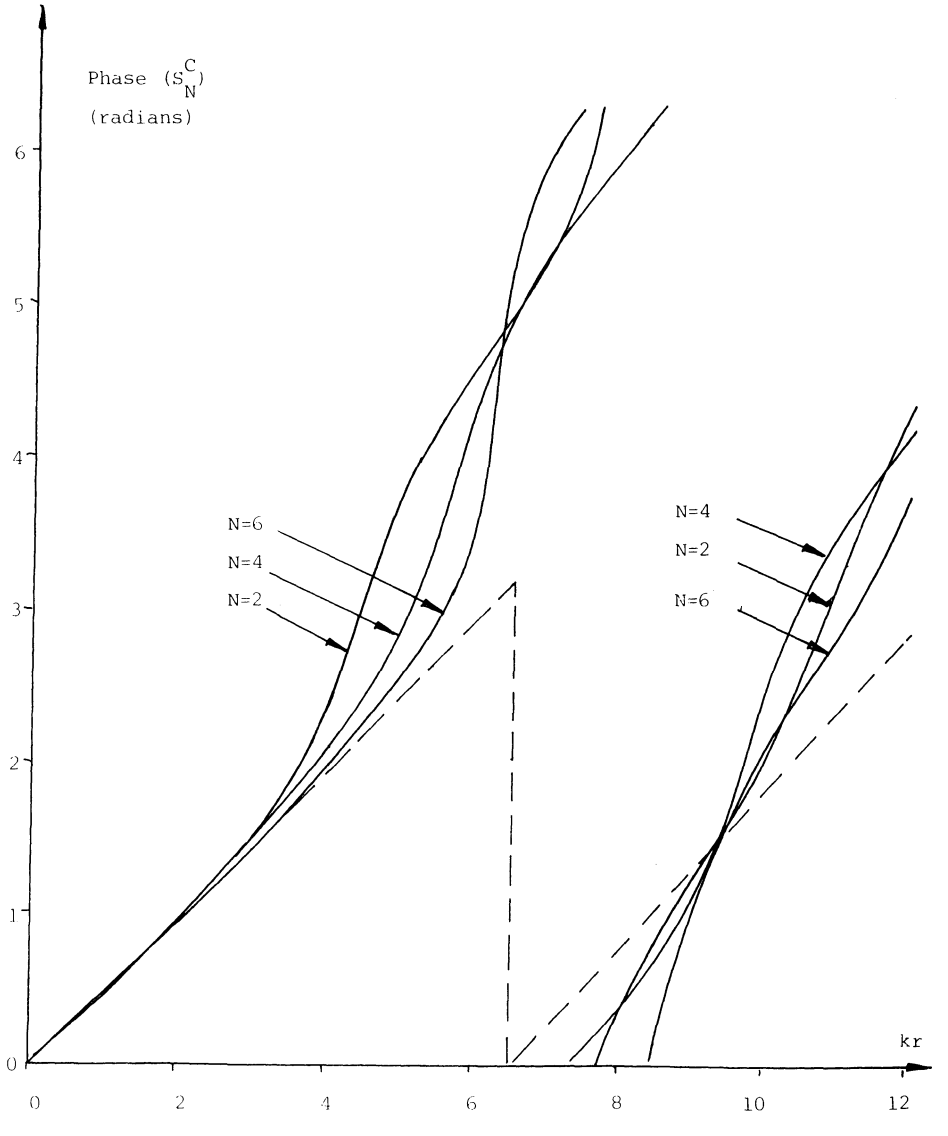

Figure 3.19(b) Spherical harmonic approximation to axial CCSD in semidiffuse field (phase). - - - true weighting

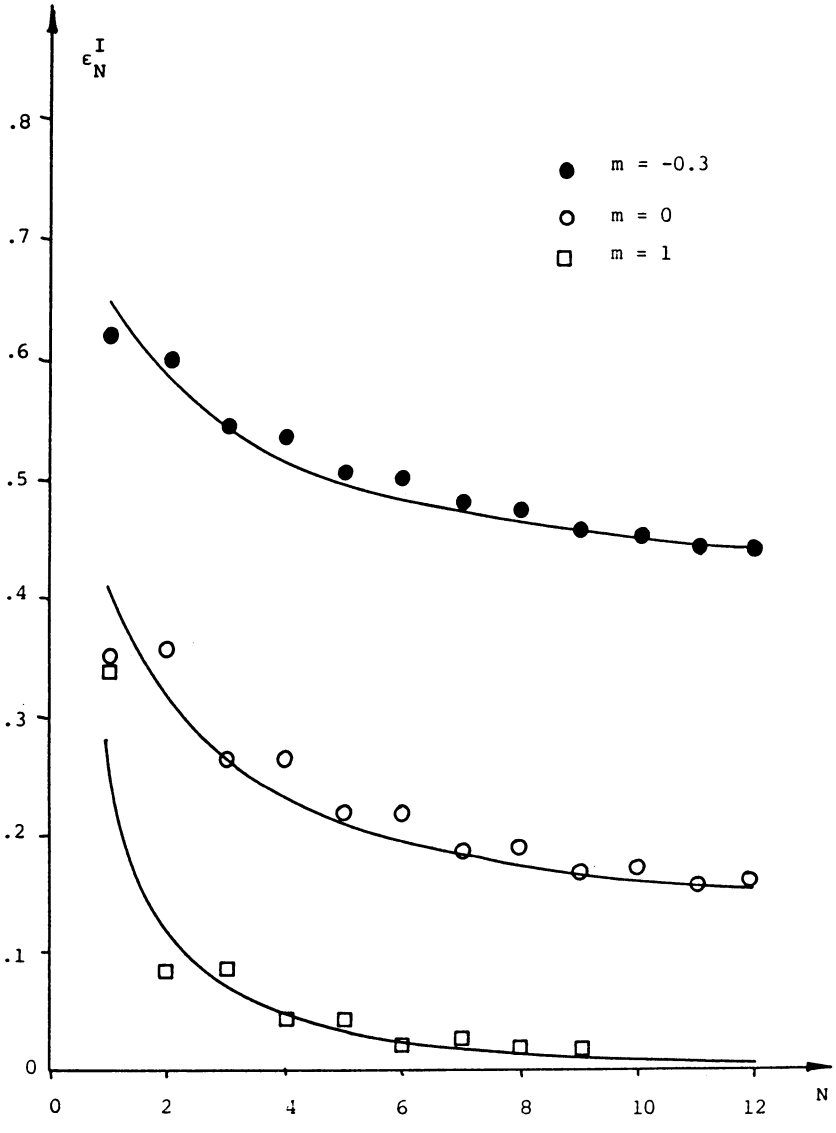

Figure 3.20 Convergence of harmonic series for plane wave weighting, various cosine-power fields.

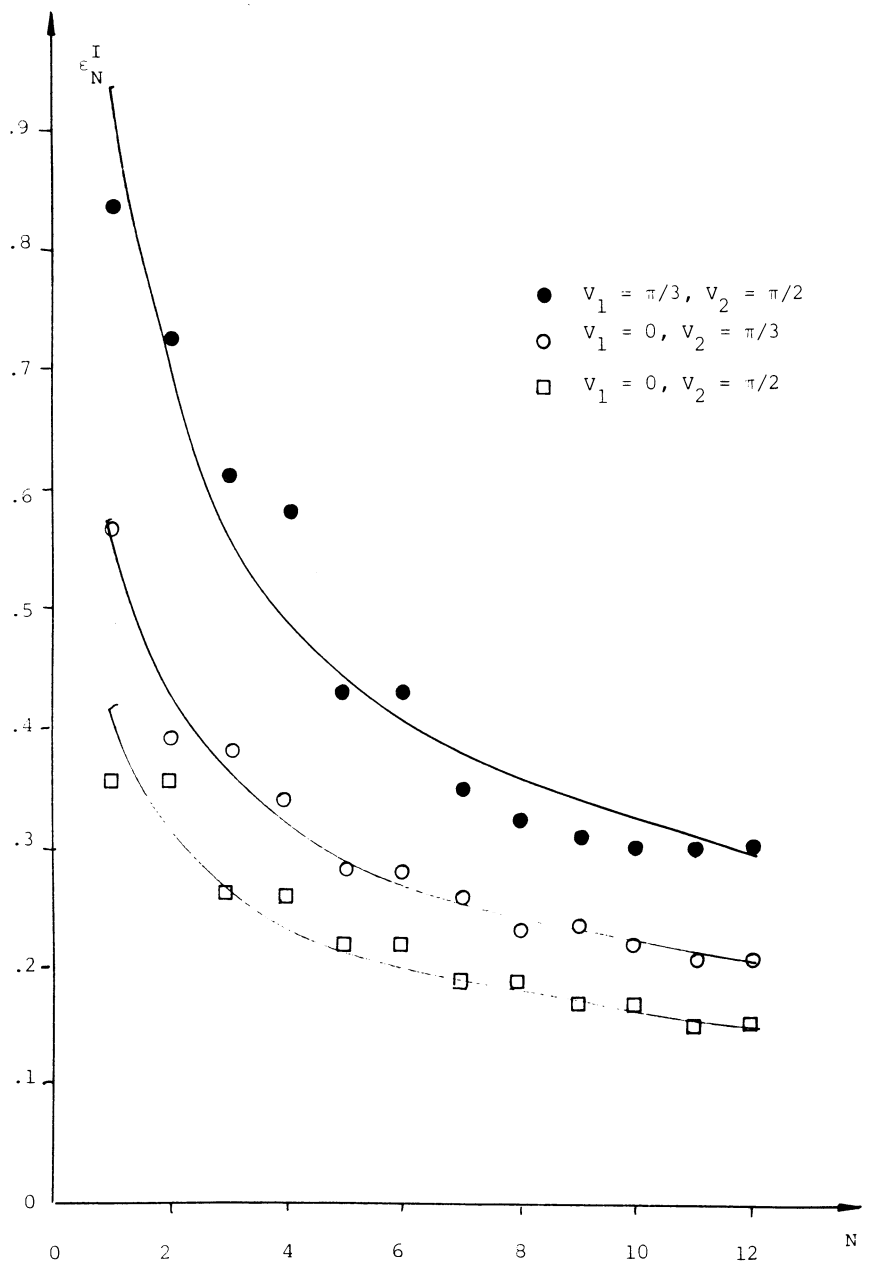

Figure 3.21 Convergence of harmonic series for plane wave weighting; various partially reverberant fields.

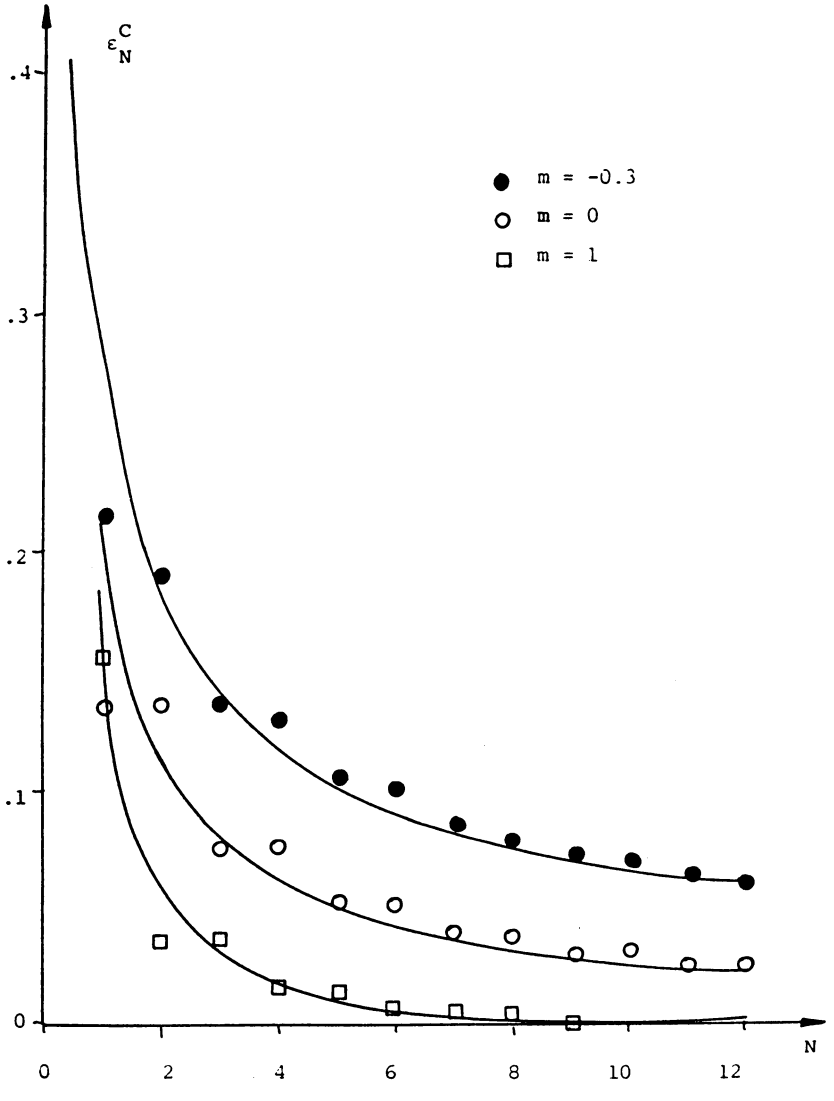

Figure 3.22 Convergence of harmonic series for CCSD, various cosine-power fields.

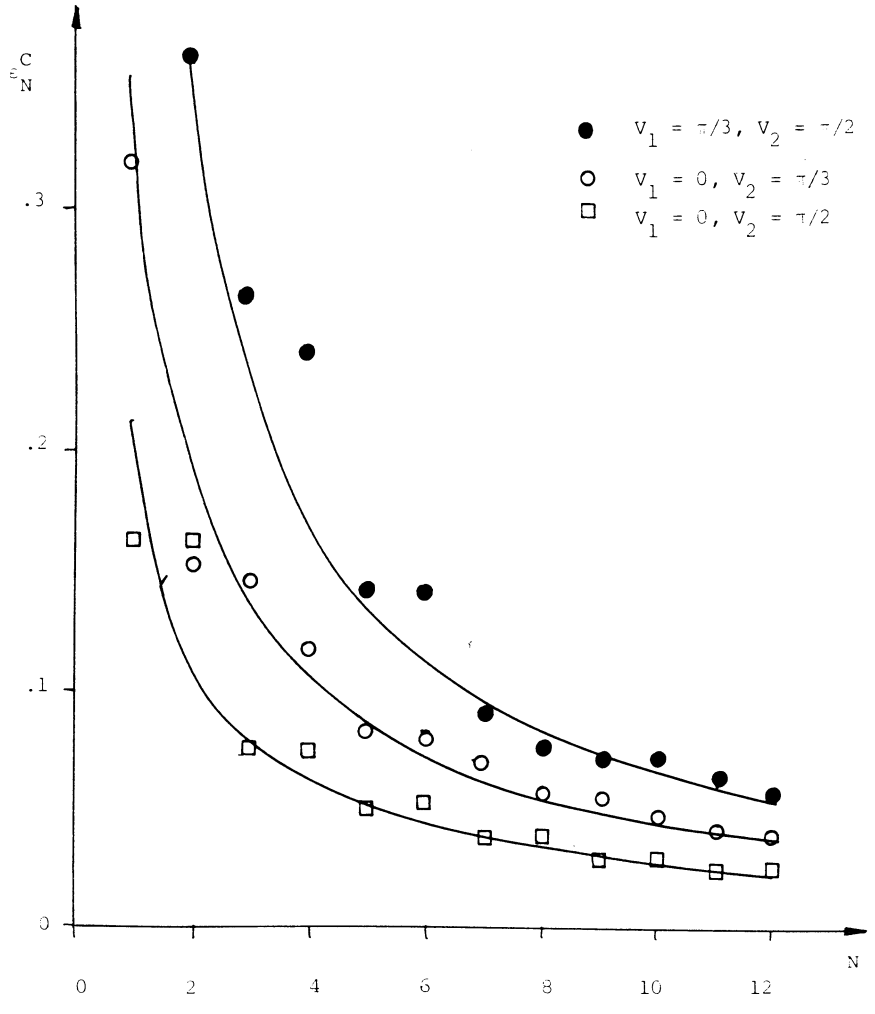

Figure 3.23 Convergence of harmonic series for CCSD, various partially reverberant fields.

CHAPTER FOUR

THE SPHERICAL HARMONIC ANALYSIS OF FREE WAVE FIELDS IN PRACTICE

4.1 INTRODUCTION

As we saw in Chapter Two, a free wave field used to model a spatially complex, random wave field may be completely described by its plane wave weighting function. Associated with the weighting function are such quantities as the energy flow directivity in the field. However, the weighting function is not directly observable, and must be inferred from measurements of complex cross-spectral density (CCSD).

There are a variety of methods by which this may in principle be done, as described in Chapter Three. Of these, the spherical harmonic analysis method has the most general applicability, and this chapter is a description of a practical algorithm for plane wave weighting inference, based on the use of spherical harmonics.

The technique as finally developed involves the least squares fitting of spherical harmonic models of free wave field plane wave weighting to CCSD data. The harmonic models are based on sets of harmonics which are chosen by a stepwise variable-by-variable search procedure. The output of computer programs written to perform the search and fitting consists, for a given input CCSD data set, of a series of plane wave weighting models which can be judged according to their statistical quality and physical plausibility.

As will be described, this method is designed to derive as much information as possible from a given set of CCSD data of a finite size, with associated errors of finite size.

The chapter opens with a detailed formulation of the central harmonic fitting problem as an exercise in regression analysis. Previous applications of spherical harmonic model fitting in various areas are then described, and the final method is presented, together with a discussion of its limitations and sensitivity to input data errors.

4.2 FORMULATION OF THE HARMONIC SEARCH PROBLEM: LEAST SQUARES FITTING

4.2.1 Preliminary Formulation

The integral relation between the plane wave weighting function characterising a free wave field, and CCSD measurements taken between signals recorded at two points in the field, was given in Chapter Two (Equation (2.14)). This integral relation may be re-expressed, as shown in Chapter Three, as a pair of spherical harmonic series. If the weighting I can be modelled by a series of the form

$$I(\omega,v,u) \simeq \hat{I}(\omega,v,u) = \sum_{\ell}^{P} \sum_{q}^{+1} I_{\ell}^{q}(\omega)\, Y_{\ell}^{q}(v,u) \qquad (4.1)$$

(equation (3.88)), with the sum taken over P+1 suitably chosen harmonics, then the correspnding normalised CCSD is given by

$$C(\omega,\underline{r}) \simeq \hat{C}(\omega,\underline{r}) = \sum_{\ell}^{P+1} 2\, I_{\ell}^{q}(\,)\, i^{\ell}\, j_{\ell}(kr)\, Y_{\ell}^{q}(\theta,\phi) \qquad (4.2)$$

(equation (3.89)).

As outlined in Chapter 3, these equations may be used in the deduction of information about weighting from CCSD samples taken over a sparse array of sampling positions. The basis of the technique is to assume a model of the weighting as expressed by equation (4.1), with the coefficients treated as unknowns. CCSD predictions based on this model weighting may be computed using equation (4.2), for each position used in the experiment. The coefficients may then be chosen by comparing the predictions to experimental measurements of CCSD. Finally, an estimate of the weighting may be reconstructed using equation (4.1).

The central problems faced by a program designed to carry out such an analysis of a given CCSD data set are: how to make an appropriate choice of a set of harmonics for the model; how to estimate the coefficient values; and how to assess the validity of the resulting model.

If the weighting varies with frequency, the coefficients will vary with frequency, and so a separate fit must be made at each frequency of interest. The following discussion concerns the estimation of coefficients from single freq-

uency data sets, and the frequency dependence of CCSD, weighting and harmonic coefficients will be omitted for convenience. Each input data set will correspond to a single frequency, and will be referred to as, for example, "a 3 kHz data set". Such a data set consists of the 3 kHz complex values of CCSD read off from CCSD frequency spectrum estimates obtained at a variety of sampling positions.

The fitting procedure may be more formally expressed as follows.
Suppose a data set

$$\{ C(\underline{r}_j); \quad j = 1,N \} \tag{4.3}$$

of N CCSD samples taken, at points $\underline{r}_j$ (j = 1,N) is available, and that the chosen model of plane wave weighting for the sound field is expressed by equation (4.1), involving P+1 harmonics. It is assumed that the harmonic sum includes the constant term

$$I^{o}_{o} = \pi^{\frac{1}{2}} \tag{4.4}$$

to ensure the correct normalisation of I (equation (2.16)), so that the model includes P unknown coefficients. The model produces a prediction $\hat{C}(\underline{r}_j)$ of the CCSD at each sampling position, a prediction which depends on the values of the P coefficients.

Then, provided P < N, the coefficient values may be chosen to minimise the weighted residual sum of squares

$$RSS = \sum_{j=1}^{N} | C(\underline{r}_j) - \hat{C}(\underline{r}_j) |^2 \, w(\underline{r}_j) \tag{4.5}$$

It was decided to develop a least squares procedure because of the well-known advantages of such methods (4.1). Because of the restriction P < N, a least squares procedure cannot yield as many coefficient values for a given data set as could be obtained by a simple simultaneous solution of N versions of equation (4.2) (one for each data point). However, in the inevitable presence of data uncertainty, a least squares procedure can be shown to produce coefficient

estimates which are of zero bias (given zero mean input errors) and whose statistical properties may be assessed in a variety of standard ways.

4.2.2 Weighting Factor; Real and Imaginary Data Fitting

The inclusion of the arbitrary weighting factor w in equation (4.5) makes the formulation of the problem as general as possible. If the plane wave weighting is azimuthally symmetric, so that the CCSD predictions would be dependent only on the axisymmetric harmonics $Y^o_\ell(\theta)$, which are Legendre polynomials in $\cos\theta$ (see Chapter 3), a suitable weighting factor would be

$$w(\theta) = \left|\frac{d}{d\theta} \cos\theta\right| = \sin\theta \tag{4.6}$$

The use of this weighting makes a distribution of samples which is uniform on an angular scale equivalent to a sample weighting which is uniform over $\cos\theta$.

Since both observed and predicted CCSD's are complex quantities, the residual sum of squares RSS splits into two separate sums:

$$RSS = RSS^R + RSS^I \tag{4.7}$$

where

$$RSS^R = \sum_{j=1}^{N} (\text{Re } C(\underline{r}_j) - \text{Re } \hat{C}(\underline{r}_j))^2 \, w(\underline{r}_j) \tag{4.8}$$

$$RSS^I = \sum_{j=1}^{N} (\text{Im } C(\underline{r}_j) - \text{Im } \hat{C}(\underline{r}_j))^2 \, w(\underline{r}_j) \tag{4.9}$$

(Re denotes real part, and Im denotes imaginary part.)

Since

$$I_{-q}^{\ell} = I_q^{\ell *} \; ; \; Y_{-q}^{\ell} = Y_q^{\ell *} \tag{4.10}$$

it is straightforward to show that

$$\hat{C}(\underline{r}) = 2 \sum_{\ell} \sum_{q \geq 0}^{P+1} i^{\ell} j_{\ell} \varepsilon_q$$

$$x \left(\mathrm{Re}\, I^q_\ell \, \mathrm{Re}\, Y^q_\ell - \mathrm{Im}\, I^q_\ell \, \mathrm{Im}\, Y^q_\ell \right) \qquad (4.11)$$

($\varepsilon_q = 1$ for $q = 0$; $\varepsilon_q = 2$ otherwise.)

It follows from the form of this sum that Re $\hat{C}$ is made up only of contributions from harmonics with the polar angle label ℓ even, while Im $\hat{C}$ is formed only by odd terms. Thus the two sums RSS^R, $RSS^{\hat{I}}$ are decoupled, and the problem of finding the best-fitting set of complex coefficients to fit to a complex CCSD data set breaks up into two separate problems: one involving the fitting of even coefficients to the real part of the data, and one involving the fitting of odd terms to the imaginary part of the data.

Henceforth the two separate problems will be referred to respectively as "the real data search" and "the imaginary data search". Note that both fitting problems involve real-valued coefficient terms and real-valued variables.

It turns out to be convenient to define "real harmonic variables" and "imaginary harmonic variables" as follows:

$$\psi^R_1 \alpha j_2 Y^0_2$$

$$\psi^R_2 \alpha j_2 \, \mathrm{Re}\, Y^1_2$$

$$\psi^R_3 \alpha j_2 \, \mathrm{Im}\, Y^1_2$$

$$\psi^R_4 \alpha j_2 \, \mathrm{Re}\, Y^2_2$$

$$\psi^R_5 \alpha j_2 \, \mathrm{Im}\, Y^2_2$$

$$\psi^R_6 \alpha j_4 \, \mathrm{Im}\, Y^2_4 \qquad (4.12)$$

$$
\begin{aligned}
\psi^{I}_{1} &\propto j_1 \, Y^{0}_{1} \\
\psi^{I}_{2} &\propto j_1 \, \mathrm{Re}\, Y^{1}_{1} \\
\psi^{I}_{3} &\propto j_1 \, \mathrm{Im}\, Y^{1}_{1} \\
\psi^{I}_{4} &\propto j_3 \, Y^{0}_{3}
\end{aligned}
\qquad (4.13)
$$

(See Appendix C, equations (C4,C7) for more detailed expressions.) These variables are all real valued. The "real" variables contribute only to the real part of $\hat{C}$, and the "imaginary" variables contribute only to Im $\hat{C}$. A convenient shorthand for the variables is the notation (ℓ,q-Re), or (ℓ ,q -Im). Thus ψ^{R}_{2} is (2,1-Re), while ψ^{R}_{3} is (2,1-Im).

4.2.3 Regression analysis: solution of problem

In Appendix C, the minimisation problems expressed by equations (4.8, 4.9) are recast into the standard notation of multiple regression analysis (4.1). This notation is simpler to manipulate than that of equations (4.8-4.11) and standard regression analysis results about the statistical quality of a fit become easily accessible. These results are summarised below, and are given in detail in the Appendix.

It may be shown that the coefficients which minimise a residual sum of squares like those of equations (4.8,4.9) can be found from a solution of a matrix equation known as the "normal equation". The elements of the matrices and vectors involved are computed from sampling position coordinates and CCSD data.

Two fundamental measures of the quality of an estimate of a random variable obtained from a regression are its "bias" and "variance". The bias measures the difference between the estimate's expected value and the "true" value of the variance, which the variance is a measure of the "spread" of estimates about their expected value. A good estimate should have low bias and low variance. However, in practice low bias estimates tend to suffer from high variances, and vice versa, and a compromise must usually be reached. An overall measure of an estimate's quality is the "mean square error" (MSE), the sum of the bias squared and the variance. An estimate will be improved by any procedure which reduces its MSE.

If we suppose that the residual data in a regression (that is, the difference between the CCSD data and the CCSD predictions produced by a harmonic model) is an unbiased, random disturbance containing no significant information, then it can be shown that the least squares coefficients and predictions are unbiassed estimates.

4.2 4 Regression Analysis: measures of statistical quality

These are various standard measures of the overall statistical quality of a least-squares fit to data (detailed in the Appendix). The most familiar is probably the ordinary correlation coefficient R. This is a measure of the ratio of the variation of the CCSD data explained by the harmonic model to the total variation of the data. If no fit is attempted, R is zero. If a perfect match is made at every data point, R has absolute value 1.

If p, the number of variables in a fitting model, is increased, then R^2 always increases. This reflects the fact that with more variables equation (4.12) can match the values of each of the n data samples more closely. In fact, if p is allowed to equal n, RSS is zero and R^2 is unity. However the true quality of the model may be poorer because the predictor function may take unrealistic values away from the data points.

This is illustrated in Figure (4.1), which is a representation of the fitting of a set of data points with polynomials of various orders. If the order is too high, the data points may be fit very well, but the predictor function oscillates to unreasonable values elsewhere.

Two more subtle measures of the qauality of a fit designed to take this feature into account are the F-statistic and the PRESS statistic. F is a function of the correlation coefficient:

$$F = \frac{R^2}{1-R^2} \Big/ \frac{p}{n-p-1} \qquad (4.14)$$

This quantity can be shown to be a random variable with the standard F probability distribution with p, n-p-1 degrees of freedom. Roughly speaking, a fit is significant if the value of F is large. This is possible if R^2 is large, but p is not too close to n.

PRESS is the "predicted residual sum of squares" defined by Allen (4.2). Its use involves a technique known as "cross validation" (CV), (4.3), which depends on the splitting up of the input data into two sets. One set is used to produce the predictor function, and the second set is used to validate the predictor function. CV allows the investigation of whether a predictor is poor away from the predictor data points on which it is based, as will be the case if too many variables are included in the model. The comparison data set, which has not been used in the formation of the predictor, is equivalent to a fresh data set against which the predictions of the model can be checked. PRESS is a measure of the deviation of the predictor function from the values of the "fresh" data set.

PRESS would be expected to be large for small p - when the fit to the data is poor - and at large p - when the fit is good, but the predictor function oscillates to unreasonable values between the data points. The best values of p would be near the PRESS minimum, representing a trade-off between goodness of fit to the data and the quality of the predictor elsewhere.

The above discussion illustrates the at first glance surprising fact that the inclusion of more harmonic variables in a model will not necessarily improve the fit. This is further shown by the properties of a measure of the contribution of an individual variable in a model, known as the t-statistic.

The t-statistic is defined as the ratio of the coefficient estimate to that estimate's standard error. The standard error is a measure of the estimate's standard deviation.

The larger the value of the t-statistic, the more important the variable is to the model. The threshold value is unity: a variable with a t-value greater than one is called "significant". It can be shown that the quality of a model is actually improved if insignificant variables are deleted from it - even though the remaining set of variables is smaller than the original. Although coefficient estimates from the smaller set suffer a worse bias than the larger, their variance is less. The decrease in variance offsets the bias increase, to give a smaller MSE.

4.2.5 Regression analysis: collinearity

An important deciding factor in the quality of a regression is the amount of collinearity among the variables. Collinearity describes the extent to which two variables appear to have a linear relationship. The relationship may be real

(for example, the dependent variable will, or should, be highly collinear with the dominant independent variables) or an artifact of the data acquisition.

Collinearity among the independent variables is purely a function of the sampling structure, and not of the values of the dependent variable data. Thus, in the present example, the independent variable collinearity depends only on the sampling position array, and not on the CCSD values, and in principle the sampling array could be designed with this in mind.

Collinearity among the independent variables makes the estimation of coefficients unstable. A coefficient estimate set may indicate a strong dependence on one variable, but a slight perturbation of the data or a marginal change in the model can "flip" this dependence to another variable, highly collinear with the first. This occurs because a linear dependence of CCSD on a given harmonic is equivalent to a linear dependence on a second harmonic, if the second variable is highly collinear with the first.

Another serious effect of collinearity is the degradation of estimates of quantities like the F- and t-statistics, making the selection and deletion of variables for a model uncertain.

Associated with a regression is a correlation vector r_{yi}, which measures the collinearity between the CCSD data and each harmonic in the fitting model, and a correlation matrix r_{ik}, each element of which measures the collinearity between the i'th and j'th harmonic variables.

A correlation matrix element can range in magnitude from zero - indicating zero collinearity between the two variables concerned - to one - indicating a perfect linear relationship. A "good" set of independent variables will have a correlation matrix with low value elements (with a magnitude $<<$ 1) away from the leading diagonal. (The leading diagonal elements r_{ii} are always unity.)

A measure of the impact on variable i of collinearity with all the other independent variables is the "variance inflation factor" (VIF) (4.4) defined by

$$VIF_i = (r^{-1})_{ii} \tag{4.15}$$

This is, the VIF is the i-th diagonal element of the inverse of the correlation

matrix. It ranges in value from one to infinity, with one indicating zero collinearity, and infinity indicating perfect collinearity with another variable or variables. In practice, a VIF larger than about 10 indicates that the variable suffers from serious collinearity.

A straightforward measure of the overall effect of collinearity in a variable set is the average of the VIF's:

$$R_L = \sum_{i=1}^{p} VIF_i/p \qquad (4.16)$$

A highly collinear variable set is characterised by a high ($R_L > 10$) value of R_L. The large value is caused by improbably large coefficient values, resulting in large fluctuations of the prediction function between data values (see Figure 4.1).

4.2.6 Summary

This concludes the formulation of the spherical harmonic fitting problem described in subsection (4.2.1) in terms of regression analysis, with the discussion of a battery of measures with which the quality of a regression may be tested.

These measures offer a way to assess the quality of a harmonic model once constructed, but as noted in subsection (4.2.1), a preliminary problem in the design of a model is the choice of a suitable set of harmonic terms. Various standard methods have been developed by regression analysts by which the selection of independent variables may be performed. However it is not clear a priori which methods are appropriate for the particular fitting problem presently considered.

There seems to have been little significant work done on harmonic model searching by previous workers in acoustics (see the discussion in Chapter 3). However, a considerable expertise has been developed in the fitting of such models by researchers on the apparently unrelated topics of the magnetic and gravitational fields of planets, and this work is the subject of the next section.

4.3 HARMONIC ANALYSIS OF THE GRAVITATIONAL AND MAGNETIC FIELDS OF PLANETS

4.3.1 Geomagnetism

Much of the inspiration for the development of the harmonic regression technique described here has come from a study of comparable work done by researchers in the field of geomagnetism (4.5).

Geomagnetism, the study of the Earth's magnetic field, is one of the oldest sciences, dating back 4000 years to studies by the ancient Chinese (4.6). The fact that the field is approximately a dipole in character was shown by Gilbert as long ago as 1600. It was realised soon after this, however, that the field has other significant components, and spherical harmonic models have been used to describe the field since the time of Gauss (1839). Harmonic models are a natural description of the field, which is a function of two spherical angles - latitude and longitude - on the Earth's surface. A dipole field can be regarded as a special case of a harmonic series, with one non-zero component ($\ell=1$, $q=0$).

The coefficients in the harmonic models produced by Gauss and later workers were determined by fitting models to measurements of the geomagnetic field made over the Earth's surface. The earliest global survey of the field seems to have been assembled by Edmund Halley in 1700. The importance of such surveys has grown with time, as a knowledge of the Earth's field yields not just information about the structure of the Earth - Gauss himself was able to show from his harmonic modelling that the magnetic field is generated inside the Earth - but also about such practical matters as the behaviour of the ionosphere, and the position of anomalies in the Earth's crust such as ore lodes. A modern survey includes many thousands of measurements made on land, at sea, in the air and in Earth orbit (4.7), sufficient to yield such harmonic models as the International Reference Geomagnetic Field (4.8), which comprises 80 variables.

The method presently accepted by workers in this area for the selection and testing of harmonic models for the geomagnetic field was presented by Fougere in 1963 (4.9). Fougere described what is basically a stepwise variable-by-variable search procedure (see section (4.4)). Recently, Whaler and Gubbins (4.10) investigated more advanced approaches to the problem, but found only marginal imporvements on Fougere's method, and concluded that the Fougere method remained the most sensible choice, being reliable and thoroughly familiar.

One interesting suggestion by Whaler and Gubbins was aimed at reducing "ringing"

- the Gibbs' phenomenon - in truncated harmonic series (see Chapter 3). Whaler and Gubbins considered the analogy between a harmonic series and a time series as employed in the frequency analysis of acoustic signals. They argued that the sharp truncation of a unweighted harmonic series is equivalent to the use of a rectangular data acquisition window, so that ringing is caused by "leakage" into "side lobes". Whaler and Gubbins proposed the use of a smoothing window, analogous to those used in signal processing, to reduce ringing by weighting out the higher order harmonic terms and so reducing the side lobe levels. However, it was found in practice that a significant reduction of the side lobes led to an unacceptably blurred final estimate. (As is familiar from frequency analysis, leakage can be reduced only at the expense of resolution.) Whaler and Gubbins concluded that "ringing seems to be a property of the spherical harmonic representation which one must live with".

4.3.2 The Magnetic Fields of Jupiter and Saturn

The expertise gained in the harmonic analysis of the Earth's magnetic field has recently been applied to data obtained from the spectacular flybys of the planets Jupiter and Saturn by unmanned American spacecraft. Each spacecraft made one pass through the gravity well of its target planet, yielding a sparse array of samples of the planetary magnetic field along a single track.

Connerney (4.11, 4.12, 4.13), describing the spherical harmonic analysis of this data, noted that a principal problem with such a limited data set is collinearity among the independent variables. This was evidenced by a model giving a good fit to the data set on which a predictor is based, but having poor behaviour elsewhere. This was shown by comparing models derived from the data from one spacecraft to further data yielded by a later spacecraft. Connerney described the development of an analysis method involving a stepwise search procedure (see section (4.4) which sought a low-collinearity variable set.

4.3.3 The Earth's Gravitational Field

Another interesting application of spherical harmonic fitting has been made in the study of the Earth's gravitational field.

The Earth's gravitational field is nonuniform because of the slightly nonspherical shape of the planet, and it can be described by a series of harmonics (4.14). The angular arguments of the harmonics are again latitude and

longitude. The orbit of an artificial satellite is a function of the coefficients in the series (among other perturbing factors such as solar and lumar gravity). Observations of satellite orbits, obtained by such means as laser and doppler tracking, can then be used to estimate the unknown coefficients.

Such modelling was performed as long ago as 1958 using observations of Sputnik 2, the second man-made object to orbit the Earth (4.15). A more recent study (4.16) involved the study of 28 satellite orbits. The resulting models, projected back to the Earth's surface, have shown that the Earth is pear-shaped, with a depression at the south pole and a spindle at the north, the variations in radius being of the order of tens of metres.

The analysis methods developed by workers in this field appear to be mostly "rule of thumb", involving the rejection on qualitative grounds of any model with excessively large high order coefficients, giving an oscillating estimated field. However, Stone (4.3) described a cross validation study of such data, involving a successful use of the PRESS statistic.

4.3.4 Summary

The main conclusion of this brief review is that the most successful formalised variable selection technique used in the construction of harmonic models of planetary magnetic and gravitational fields has been the relatively simple variable-by-variable stepwise search method (to be described below). More advanced techniques have been proposed but not generally accepted. Collinearity among the independent variables is a weakness of more restricted data sets, such as those acquired by the sampling of a planetary magnetic field during a single spacecraft flyby.

The plane wave weighting harmonic model construction technique developed in the present study has been based on a stepwise search procedure, with safeguards against collinearity incorporated into the search. The development of the search technique is described in the next section.

4.4 DEVELOPMENT OF HARMONIC SEARCH PROCEDURE

4.4.1 Introduction

The standard statistical results described in section (4.2) may be used to assess

the goodness of fit of a model composed of p spherical harmonic terms to n CCSD data samples, with $p < n$. There are, however, an infinite number of harmonic terms to choose from, and so an infinite number of possible models of size p. The basic requirement of a harmonic fitting procedure is therefore a method to find harmonic models which are likely to give a good fit to the data. The goodness of fit of each model can then be measured using the criteria described earlier, and the models further judged in terms of their physical plausibility.

A reasonable preliminary criterion, giving n data points, is to restrict the harmonic variable set out of which models are to be constructed to the first n harmonic terms (with the variables arranged in the order of increasing complexity described in equations (4.12, 4.13).) It is likely that any higher order harmonic variables would suffer from aliasing, and would worsen the collinearity of any model.

Even this restricted set, however, has a total of $2^n - 1$ subsets from which harmonic models could be chosen. In principle, $2^n - 1$ separate regressions would be required to evaluate all the possible models, and even for moderate values of n this is impractical. (For example, for $n = 12$, $2^n - 1 = 4095$.)

As mentioned in section (4.3), the approach adopted by workers in the field of geomagnetism is that of Fougere (4.9), who described a "stepwise" search procedure (4.1). This is a search through likely combinations of harmonic variables, performed by adding to or deleting from a model one variable at a time. Such a search cannot be exhaustive and is not guaranteed of success, in that it is possible that a good model or group of models may be missed altogether. However, it is practical and economical and, as noted in section (4.17), has been proven successful.

Such a search procedure is described in the present section. The motivation for the inclusion of each feature of the final method is illustrated by a series of example runs of a computer program, made as the method evolves.

4.4.2 Basis of Development

The operation of a computer program performing a stepwise search for harmonic variable combinations to fit to a given set of data can be described as follows. At any point in the search, the program has a "model", that set of harmonics yielded by the search so far. The program compares its model with the given data and considers its quality using the statistical measures described in section

(4.2), and changes the model by adding or deleting one variable, in such a way as seems likely to improve the model's quality. The new model can be compared to the data and assessed, and a further change made; and so on.

The two basic operations involved in such a search are known as "forward search" (FS) and "backward elimination" (BE). FS involves the inspection of all the variables in some allowed set outside the model (called the "hopper"). The variable which seems most likely to improve the model, by some external criterion, is taken from the hopper and added to the model.

A straightforward way to perform a FS stepwise search is simply to scan through the variables in the hopper in the order defined by equations (4.12, 4.13). Another external criterion commonly used is that the variable selected should be the one whose correlation with the residual data is the highest. The residual data is the difference between the data and the present model's prediction. This criterion seeks to ensure the selection of an improving variable by using any systematic information still left in the residual data. A FS can be initiated by choosing, for the first variable in a model, that variable in the hopper with the highest correlation to the data.

BE (backward elimination) involves the examination of the variables within the present model. A variable may be deleted from the model and returned to the hopper if this seems likely to improve the model's quality, according to some internal criterion. The criterion most commonly used is that of significance as measured by the t-statistic (subsection (4.2.4)), since the deletion of variables insignificant by this criterion leads to a definite imporvement in the quality of a model. A model variable may become insignificant as the model evolves through the inclusion in the model of variables with which it is collinear. In practice, the least significant variable (the one whose t-statistic is smallest in magnitude) is deleted.

The two simplest methods to perform a stepwise search are to FS until the hopper is empty, or BE from a model initially composed of all the hopper variables, until the model has been reduced to purely significant variables or emptied. Mantel (4.18), studying these two methods, recommended the BE procedure because the deletion of insignificant variables is guaranteed to improve the model, while FS brings no guarantee of improvement. Furthermore, the BE technique can be shown to be more economical in computer time.

More sophisticated searches involve a combination of the two basic operations, with the selection of fresh variables for the model followed by the pruning out

of insignificant terms. This sort of approach offers the prespect of finding more good quality models than do the two simple methods described in the last paragraph. In principle, if deleted variables are returned to the hopper for reconsideration later, all the $2^n - 1$ possible models derivable from a hopper of size n can be reached.

This is desirable because a model searching procedure cannot be expected to be fully automated, with no need for the further judgement of results. A search program seeks models according to criteria of statistical quality, which are not equivalent to criteria of physical plausibility. Two models may have comparably good statistical behaviour, with one making good physical sense and the other not. However, it is unlikely that a model which is poor statistically will be worthwhile physically. A good search program therefore filters out statistically bad models from the possible combinations of harmonics. The remaining statistically good models may then be further reviewed to remove the physically implausible, leaving a residue of sound models.

A drawback of any variable selection technique is that in the presence of significant collinearity among the variables, estimates of the statistics on which the selection is based are unreliable, and the selection procedure can become unstable. A check on the level of collinearity in the models is therefore desirable.

4.4.3 Model Experiment Data

The search procedure described below was originally designed for the analysis of acoustic duct data, and was tailored to suit properties of the data to be analysed. Modifications may be necessary if the procedure is applied in other areas.

Input CCSD data for use as a development example was obtained from a microphone traverse experiment performed in a hardwalled circular duct of radius 34.3 cm and uniform length 2.96 diameters. At one duct termination was a reverberation chamber containing four Hartmann generators. The generators excited a reverberant field in the chamber which in turn excited the duct sound field. The duct terminated in a second reverberation chamber.

It is worth pausing to consider the geometry of this experiment in some detail. It illustrates an attempt to produce a useable set of CCSD data from a straightforward experimental set-up.

Two 1/4 in. microphones were used in the experiment, and their placing in the duct sound field is shown schematically in Figure (4.2). The microphones were attached to a pair of traverse rods which stretched across a horizontal diameter of the duct; the rods were at the mid-point of the working section length. The microphones were attached with their axes perpendicular to the traverse rods, so that the diaphragm of the moving microphone swept out an arc of a circle as the rod was twisted, as indicated in the Figure.

The microphones were initially positioned with their axes parallel to each other and to the duct axis, with the centre ponts of their diaphragms held a distance d = 2.54 cm apart. Both microphones pointed towards the source reverberation chamber. One rod was then twisted to move the microphone marked $\underline{x}$ in Figure (4.3) to a total of 12 positions relative to the microphone marked $\underline{x}'$, which was held stationary. These positions were parametrised by the angle α through which microphone $\underline{x}$ had been rotated from its initial position.

An input data set for the harmonic search procedure would consist of twelve complex values of CCSD read off at a particular frequency from the twelve sampling positions.

It is convenient to study the geometry of the chosen set of sampling positons in terms of a coordinate system defined as in the Figure, with a Cartesian z-axis taken along the duct axis. The origin of coordinates is located at the mid-point of the duct length, at the centre of a circular cross-section. As shown in the Figure, the y-axis is vertical, so that the x-axis is horizontal. Information about the chosen set of sampling positions is summarised in Table (4.1). A range of values of turning angle α from -37^{o} to 42^{o} was used. The position vectors $\underline{x},\underline{x}'$ are given in terms of Cartesian and polar coordinates relative to the above axes by

$$\underline{x} = (-d, R \sin(\alpha_o + \alpha), -R \cos(\alpha_o + \alpha)) \qquad (4.17)$$

$$\underline{x}' = (0, R \sin \alpha_o, -R \cos \alpha_o) \qquad (4.18)$$

d is the microphones' minimum separation distance, 2.54 cm. R is the radius of the turning circle of the diaphragm of the moving microphone (Figure 4.3)), while $_o$ is the angle made by the z-axis to the line joining the microphone diaphragm to the centre of the mounting rod. The separation vector $\underline{r} = \underline{x}-\underline{x}'$ of the two

microphones is given in terms of Cartesian and cylindrical polar coordinates for each of the twelve positions in Table (4.1).

4.4.4 Design of Experiment: CCSD Sampling

The twelve sampling positions were chosen with three criteria in mind: that the positions should be close enough together for the sampled sound field to be considered homogeneous; that the microphones should always be far enough apart for scattering to be negligible; and that the expected spatial variation of CCSD should be well sampled.

The distance scale of variation of CCSD might reasonably be expected to be comparable to the distance scale of Cook's diffuse field CCSD sin(kr)/kr. The twelve separations were chosen to give eight samples distributed in terms of separation distance approximately uniformly over the interval from the minimum separation d up to a wavelength of sound at 3 kHz (11.35 cm), interwoven with eight samples distributed uniformly over the interval from d up to a wavelength of 5 kHz (6.81 cm). This is illustrated in Figure (4.4). The Figure shows that this choice would ensure that the first lobe of the diffuse field CCSD would be well sampled.

The Table shows that the twelve sampling positions cover a range of polar angle of width 0.494 (= $\pi/6.4$) radians. Thus is would be anticipated that axisymmetric spherical harmonics up to order at least 3 could be considered well sampled without fear of aliasing. Figure (4.5) shows that the twelve angular separations cover roughly half the interval between successive zeroes of $Y_3^0(\theta)$. The aliasing of harmonics is considered further in subsection (4.4.10).

As well as the measured experimental data, artificial data was computed. The value of CCSD which would be obtained in a free wave field with a cosine-power weighting of m = 1 (see Chapter 3) at a frequency of 3 kHz was calculated for each of the twelve microphone separation positions used in the experiment. The calculation was made using a program based on the strip-function method outlined in Chapter 3. The true harmonic coefficients for this field can be calculated so that the results of the procedure could be readily judged. If computing rounding errors are neglected, this data set can be regarded as an ideal input set, completely free of measurement error.

4.4.5 Design of Variable Hoppers

A suitable choice of initial hoppers of harmonic variables for each of the real and imaginary data model searches performed by the program in its earliest form is illustrated in Figure (4.6). As shown in the Figure, there are five real harmonic variables with polar angle index $\ell \leq 2$. They are (2,0), (2,1 - Re), (2,1 - Im), (2,2 - Re), (2,2 - Im). Similarly there are fourteen variables with $\ell \leq 4$ and in general, there are

$$\tfrac{1}{2}\ (\ell^2 + 3\ell)$$

real variables up to polar index ℓ(ℓ even).

Given twelve data points, the inclusion of more than the five variables with $\ell \leq 2$ in the initial hopper would necessitate the inclusion of some but not all the variables from the nine-member set with $\ell = 4$. The choice of which variables to include would be somewhat arbitrary, and could influence the nature of the final regressions. The neglect of terms with higher q values, for example, would effectively weight the choice of harmonic models in favour of models with a more complex polar angle dependence than azimuthal angle dependence. If, for example, twenty data points were available, then an appropriate choice of initial hopper variables would be the fourteen with $\ell \leq 4$; and so on.

Similar considerations apply for the selection of a hopper for the imaginary fit variables. It can be seen from Figure (4.6) that there are three variables with $\ell \leq 1$, and ten with $\ell < 3$. In general, there are

$$\tfrac{1}{2}\ (\ell^2 + 3\ell\ + 2)$$

variables up to polar angle order ℓ. The initial hopper in this case is the set of ten variables with $\ell \leq 3$.

4.4.6 Simple FS, BE Search Procedures

The results of the application of the simple FS (forward search) procedure described in subsection (4.4.2) to the set of artificial data is shown in Table (4.2).

Each column of the table represents one iteration of the search procedure. The program begins by choosing that variable in the hopper which has the highest correlation with the data, and proceeds to select at each iteration one more variable to include, according to the best residual data correlation criterion described in subsection (4.4.2). The table records each harmonic coefficient estimate value and the corresponding t-statistic. It can be seen from a comparison of the estimated coefficients with the true values given in the table that the searches in the early stages successfully found the "correct" harmonic variables; the non-zero coefficient estimate values are within a few per cent of the theoretical values for the first few iterations, while the t values indicate the relative contribution to the fit of the correct terms. Once the contribution of these correct variables has been removed, the residual "data" is due to higher order harmonic variables than are present in the hoppers, and appears to the present program as non-systematic error; the table indicates the largely unsuccessful attempts of the program to fit further terms to the residual data.

The later iterations in the imaginary data search show the hazards of using a collinear set of variables. Collinearity is significant by the fifth iteration ($R_L > 10$), and by the twelfth the collinearity is enormous. Some of the coefficient values are unrealistically large, the estimates of coefficients and t-statistics have been thrown awry, and the true harmonic structure of the field is not discernible. The harmonic content of the field in this case is quite simple; these problems would be aggravated for fields with more complex structures, as would be anticipated in practice.

The collinearity problem is evident in Table (4.3), which shows the results of a straightforward BE search applied to the same data set. The same hoppers were used as in the FS run described above; the program begins with models composed of all the hopper variables and deletes the least significant term at each iteration until only one is left. The "correct" coefficient emerges from the real data search, but in the imaginary data case the t-statistic estimates are so distorted by collinearity that the correct term is deleted at the first iteration, and the correct harmonic dependence is not found in the later stages of the search.

Because of the need for BE searches to start from quite large variable sets, with the consequent hazards of collinearity (the only way to avoid this being to make an arbitrary choice of initial hopper variables), it seems best to build the final program around what is essentially a FS procedure.

The most encouraging feature of the results in Table (4.2) is the good statist-

ical quality of the early models, with good estimates of the correct coefficients, large values of R and t where appropriate, and reasonable levels of collinearity as indicated by R_L. This indicates that the method is workable in principle.

The behaviour of the PRESS statistic, as shown in Table (4.2), is disappointing. The PRESS results alone do not indicate unambiguously which model or models would be preferred: the statistic does not vary monotonically with the number of variables in a model, and its minima do not correspond to the best models.

Throughout the rest of the regression exercise described in this Chapter, the PRESS statistic was not found to be of any practical value. There are various possible explanations: for example, it is possible that the numbers of variables involved here were too small to be meaningful. Stone (4.3) in his harmonic analysis of the Earth's gravitational field using satellite data, used a much larger data set than that available here.

However, PRESS has been introduced here in order to illustrate its possible use. PRESS is a novel and intuitively appealing statistic which may be of value to future workers.

4.4.7 Stepwise Search Procedure

The first improvement we can try over a simple FS (forward search) procedure for the next generation of the program is to incorporate a BE (backwards elimination) routine into the program, so that the program has the option of deleting variables which become insignificant from the models it builds up.

Table (4.4) shows how this version of the program works in practice. This table is based on experimental data; the data set used here is made up of twelve measurements of CCSD taken at 4743 Hz.

The real data search results show how at first the program successively selects the harmonic variables from the hopper which fit best to the residual data, just as did the simple FS procedure described earlier. However, after each selection the program scans through its new model to check if any variables have become insignificant - as is indeed the case at iteration 4. The programe prunes away the insignificant variables, until a new combination of significant variables has been found, at iteration 6. This exemplifies the value of the more complex search procedure; this model could not have been found with a simple FS

procedure.

After deletion from the model, the variables are returned to the hopper for possible reselection later. This is done to maximise the number of significant variable combinations the model is likely to find. For example, in the real data search shown in Table (4.4) the program reselects variable (2,2 - Im) at iteration 7. However, this variable proves to be insignificant and is immediately dropped at the next step.

The selection and deletion in successive iterations of a variable is a sensible choice as the program's basic stopping criterion. The argument for this is that the variable just selected was chosen on the basis of any systematic information left in the residual data. Once in the model, however, the variable proves to be an insignificant part of the fit, and so the residual information to which it fits may also be regarded as insignificant. That is, there is no significant information left in the residual data, and the search may end.

The imaginary data search presented in Table (4.4) also shows the operation of this termination criterion.

4.4.8 Statistical Properties of Results

An inspection of the statistical parameters of the models found during this analysis is encouraging. Values of the correlation coefficient are quite high, though not so high as those achieved by fits to the noise-free artificial data considered earlier. The most probable cause of this is the presence of estimation error in the experimental data. The degrading effect of error is also the probable cause of lower t values than were computed in the artificial data fits. The F-statistic shows the significance of the models to be high, and the coefficients of the dominant terms are stable during the perturbation of the rest of the model caused by the introduction and deletion of higher order terms.

These observations reinforce the remarks made in subsection (4.4.6) that the search method is workable in principle and delivers good, statistically reliable models. The performance of the method may be further improved by subsequent developments, described in the rest of this section.

4.4.9 Collinearity Safeguards

As noted earlier, the presence of collinearity in the data makes variable

selection techniques hazardous, as the statistics on which they are based become unreliable. That collinearity is a danger with the example duct data sets is demonstrated by the early stages of the BE search shown in Table (4.3), and also by the typical independent variable correlation matrix shown in Table (4.5).

The simplest safeguard against collinearity is to terminate the search procedure as soon as the level of collinearity in the model becomes unacceptably high. The search would become questionable after this point, since the basic variable selection criteria are unreliable when collinearity is significant. A simple criterion may be based on the value of R_L (equation (4.16)). If R_L for a model is greater than 10, the program stops.

A complementary approach is to attempt to reduce the levels of collinearity in the variable sets used in the search procedures by "screening out" collinear pairs from the initial hoppers of variables. This may be done by removing from the hopper the higher order member of any pair of variables whose collinearity (as measured by the elements of the correlation matrix) is unacceptably high.

The justification for removing the higher order member of the pair, rather than the lower order, comes from an Occam's razor argument. A model made up of low order variables represents a simpler physical hypothesis about the duct sound field in question than one made up of high order variables. A suitable level of unacceptability is a correlation matrix element value of 0.9. Thus, in the 3 kHz example shown in Table (4.5), the only variable deleted would be (3,2 - Re). This level of acceptability is quite high, but a more restrictive criterion could lead to an unacceptable reduction in the number of models found by the search procedure. The introduction of this fairly lax screening technique is intended to reduce the risk of finding models becoming unacceptably collinear with a small number of variables. However, collinearity will still be present and will adversely affect larger models.

An example of the difference made by the introduction of the collinearity safeguards is shown by Table (4.6), which presents the results of a search procedure as applied to the 3 kHz data set. Table (4.6a) shows the real data search which was unaffected by the new measures. Table (4.6b) shows an imaginary data search performed without prescreening of the hopper, and models are found featuring the variable (3,2 - Re). Table (4.6c) shows a run with pre-screening, and models are found featuring the variable (3,0), the other half of the high collinearity pair. The results of the new procedure are satisfactory because it has yielded two significant models as opposed to one found by the replaced procedure, indicating that (3,0) was a more correct choice.

4.4.10 Origin of Collinearity

The properties and origins of collinearity in the present harmonic variable set are of interest, since they throw some light on facets of the harmonic analysis method.

A more complete analysis of correlation matrices like that in Table (4.5) reveals that collinearity in the present example has certain properties. First, the general level of collinearity tends to decrease with higher frequency. Second, if a pair of variables are highly collinear at any frequency, they may be expected to be collinear at all frequencies. Third, the highest levels of collinearity tend to occur between pairs of higher-order (i.e. spatially complex) variables. Finally, the correlation between a low-order/high-order variable pair can often be virtually independent of the choice of higher-order variable: that is, the collinearity is dominated by the identity of the low order terms.

The most obvious candidate for the primary cause of collinearity among the variables is "spatial aliasing" among the harmonic variables. Such aliasing is familiar by analogy with similar problems encountered during the digital sampling of time series. If a field is under-sampled spatially, it is impossible to determine whether an observed variation is due to the presence of a given harmonic variable, or to the presence of another, higher-order term. Another way of expressing the same problem is to note that if only a small, sparse set of sampling positions is available, a linear combination of high-order variables can be formed whose sum is close to zero at each of the given sampling positions. It is then impossible to tell from a given data set whether these higher order variables are present or not.

However, spatial aliasing alone does not explain the features of the correlation matrices described above. Aliasing would be expected to produce high collinearity between low order/high order variable pairs, but the general trend observed is for high collinearity to occur between high order/high order pairs. Collinearity due to aliasing would tend to increase with frequency, since the spatial structure of a harmonic variable depends on the dimensionless combination kr: at higher frequencies, the zeroes of a variable move closer together in position, and a given set of sampling positions becomes effectively more sparse. In contrast, however, we have observed a general reduction in the level of collinearity with increasing frequency.

An alternative hypothesis for the cause of collinearity comes from a consideration of the distance dependence of the variables. A harmonic variable

of polar angle order ℓ is proportional to the spherical Bessel function j_ℓ (kr) (see Equations (4.12, 4.13)). When ℓ is large (i.e. $\ell >> kr$)

$$j_\ell(kr) \alpha \quad e^{\ell}(kr)^{\ell} \quad (\ell + \tfrac{1}{2})^{-\ell} \tag{4.19}$$

(reference 2.31, Chapter 10).

A variable with large ℓ will thus take very small values at any data point where kr is not large. In the present experiment, at 2 kHz kr ranges in value from 0.94 to 4.24. At a typical value, say kr = 2, $j_\ell(kr)$ takes the values .2 for ℓ = 2, 0.14 for ℓ = 4, 4 x 10^{-4} for ℓ = 6, and 7 x 10^{-6} for ℓ = 8. It can be seen that the independent variables with higher ℓ will take significantly non-zero values at only a few of the twelve sampling positions. At higher frequencies, kr takes higher values: in the present example, kr ranges from 2.35 to 10.6 at 5 kHz. The number of positions where the high ℓ independent variables take significantly non-zero values is therefore increased.

This appears to explain the observed features of the correlation matrices. The details of the argument may be found in Appendix C; the key idea is that a high order variable will take a significantly non-zero value at only one data point. Thus the correlation r_{ik} between two variables i,k which are both high order will be approximately unity, since correlations computed on the basis of one data point are by definition unity. If i is low order and k is high order, only i takes significant values at most of the sampling points, so the structure of variable i dominates the value of r_{ik}.

At higher frequencies, with increasing kr, a higher order variable will take significantly non-zero values at more sampling positions, and these tendencies are reduced - as observed.

This hypothesis is therefore consistent with the observed features of the matrices discussed above, and appears the most plausible principle cause of collinearity among the harmonic variables. The persistence of high correlation between certain low order variable pairs may however be evidence of spatial aliasing. This could be tested by a consideration of the correlation matrices corresponding to different arrays of sampling positions at the same frequencies.

A final remark concerning collinearity is that the collinear behaviour of the variable sets considered here is in general encouragingly good. This is further

improved by the anticollinearity screening procedure described earlier.

4.4.11 Final program

The above ideas may be incorporated into a final program to take in complex values of CCSD recorded at a given frequency for a given set of sampling position separations, and to perform both the real and imaginary data model searches described above.

The execution of each of the search procedures (for real and imaginary data) is illustrated in flow diagram form in Figure (4.7). The operation and stopping criteria are essentially as described above. The terminating case in which a variable is selected and deleted immediately, described in subsection (4.4.7), is detected by comparing the contents of a model before and after each process of selection and deletion. In the terminal condition described above, the process would leave the model unchanged, and the program is instructed to stop. However the casting of the criterion in this form also ensures that the program stops if, through any peculiarity of the data, an infinite loop of selection and rejection of any form is entered, making the program more reliable than if a simpler form of the criterion were used (see for example (4.1)).

4.5 DEVELOPMENT OF AXISYMMETRIC HARMONIC SEARCH PROCEDURE

With the application of the stepwise search procedure described above to several sets of data from the example experiment, it became apparent that the program was consistently finding models composed of or dominated by axisymmetric harmonic variables (variables with $q = 0$). This fact motivates the development of an alternative version of the program described above, involving searches through hoppers composed purely of axisymmetric harmonic variables.

Such a restricted search offers the hope of extracting more information from a given set of data. For example, the search procedure described in section (4.4) could yield axisymmetric models fitting to the real data composed of variables of order no higher than $\ell = 2$; in principle an axisymmetric variable search could yield more detailed models of plausible weightings composed of higher order variables.

The development of the program follows similar lines to that of the program described above; the principal difference is in the choice of selection

criterion for the FS operation. The motivation for the alternative choice is described in the next subsection.

4.5.1 Simple FS Search Procedure

The hoppers of variables used for this search procedure may be initially chosen to be simply the first ten real or imaginary axisymmetric harmonic variables, in the order described in subsection (4.2.2).

Table (4.7) illustrates the preliminary application of a simple FS procedure to the 3 kHz duct data set. The external criterion by which the next variable for inclusion in the model was selected was to choose the next highest order variable in the hopper. The entire hopper was scanned through in increasing order. The use of this criterion as an alternative to the highest-residual-correlation criterion employed in the development of the previous program is satisfactory since the dominant terms in the axisymmetric models in this case seem in general to be the lower order variables. This is evidenced by the t values in the table. The program is therefore built on this framework, incorporating a BE option and collinearity safeguards as described above.

4.5.2 Stepwise Procedure: Collinearity Safeguards

The structure of the final program involves the use of two hoppers of variables outside the model: hopper 1, from which variables are selected for fitting into the model by the FS operation, and hopper 2, in which are stored variables deleted from the model by the BE option. The program searches through the variables in hopper 1 in increasing order. Each variable is included in the model and tested for significance using the t-statistic criterion. Significant variables are retained; insignificant variables are rejected and stored in hopper 2. When hopper 1 is exhausted, it can be refilled from hopper 2, and the search begun again. The search stops when both hoppers are empty, or when no variables are retained from hopper 1 after a complete scan through its contents. This two-hopper structure was designed to give the program as much scope as possible in the building of models, in the hope that many good models would be generated.

As might be expected, collinearity is a more serious problem for the sort of variable set used for this version of the program than for the lower order variable sets employed previously.

This can be seen from the results of Table (4.7), not only from the large values of R_L for later iterations but also from the large and fluctuating coefficient estimates, characteristic of highly collinear data sets. The correlation matrices for the 3 kHz data shown in Table (4.8) show serious collinearity occurring among the higher order terms.

To counteract this, anticollinearity safeguards as described in the last section, comprising a pre-screening of the initial hopper's contents and a level of acceptability of collinearity for the search to continue, may be included.

The operation of the final version of the program is illustrated by Table (4.9), which shows the results of a search for axisymmetric harmonic models to fit to the 3kHz data set. The table shows the program scanning repeatedly through the hoppers, deleting redundant variables from the models as it proceeds. Both real and imaginary data searches are stopped when no variables are retained from hopper 1 after a complete scan through its contents.

The execution of the final version of the axisymmetric model search procedures (for real and imaginary data) is illustrated in flow diagram form in Figure (4.8). Given n complex values of CCSD recorded at a given frequency the program performs both the real and imaginary data searches described above.

4.6 PROPERTIES OF ANALYSIS RESULTS

4.6.1 Results of Analysis

A typical product of the harmonic analysis method is illustrated in Figure (4.9). This Figure is an estimate of the plane wave weighting function at 5 kHz in the example duct used in the present experiment. Included in the Figure for comparison is the plane wave weighting corresponding to an equal modal power distribution in an anechoically terminated duct. The weighting function estimate was made using the axisymmetric model version of the search program.

We can make physical interpretations of such a Figure. Most of the sound power appears to be concentrated in the modes with large $|\cos v|$; that is, with propagation angles close to the duct axis. In the present example, this is thought to be due to the focussing effect of the tapered inlets to the duct from the reverberation chambers at its terminations. The symmetry of the Figure suggests a significant reflection of sound back up the duct towards the source;

this may be due to the excitation of a reverberant field in the receiver reverberation chamber, which in turn re-excites the duct field.

This symmetry is also reflected in the fact that the imaginary harmonic variable coefficients take small values compared to the real. The imaginary terms made up the antisymmetric part of the field, while the real terms make up the dominant symmetric part.

However, such hypotheses depend on the reliability of the weighting estimate. As noted above, the search procedures do not deliver just one model of the weighting, but several with similar statistical properties. An estimate like that given in Figure (4.9) cannot be treated as the 'best' model or definitive in any sense; associated with it is an uncertainty due to the presence of similar, comparable models.

In addition, there is an uncertainty due to the harmonic analysis method's sensitivity to error in the input data, which is the subject of the next subsection.

4.6.2 Sensitivity to data errors

The two principal limitations of the input data set are the finite size of the sample array on which it is based, and estimation errors associated with the CCSD values. A parameter to describe the sample array size is simply the number of points in the array, n_p. Two parameters describe the CCSD estimation errors: the frequency bandwidth, and the number of degrees of freedom n_d. If it is assumed that the data set is large enough that a sufficiently small choice of bandwidth may be made to resolve the significant frequency variation of CCSD, then estimate errors may be assumed to depend only on the number of degrees of freedom. It may be shown (4.19) that the mean square error of CCSD estimates is inversely proportional to n_d.

The impact of the error sources controlled by the parameters on the harmonic search technique is indicated schematically in Figure (4.10). Estimation errors corrupt the data input to the analysis procedure. As the sample array size is increased, it would be expected that the number of terms in a possible model, and the accuracy of the estimation of coefficients in each model, would increase. Furthermore the onset of spatial aliasing would be delayed to higher harmonics, as the sample density of the sound field was increased.

To study the practical consequences of adjusting the two error parameters n_p, n_d, an investigation was made of the following axisymmetric models of the 5 kHz data set: (2,0), (4,0), (6,0) for the real data set, and (1.0), (3,0), (5,0) for the imaginary data set. During the runs of the axisymmetric harmonic search program described in the last section, which were based on data with n_p = 12, n_d = 3000, each of these models was found to consist of two significant terms and one insignificant term. The insignificant term in the real data model was (6,0), and (1,0) was insignificant in the imaginary data model. The separate effects of the two error sources are discussed in the following.

The impact of raising the level of estimation error in the data was investigated by repeating the axisymmetric search procedure, keeping the number of sampling positions fixed at 12, but using CCSD data sets estimated using 1000, 400, 150, 50 and 24 degrees of freedom. The results are shown in Figures (4.11, 4.12) which illustrate the dependence of the model coefficient values and their associated t-values on the number of degrees of freedom. Figure (4.11) shows the coefficients and t-statistics to be fairly stable for $n_d > 400$. For n_d below this value, the magnitude of the coefficient estimates for the significant variables tend to drop, and that of the spurious variable (6,0) tends to increase. The t-values for the 'correct' terms also drop, while that of the spurious variable increases. Thus the introduction of estimation error gradually swamps the true harmonic structure of the model, by corrupting the 'correct' contributions and magnifying the contributions of spurious terms. However, if n_d is higher than 400, the errors are sufficiently small that the spurious term in the model is well suppressed.

Figure (4.11) therefore allows another encouraging conclusion to be drawn. The results of the search procedure are stable to small perturbations of the data, represented by the small but increasing error in the range n_d = 3000 to n_d = 400. This provides further confidence in the analysis method.

The same trends are evident in the imaginary data model results presented in Figure (4.12). The onset of instability occurs at larger n_d, and the corruption of the model is more dramatic, with the structure of the model breaking down altogether. This is probably because the 'correct' coefficient and t values are smaller than those in the real data model at n_d = 3000, reflecting the comparatively small amount of significant information in the imaginary data set noted earlier.

The effect of reducing the number of sampling positions n_p on the models is illustrated in Figures (4.13, 4.14). The Figures summarise the results of

applying the axisymmetric model search program to CCSD data sets estimated with 3000 degrees of freedom, with n_p reduced from 12 to 10, 8 and 6.

Figure (4.13) shows that the increase in error from this source has a similar effect on the real data model to that of the increase in estimation error: the coefficient values for the 'correct' variables tend to decline, while that of the spurious variable (6,0) increases, and the t-statistics for the correct variables decrease, while that of the spurious variable increases. Thus, as before, the introduction of error tends to swamp the harmonic structure of the model. Similar trends can be observed in the imaginary data results shown in Figure (4.14), although once again the onset of instability occurs for higher values of n_p.

The assertion that the number of sampling positions n_p = 12 is high enough for these models to be reasonably stable to errors from the array size limitation is not really justified by the above results. If n_p were increased, the results suggest that the accuracy of estimates of the model coefficients and the number of terms in possible models might increase significantly.

This study of the stability of the harmonic analysis method to input data errors cannot claim to be exhaustive or definitive, being based on the results of one experiment. A useful future project would be a thorough study of the stabilty of the method based on sets of artificial data with known "target" harmonic coefficients, corrupted by known levels of random errors.

4.7 CONCLUSIONS

The scope of this chapter has been a description of the role of techniques from regression analysis in the development of a method to implement the duct sound field plane wave weighting harmonic modelling procedure first outlined in Chapter 3. With the input of ideas generated by work done on comparable problems concerning the magnetic and gravitational fields of planets, the discussion has concluded with a listing of programs to perform the analysis of CCSD data.

The analysis performed may be claimed a success, within the limitation of the input data set. The harmonic models produced have been shown to have good regression statistics, and to be stable to small errors in the data.

The plane wave weighting results produced, while hedged with qualifications, appear physically reasonable in the present instance. The value of the new

technique may be gauged from the fact that for the first time a glimpse has been obtained of the modal power distribution in a duct at frequencies high enough to allow as many as 500 modes to propagate.

REFERENCES

4.1 YOUNGER, M.S., A Handbook for Linear Regression. Duxbury Press, Massachusetts. (1979).

4.2 ALLEN, D.M., Technometrics 13, 469-475 (1971). Mean square error of prediction as a criterion for selecting variables.

4.3 STONE, M., Journal of the Royal Statistical Society, B 36, 111-147 (1974). Cross-validatory choice and assessment of statistical predictions.

4.4 MARQUADT, D.W. and SNEE, R.D., The American Statistician 29, 3-20, (1975). Ridge regression in practice.

4.5 BARRACLOUGH, D.R., Geomagnetism Unit, Institute of Geological Sciences, Edinburgh. Private communication (1982).

4.6 JACOBS, J.A., The Earth's Core and Geomagnetism. Pergamon Press, Oxford (1963).

4.7 ZMUDA, A.J., Transactions of the American Geophysical Union 52, 60-66 (1971). The World Geomagnetic Survey 1957-1969.

4.8 International Association of Geomagnetism and Aeronomy, Journal of Geophysical Research 81, 5163-5164 (1976). The International Geomagnetic Reference Field 1975.

4.9 FOUGERE, P.F., Journal of Geophysical Research 68, 1131-1139 (1963). Spherical harmonic analysis I: a new method and its verification.

4.10 WHALER, K.A. and GUBBINS, D., Geophysical Journal of the Royal Astronomical Society 65, 645-693 (1981). Spherical harmonic analysis of the geomagnetic field: an example of a linear inverse process.

4.11 CONNERNEY, J.E.P., Journal of Geophysical Research 86, 7679-7693 (1981). The magnetic field of Jupiter: a generalised inverse approach.

4.12 CONNERNEY, J.E.P., ACUNA, M.H. and NESS, N.F., Journal of Geophysical Research 86, 3623-3627 (1981). Voyager 1 assessment of Jupiter's planetary magnetic field.

4.13 CONNERNEY, J.E.P., NESS, N.F. and ACUNA, M.H., Nature 298, 44-46 (1982). Zonal harmonic model of Saturn's magnetic field from Voyager 1 and 2 observations.

4.14 KING-HELE, D.G. and COOK, G.E., Nature 246, 86-88 (1973). Redefining the Earth's pear shape.

4.15 MERSON, R.H. and KING-HELE, D.G. Nature 182, 640-641 (1958). Use of artificial satellites to explore the Earth's gravitational field: results from Sputnik 2.

4.16 KING-HELE, D.G., BROOKES, C.J. and COOK, G.E., Geophysical Journal of the Royal Astronomical Society 64, 3-30 (1981). Odd zonal harmonics in the geopotential from analysis of 28 satellite orbits.

4.17 CHATTERJEE, S. and PRICE, B., Regression Analysis by Example. J. Wiley, New York (1977).

4.18 MANTEL, N., Technometrics 12, 621-625 (1970). Why stepdown procedures in variable selection.

4.19 OTNES, R.K., and ENOCHSON, L., Applied Time Series Analysis. Wiley, New York (1978).

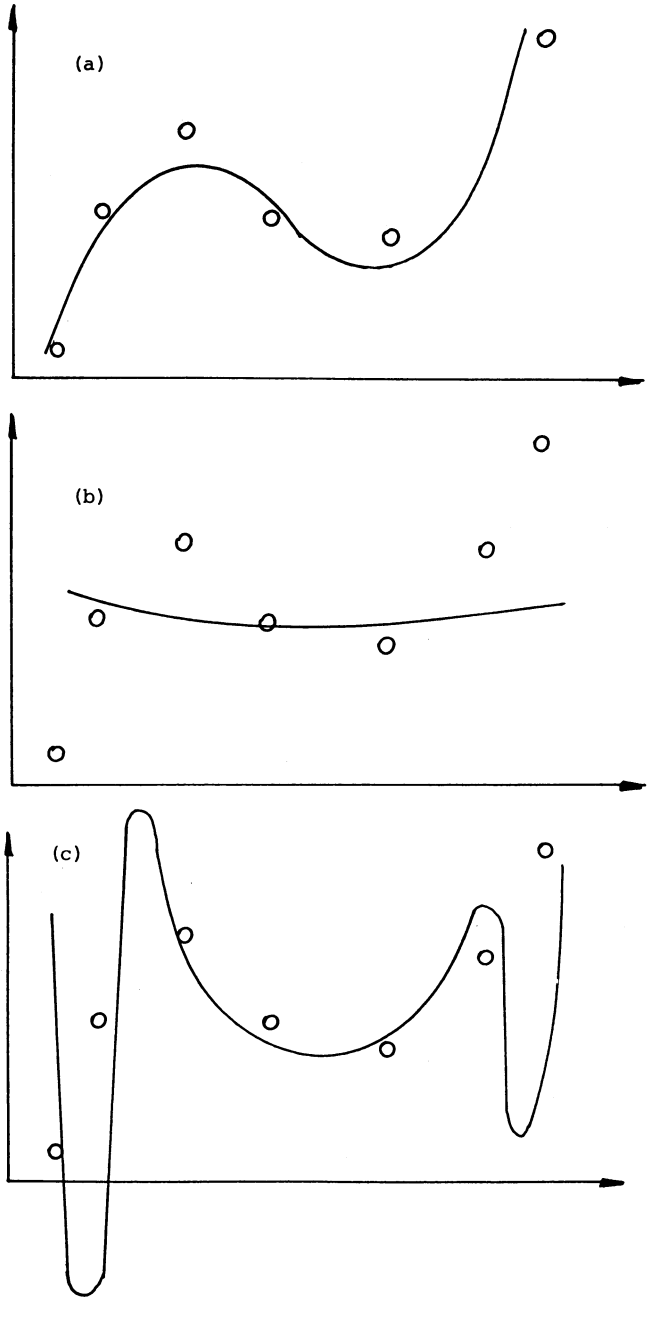

Figure 4.1 Polynomial fits to seven data points. (a) Good choice of order; (b) Low order (c) High order.

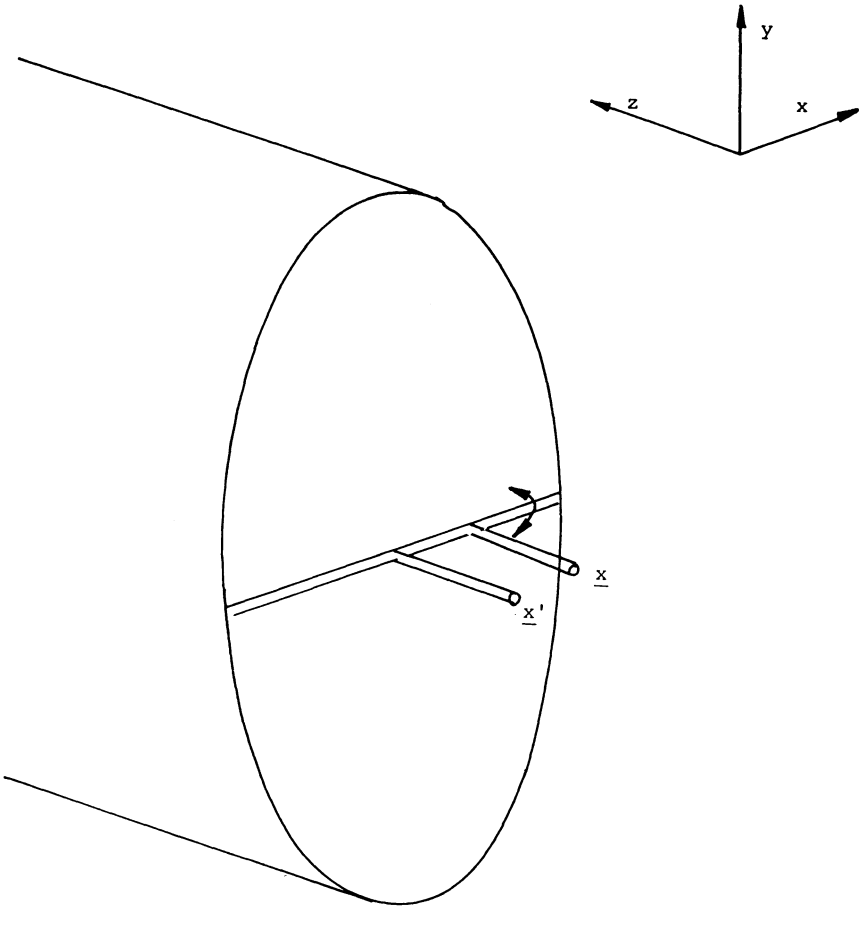

Figure 4.2 Schematic representation of microphone positioning in test duct

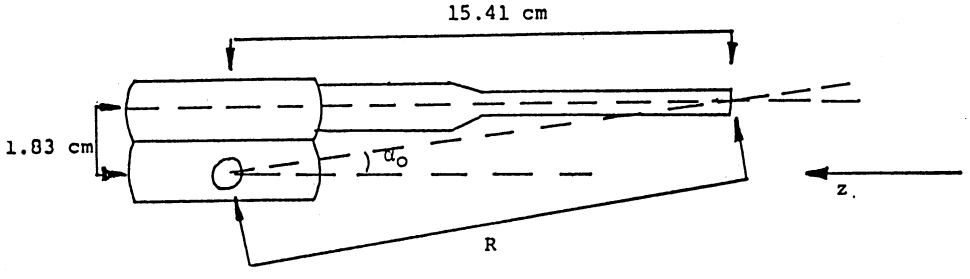

Figure 4.3 Details of microphone mounting. R is turning circle of microphone diaphragm; α_o is made by z-axis with the rod-diaphragm line.

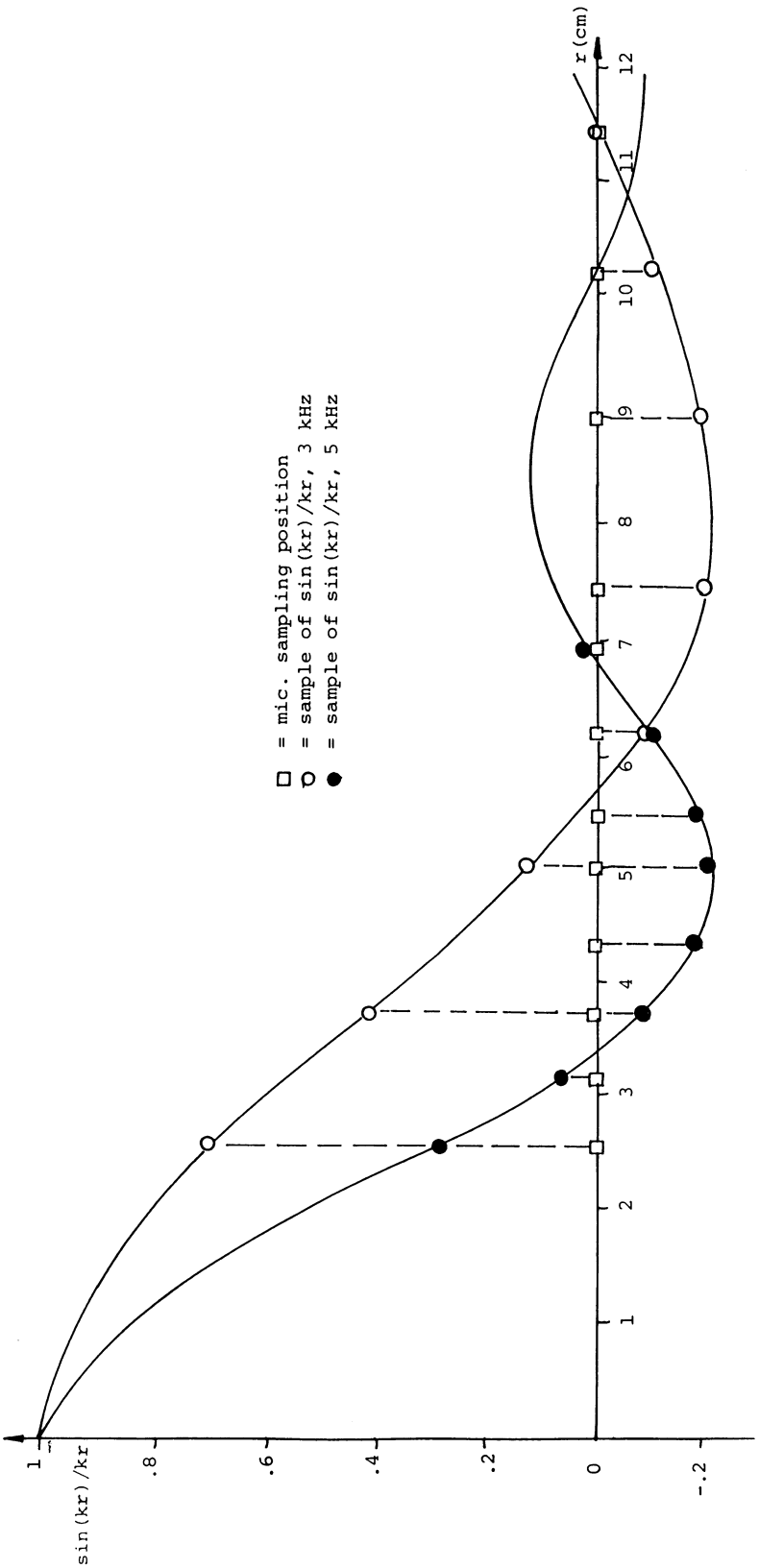

Figure 4.4 Distance distribution of sampling separations. The Figure shows how C = sin(kr)/kr would be sampled.

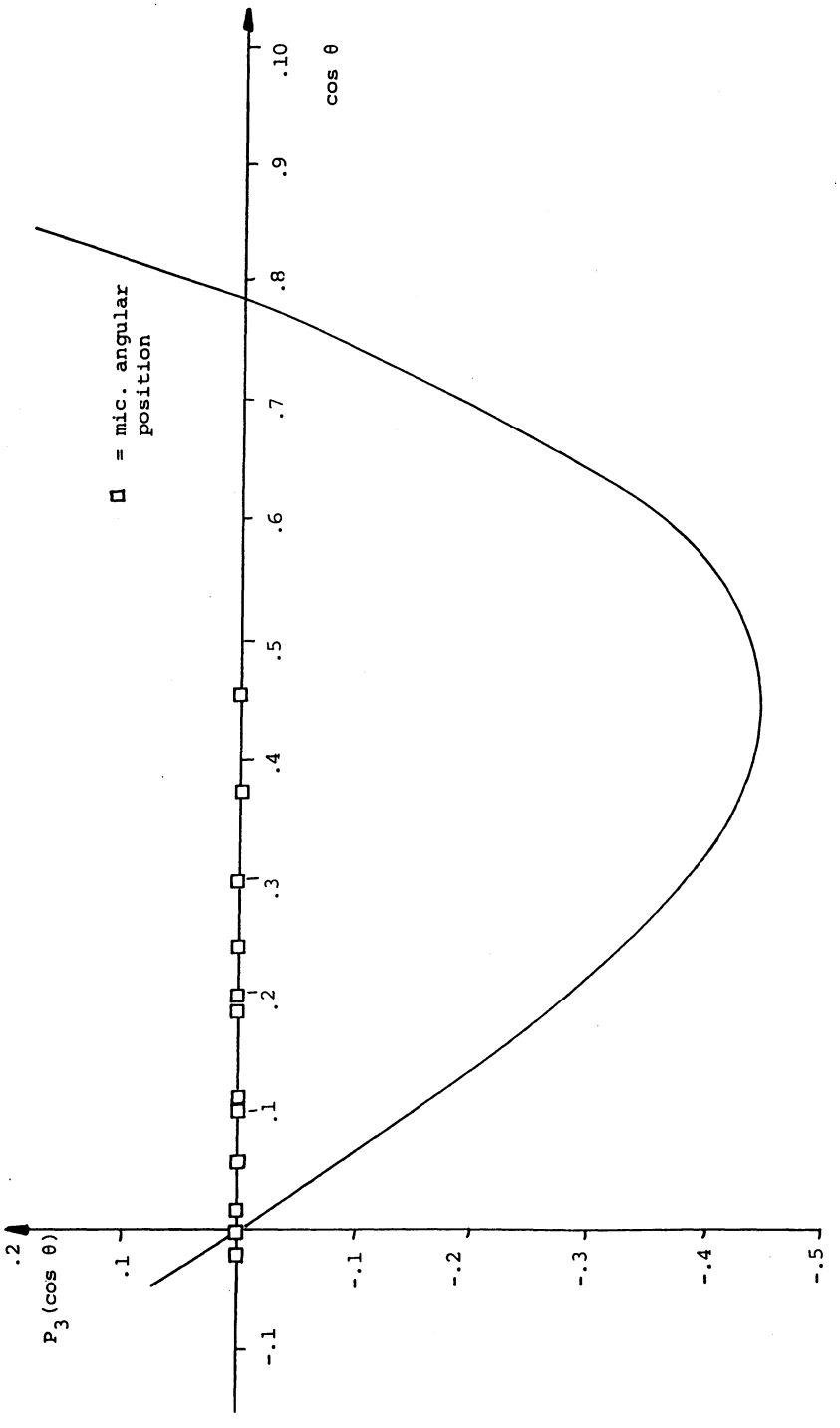

Figure 4.5 Angular distribution of sampling separations. All the points are within successive zeroes of $P_3(\cos\theta) \propto Y_3^0(\theta)$.

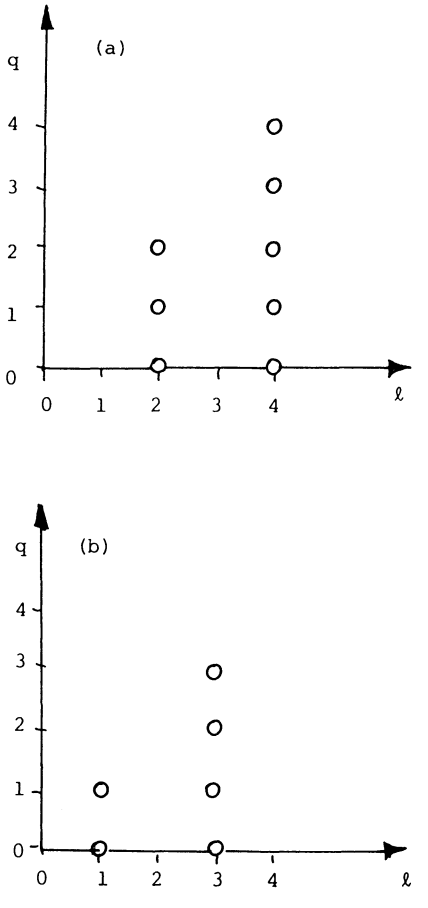

Figure 4.6 Section of variable hoppers.
(a) Real harmonic variables;
(b) Imaginary harmonic variables.
Each circle represents two variables, except for those on the q = 0 axis, which represent one. For example, the circle ℓ =2, q=1 in (a) represents the variables (2,1-Re), (2,1-Im).

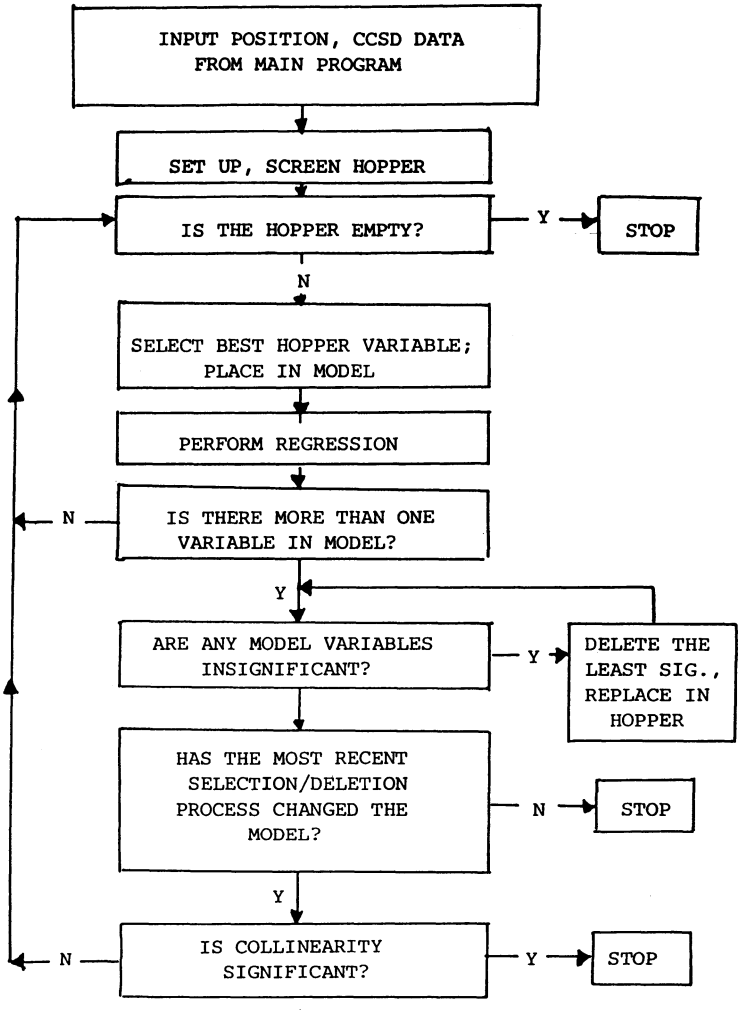

Figure 4.7 Flow diagram to illustrate operation of harmonic search subroutines.

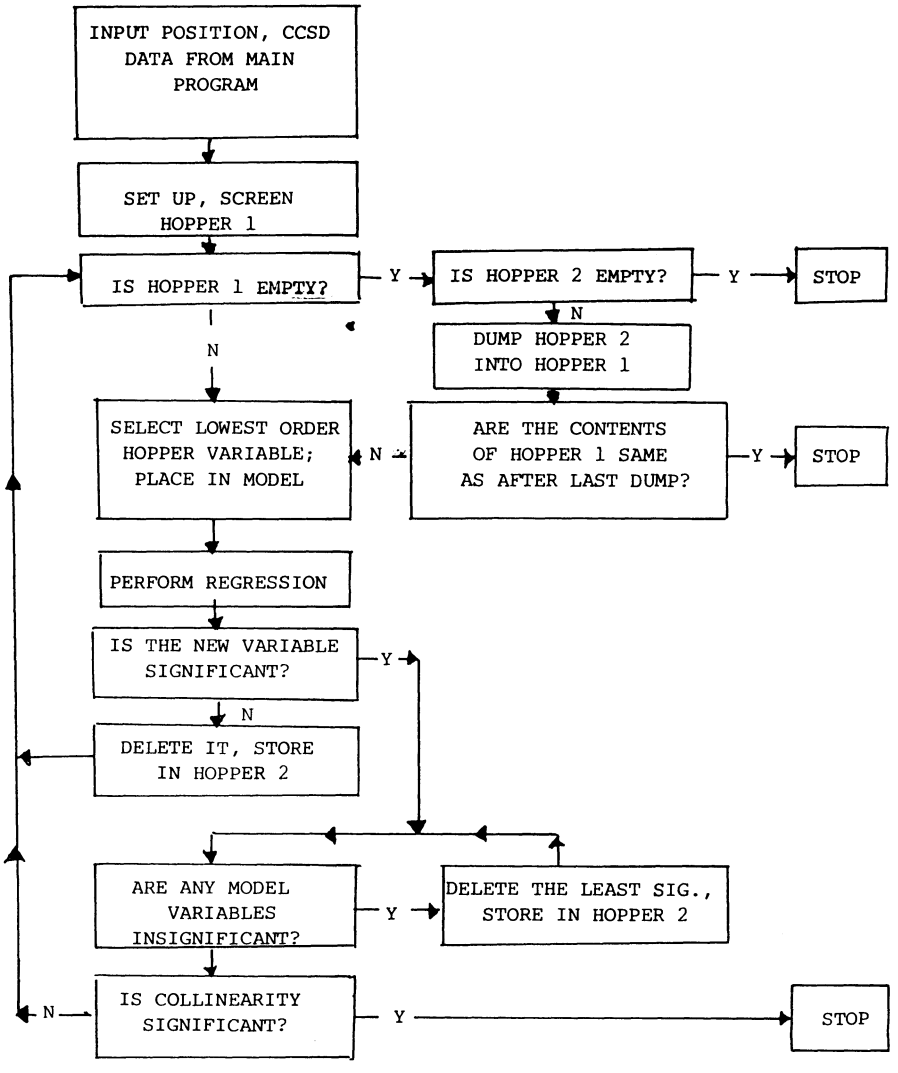

Figure 4.8 Flow diagram to illustrate operation of harmonic search subroutines; axisymmetric version.

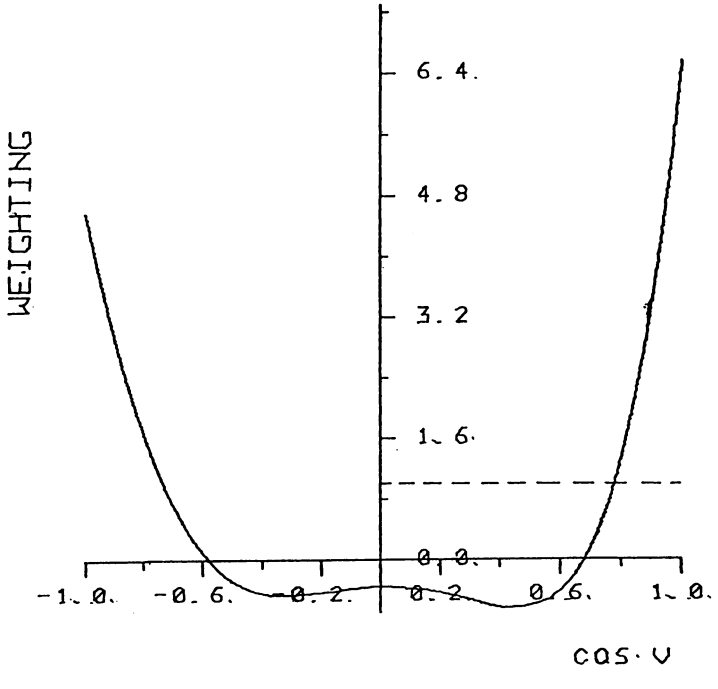

Figure 4.9 Harmonic search results: axisymmetric version, 5 kHz real and imaginary data. Broken line: equal modal power weighting (zero for cos v < 0).

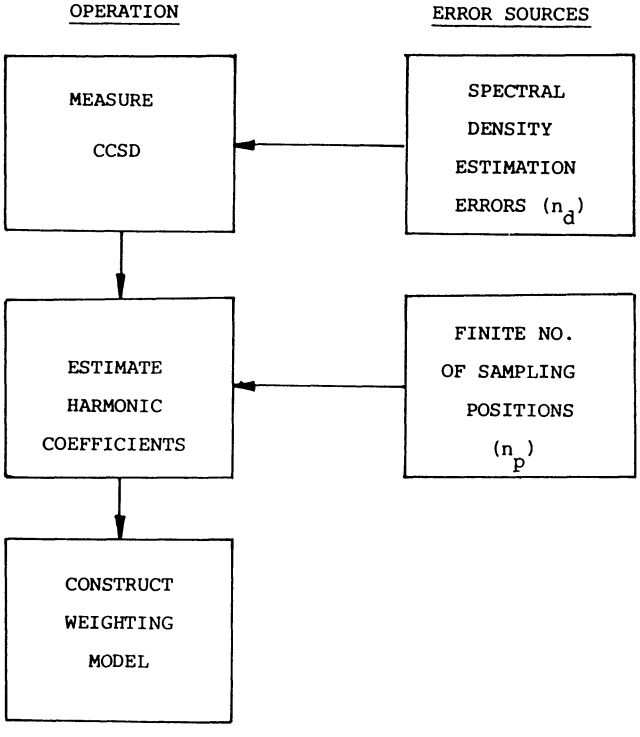

Figure 4.10 Schematic representation of harmonic analysis procedure and associated error sources, with their controlling parameters.

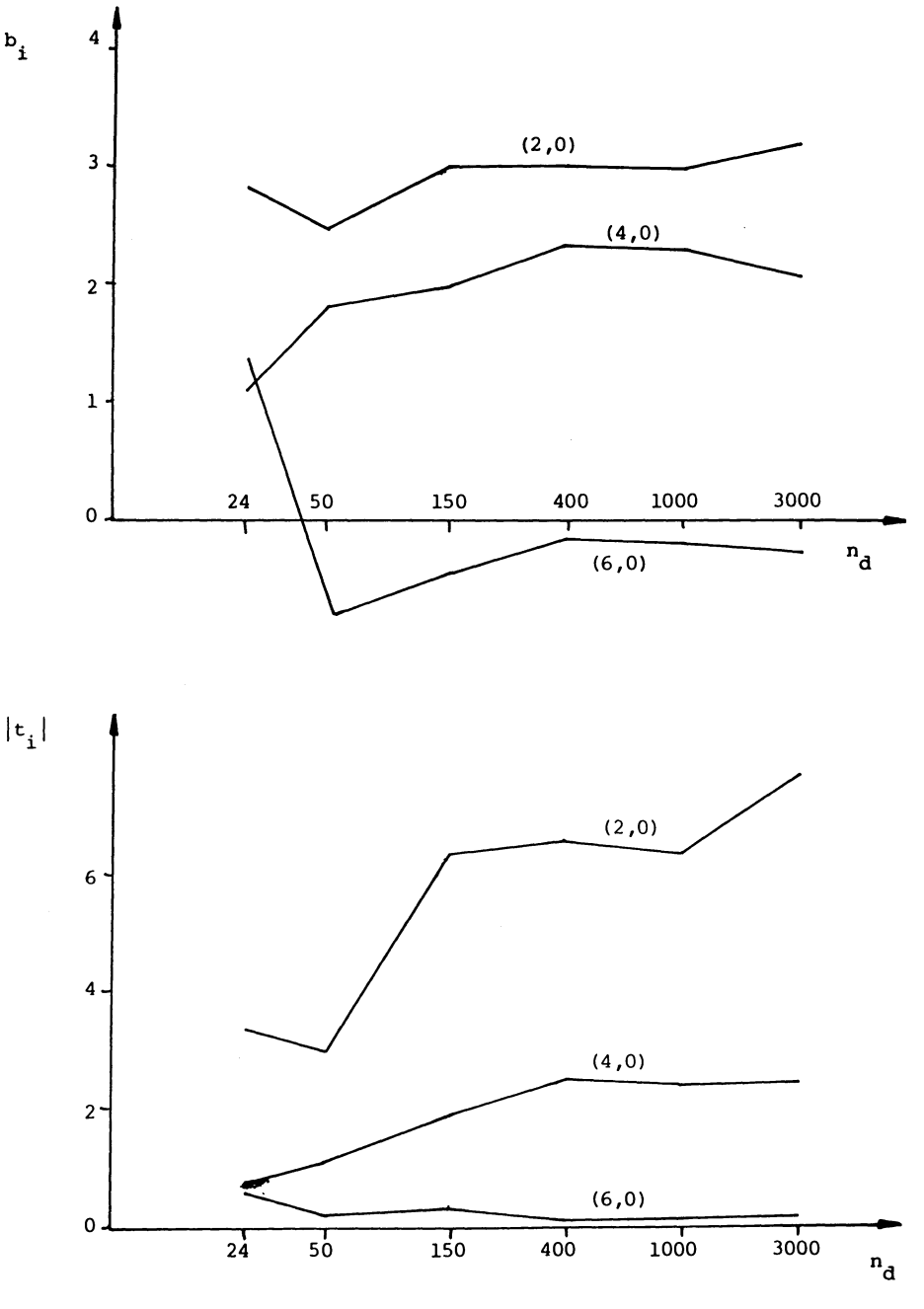

Figure 4.11 Dependence of harmonic model on degrees of freedom of input CCSD data. 5 kHz real data; 12 sampling positions.

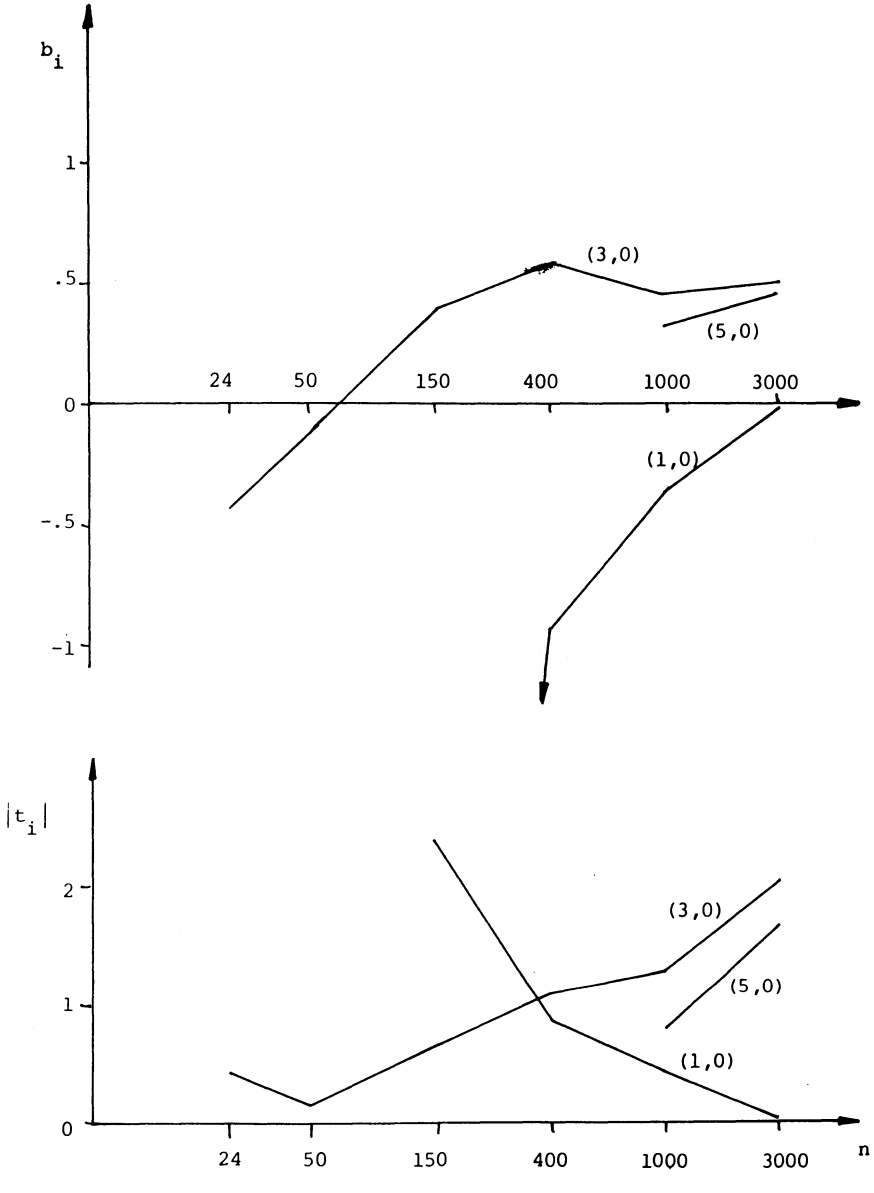

Figure 4.12 5 kHz imaginary data.

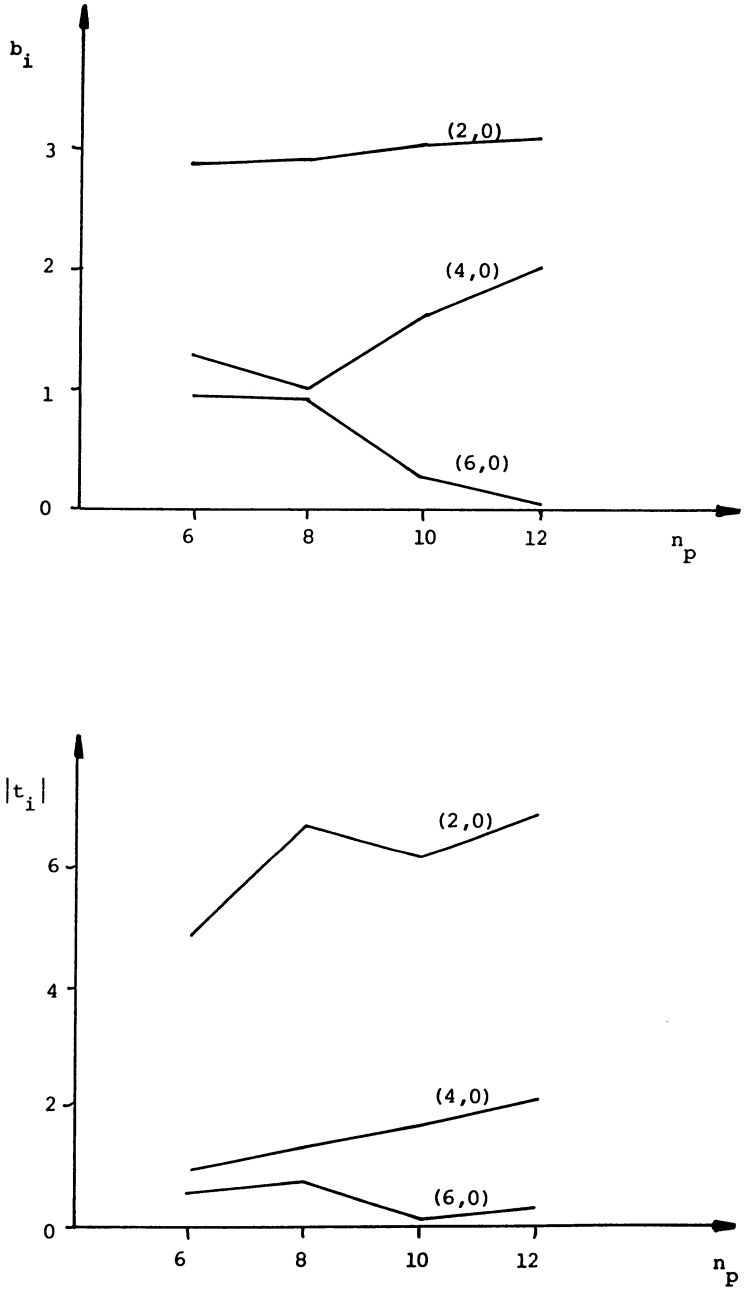

Figure 4.13 Effect of reducing number of sampling positions on harmonic model. 5 kHz real data, 3000 degrees of freedom.

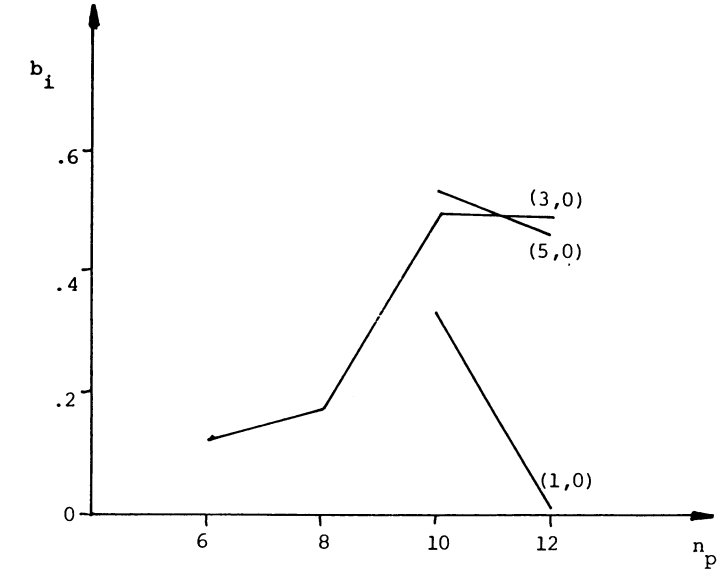

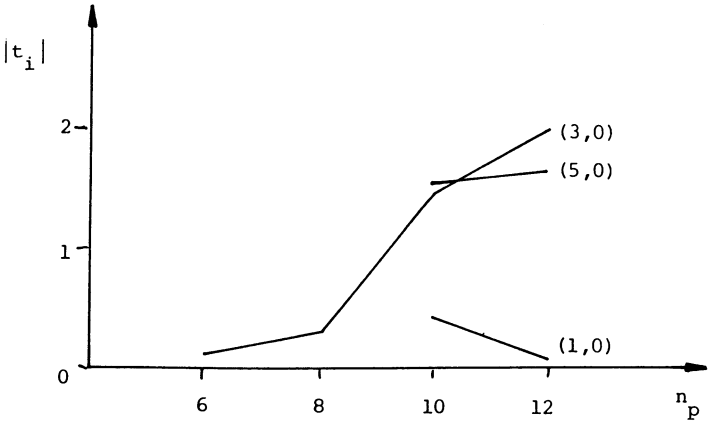

Figure 4.14 5 kHz imaginary data.

Distances in cm; α in degrees; other angles in radians

Position		x	y	z	r		
1	0	-2.54	0	0	2.54	1.57	3.14
2	7	-2.54	1.86	0.34	3.17	1.46	2.51
3	13	-2.54	2.42	0.81	4.34	1.38	2.21
4	18	-2.54	4.67	1.32	5.48	1.33	2.07
5	24	-2.54	6.11	2.08	6.93	1.27	1.97
6	32	-2.54	7.89	3.31	8.92	1.19	1.88
7	42	-2.54	9.84	5.18	11.41	1.10	1.82
8	-10	-2.54	-2.70	-0.08	3.71	1.59	2.96
9	-16	-2.54	-4.32	.093	5.01	1.55	4.18
10	-21	-2.54	-5.64	.37	6.20	1.51	4.29
11	-26	-2.54	-6.94	.76	7.43	1.47	4.36
12	-37	-2.54	-9.64	2.00	10.17	1.37	4.46

Table 4.1 Microphone separation position vectors

Variable	Iteration No. 1	2	3	4	5
2.0	.951 45.0	.938 44.7	.966 30.9	.963 28.6	1.25 4.40
2,1-Re	-	-	-	-	1.46 1.03
2,1-Im	-	-.037 -1.64	-.042 -1.87	-.058 -1.34	-.120 -1.62
2,2-Re	-	-	-.023 -1.16	-.026 -1.184	.112 .826
2,2-Im	-	-	-	.008 .436	-.165 -.979
Statistics					
RSS	7.1×10^{-4}	5.5×10^{-4}	4.7×10^{-4}	4.6×10^{-4}	3.9×10^{-4}
R	.993	.994	.995	.995	.996
s	8.5×10^{-3}	7.8×10^{-3}	7.7×10^{-3}	8.1×10^{-3}	8.1×10^{-3}
PRESS	7.9×10^{-3}	6.4×10^{-3}	5.7×10^{-3}	5.8×10^{-3}	5.3×10^{-3}
R_L	1	1.03	1.62	2.77	200

Table 4.2(a): Harmonic search results: artificial real data.
Simple FS procedure

True values: (2,0): 0.9908; other coefficients zero.

The pairs of values in this Table and those following are coefficient estimates (uppermost) and t-statistics.

Variable	Iteration No. 1	2	3		
1,0	2.10 164	2.11 154	2.12 141	2.12 110	2.12 76.4
1,1-Re	-	-	-	-	-
1,1-Im	-	-	-	-	-
3,0	-	-	-	-	.003 .099
3,1-Re	-	-.009 -.956	-.022 -1.84	-.032 -1.00	-.032 -.896
3,1-Im	-	-	-.008 -1.60	-.009 -1.49	.010 -.910
3,2-Re	-	-	-	-	-
3,2-Im	-	-	-	-	-
3,3-Re	-	-	-	.002 .340	.001 .064
3,3-Im	-	-	-	-	-
Statistics					
RSS	3.5×10^{-5}	3.2×10^{-5}	2.4×10^{-5}	2.4×10^{-5}	2.4×10^{-5}
R	1	1	1	1	1
s	1.9×10^{-3}	1.9×10^{-3}	1.7×10^{-3}	1.8×10^{-3}	2.0×10^{-3}
PRESS	5.5×10^{-5}	5.3×10^{-5}	4.7×10^{-3}	5.4×10^{-3}	6.6×10^{-5}
R_L	1	1.39	5.90	8.70	22.4

Table 4.2(b): Harmonic search results: artificial imaginary data. Simple FS procedure.

True values: (1,0): 2.047: other coefficients zero.

Variable	Iteration No. 6	7	8	9	10
1,0	2.22 30.9	2.22 11.8	2.20 323	2.15 304	-.145 -.040
1,1-Re	-	-	-	-	3.21 .640
1,1-Im	-.009 -1.46	-.021 -9.67	.009 1.77	.018 9.45	.210 .701
3,0	.100 1.37	.172 8.25	.124 123.1	.470 8.91	14.3 .662
3,1-Re	-.051 -1.45	-.020 -2.00	-.007 -1.91	-.019 -9.28	-40.3 -.640
3,1-Im	-.035 -1.76	.052 4.43	-.009 -.886	-.057 -7.37	-.563 -.712
3,2-Re	-	-	-	.211 -6.58	-12.6 .651
3,2-Im	-	.139 8.29	.179 21.17	.197 57.3	6.15 .661
3,3-Re	-.033 -1.19	-.017 -2.28	-.003 -.982	-.014 -7.59	11.63 .639
3,3-Im	-	-	.010 6.13	.153 16.7	1.95 .694
Statistics					
RSS	1.7×10^{5}	9.2×10^{-7}	6.8×10^{-8}	3.0×10^{-9}	2.1×10^{-9}
R	1	1	1	1	1
s	1.8×10^{-3}	4.8×10^{-4}	1.5×10^{-4}	3.9×10^{-5}	4.6×10^{-5}
PRESS	7.4×10^{-5}	8.0×10^{-6}	2.9×10^{-6}	1.5×10^{-7}	2.4×10^{-6}
R_L	161	2320	5800	7.3×10^{6}	2.1×10^{11}

Table 4.2(b) Continued.

Variable	Iteration No. 1	2	3	4	5
2.0	1.25 4.40	1.03 14.7	.964 26.5	.938 44.7	.951 45.0
2,1-Re	1.46 1.03	.306 1.37	.122 .868	-	-
2,1-Im	-.122 -1.62	-.074 -1.58	-.073 -1.54	-.037 -1.64	-
2,2-Re	-.165 -.979	-.028 -1.06	-	-	-
2,2-Im	-	-	-	.008 .436	-.165 -.979
Statistics					
RSS	3.9×10^{-4}	4.3×10^{-4}	5.0×10^{-4}	5.5×10^{-4}	7.1×10^{-4}
R	.996	.996	.995	.994	.993
s	8.1×10^{-3}	7.9×10^{-3}	7.9×10^{-3}	7.8×10^{-3}	8.4×10^{-3}
PRESS	5.3×10^{-3}	5.4×10^{-3}	6.2×10^{-3}	6.4×10^{-3}	7.9×10^{-3}
R_L	200	8.10	3.90	1.03	1

Table 4.3(a): Harmonic search results: artificial real data.
Simple BE procedure

Variable	Iteration No. 1	2	3	4	5
1,0	-.145 -.040	-	-	-	-
1,1-Re	3.21 0.640	3.00 361	3.75 18.0	3.54 12.1	.005 .146
1,1-Im	.210 .702	.198 157	.089 2.53	-	-
3,0	14.3 .662	13.4 900	12.6 17.4	14.2 25.2	9.4 4.32
3,1-Re	-40.3 -.640	-37.8 -366	-47.0 -18.1	-44.5 -12.1	-.160 -.560
3,1-Im	-.563 -.713	-.531 -99.5	-	-	-
3,2-Re	-12.6 -.651	-11.8 -1320	-12.3 -27.3	-12.8 -20.9	-5.80 -5.51
3,2-Im	6.15 .661	5.78 437	6.92 18.5	6.43 13.0	.640 1.00
3,3-Re	11.6 .639	10.9 346	13.7 17.6	12.8 12.1	-
3,3-Im	1.95 .695	1.84 471	1.50 13.3	1.26 14.0	.414 1.33
Statistics					
RSS	0	0	1.1×10^{-5}	3.3×10^{-5}	1.2×10^{-3}
R	1	1	1	1	.993
s	4.6×10^{-5}	3.3×10^{-5}	1.9×10^{-3}	2.9×10^{-3}	.016
PRESS	2.0×10^{-6}	2.2×10^{-7}	3.1×10^{-4}	3.5×10^{-4}	4.9×10^{-3}
R_L	2.1×10^{11}	1.1×10^{9}	2×10^{6}	9.1×10^{5}	304

Table 4.3(b): Harmonic search results: artificial imaginary data. Simple BE procedure.

Variable	Iteration No. 6	7	8	9	10
1,0	-	-	-	-	-
1,1-Re	-	-	-	-	-
1,1-Im	-	-	-	-	-
3,0	8.21 7.57	7.22 21.3	7.00 15.5	- -	- -
3,1-Re	-.127 -.796	-	-	-	-
3,1-Im	-	-	-	-	-
3,2-Re	-5.72 -6.88	-5.24 -9.46	-4.75 -21.7	-4.59 15.9	-.163 -.710
3,2-Im	.586 1.23	.340 .962	-	-	-
3,3-Re	-	-	-	-	-
3,3-Im	.391 1.60	.280 1.43	.095 2.94	-	-
Statistics					
RSS	1.2×10^{-3}	1.4×10^{-3}	1.6×10^{-3}	3.2×10^{-3}	9.0×10^{-2}
R	.993	.993	.992	.983	.209
s	.014	.014	.014	.019	.095
PRESS	4.2×10^{-3}	3.4×10^{-3}	3.0×10^{-3}	5.2×10^{-3}	.108
R_L	332	99.3	13.1	18.8	1

Table 4.3(b): Continued

Variable	Iteration No. 1	2	3	4	5
2.0	3.29 7.79	23.26 8.67	3.24 8.95	3.02 6.18	2.92 6.59
2,1-Re	-	-	-	-	-
2,1-Im	-	-	-	-.750 -.672	-1.17 -1.33
2,2-Re	-	-	.375 1.32	.234 .649	-
2,2-Im	-	-.329 -1.92	-.350 -2.12	-.229 -.922	-.153 -.724
Statistics					
RSS	.271	.192	.158	.148	.157
R	.927	.949	.958	.961	.958
s	.165	.146	.141	.146	.146
PRESS	.320	.246	.249	.246	.225
R_L	1	1	1.02	2.03	1.67
F	60.7	40.4	29.7	20.9	29.8

Table 4.4(a): Harmonic search results: 4743 Hz real data
Stepwise procedure

Variable	Iteration No. 6	7	8	
2.0	2.81 69.92	2.92 6.59	2.81 6.92	
2,1-Re	-	-	-	
2,1-Im	-1.57 -2.36	-1.17 -1.33	-1.57 -2.36	
2,2-Re	-	-	-	
2,2-Im	-	-1.53 -.724	-	
Statistics				
RSS	.168	.157	.168	
R	.955	.958	.955	
s	.137	.140	.137	
PRESS	.209	.225	.209	
R_L	1.21	1.67	1.21	
F	46.9	29.8	46.9	

Table 4.4(a): Continued

Variable	Iteration No. 1	2	3	4	5
1,0	-	-	-	-.281 -.522	-
1,1-Re	-	-.114 -2.40	-.114 -2.45	-.103 -1.93	-.114 -2.45
1,1-Im	-	-	-	-	-
3,0	-	-	-	-	-
3,1-Re	-	-	-	-	-
3,1-Im	.296 3.20	.308 4.05	.328 4.25	.336 4.08	.328 4.25
3,2-Re	-	-	-	-	-
3,2-Im	-	-	-	-	-
3,3-Re	-	-	.054 1.11	.051 .988	.054 1.11
3,3-Im	-	-	-	-	-
Statistics					
RSS	.022	.013	.011	.011	.011
R	.712	.836	.860	.866	.860
s	.046	.038	.038	.040	.038
PRESS	.023	.015	.015	.018	.015
R_L	1	1.01	1.13	1.20	1.13
F	10.3	10.5	7.57	5.23	7.57

Table 4.4(b): Harmonic search results: 4743 Hz imaginary data. Stepwise procedure.

Variables

i	k	r_{ik}
2,0	2,0	1
2,0	2,1-Re	-.419
2,0	2,1-Im	-.160
2,0	2,2-Re	.687
2,0	2,2-Im	.226
2,1-Re	2,1-Re	1
2,1-Re	2,1-Im	.856
2,1-Re	2,2-Re	-.508
2,1-Re	2,2-Im	.744
2,1-Im	2,1-Im	1
2,1-Im	2,2-Re	-.272
2,1-Im	2,2-Im	.754
2,2-Re	2,2-Re	1
2,2-Re	2,2-Im	.141
2,2-Im	2,2-Im	1

Table 4.5 (a) Correlation matrix, 3 kHz real data

Variables i	Variables k	r_{ik}
1,0	1,0	1
1,0	1,1-Re	.460
1,0	1,1-Im	.608
1,0	3,0	-.083
1,0	3,1-Re	.462
1,0	3,1-Im	.379
1,0	3,2-Re	-.323
1,0	3,2-Im	-.234
1,0	3,2-Re	.158
1,0	3,3-Im	-.116
1,1-Re	1,1-Re	1
1,1-Re	1,1-Im	.088
1,1-Re	3,0	-.747
1,1-Re	3,1-Re	.077
1,1-Re	3,1-Im	.198
1,1-Re	3,2-Re	-.808
1,1-Re	3,2-Im	.158
1,1-Re	3,3-Re	-.645
1,1-Re	3,3-Im	.007
1,1-Im	1,1-Im	1
1,1-Im	3,0	.290
1,1-Im	3,1-Re	-.207
1,1-Im	3,1-Im	.558
1,1-Im	3,1-Re	.112
1,1-Im	3,2-Im	-.320
1,1-Im	3,3-Re	-.112
1,1-Im	3,3-Im	-.178
3,0	3,0	1

Variables i	Variables k	r_{ik}
3,0	3,1-Re	-.253
3,0	3,1-Im	.394
3,0	3,2-Re	.969
3,0	3,2-Im	.682
3,0	3,3-Re	.532
3,0	3,3-Im	.376
3,1-Re	3,1-Re	1
3,1-Re	3,1-Im	-.558
3,1-Re	3,1-Re	-.352
2,1-Re	3,1-Im	.415
3,1-Re	3,3-Re	.646
3,1-Re	3,3-Im	-.492
3,1-Im	3,1-Im	1
3,1-Im	3,2-Re	.289
3,1-Im	3,2-Im	-.880
3,1-Im	3,3-Re	-.305
3,1-Im	3,3-Im	.704
3,2-Re	3,2-Re	1
3,2-Re	3,1-Im	-.602
3,1-Re	3,3-Re	.463
3,2-Re	3,3-Im	.407
3,2-Im	3,2-Im	1
3,2-Im	3,3-Re	-.092
3,2-Im	3,3-Im	-.829
3,3-Re	3,3-Re	1
3,3-Re	3,3-Im	-.146
3,3-Im	3,3-Im	1

Table 4.5 (b) Correlation matrix, 3 kHz imaginary data

Variable	Iteration No. 1	2	3	4	5
2.0	3.34 6.28	2.81 6.91	2.20 3.90	2.10 3.50	2.20 3.90
2,1-Re	-	-	-	-	-
2,1-Im	-	-1.58 -3.32	-1.45 -3.18	-1.96 -2.27	-1.45 -3.18
2,2-Re	-	-	.551 1.49	.447 1.09	.551 1.49
2,2-Im	-	-	-	.227 .709	-
Statistics					
RSS	.537	.241	.189	.176	.189
R	.893	.953	.964	.966	.964
s	.232	.164	.154	.159	.154
PRESS	.582	.327	.289	.339	.289
R_L	1	1.03	1.66	2.84	1.66
F	39.4	45.0	34.8	24.5	34.8

Table 4.6(a): Harmonic search results: stepwise procedure
3 kHz real data

Variable	Iteration No. 1	2	3	
1,0	-	-	-	
1,1-Re	-	-.068 -.980	-	
1,1-Im	-	-	-	
3,0	-	-	-	
3,1-Re	-	-	-	
3,1-Im	-	-	-	
3,2-Re	.478 2.535	.490 2.59	.478 2.535	
3,2-Im	-	-	-	
3,3-Re	-	-	-	
3,3-Im	-	-	-	
Statistics				
RSS	.045	.040	.045	
R	.625	.671	.625	
s	.067	.067	.067	
PRESS	.063	.060	.063	
R_L	1	2.88	1	

Table 4.6(b): Harmonic search results: stepwise procedure without collinearity screening, 3 kHz imaginary data.

Variable	Iteration No. 1	2	3	4	
1,0	-	-	-	-	
1,1-Re	-	-.086 -1.22	-.088 -1.20	-.086 -1.22	
1,1-Im	-	-	-	-	
3,0	.691 2.36	.749 2.59	.759 2.50	.749 2.59	
3,1-Re	-	-	-	-	
3,1-Im	-	-	-.071 -.473		
3,2-Re	-	-	-	-	
3,2-Im	-	-	-	-	
3,3-Re	-	-	-	-	
3,3-Im	-	-	-	-	
Statistics					
RSS	.047	.040	.039	.040	
R	.599	.671	.682	.671	
s	.069	.067	.070	.067	
PRESS	.065	.058	.061	.058	
R_L	1	2.26	5.69	2.26	

Table 4.6(c): Harmonic search results: stepwise procedure with collinearity screening, 3 kHz imaginary data.

Variable	Iteration No. 1	2	3	4	5
2.0	3.34 6.28	3.05 4.58	3.31 4.37	3.91 3.27	2.41 4.25
4,0	-	1.52 .747	-.244 -.081	-4.78 -.620	8.33 2.10
6,0	-	-	3.81 .813	28.2 .738	74.5 3.10
8,0	-	-	-	-143 -.644	409 3.06
10.0	- -	- -	- -	- -	-1290 -5.77
12.0	-	-	-	-	-
14.0	-	-	-	-	-
16,0	-	-	-	-	-
18,0	-	-	-	-	-
20,0	-	-	-	-	-
Statistics					
RSS	.537	.506	.467	.441	.067
R	.724	.743	.765	.780	.970
s	.232	.237	.242	.251	.106
PRESS	.583	.697	4.50	4.46	28.9
R_L	1	1.26	3.32	145	149

Table 4.7(a): Harmonic search results: simple FS procedure, axisymmetric variables, 3 kHz real data.

Variable	Iteration No. 6	7	8	9	10
2,0	1.39 1.58	.947 .816	.513 .306	.916 .368	.714 .096
4,0	27.0 2.01	33.3 1.92	38.4 1.67	32.5 .936	36.4 .271
6,0	-377 -1.79	-472 -1.76	-537 -1.58	-442 -.828	-514 -.209
8,0	4.7×10^3 1.58	6.0×10^3 1.60	6.8×10^3 1.46	5.4×10^3 .697	6.6×10^3 .1614
10.0	-5.3×10^4 -1.51	-6.8×10^4 -1.54	-7.7×10^4 -1.42	-5.9×10^4 -.652	-7.5×10^5 -.148
12,0	3.3×10^5 1.44	4.3×10^5 1.49	4.9×10^5 1.37	4.0×10^5 .745	4.7×10^5 .203
14.0	- -	2.4×10^3 -.643	-1.6×10^5 -.418	-6.8×10^5 -.351	-3.4×10^4 -.002
16,0	-	-	348 .412	5.9×10^3 .294	-238 -.001
18,0	-	-	-	-7.47 -.277	5.66 .013
20,0	-	-	-	-	-.007 -.031
Statistics					
RSS	.048	.043	.041	.039	.039
R	.979	.981	.982	.982	.982
s	.098	.104	.117	.140	.198
PRESS	57.2	81.1	66.0	307	9.1×10^4
R_L	7.1×10^4	6.3×10^4	6.5×10^4	9.1×10^5	7.3×10^7

Table 4.7(a): Continued.

Variable	Iteration No. 1	2	3	4	5
1,0	.062 -.109	-.221 -.460	-.707 -1.01	-1.59 -3.73	-.731 -8.29
3,0	-	.710 2.31	1.38 1.82	2.23 4.95	-0.79 -.037
5,0	-	-	-1.50 -.961	-3.95 -3.94	8.16 .743
7,0	-	-	-	8.46 4.51	-57.4 -.964
9,0	-	- -	-	250	1.11
11,0	-	-	-	-	-
13,0	-	-	-	-	--
15,0	-	-	-	-	-
17,0	-	-	-	-	-
19,0	-	-	-	-	-
Statistics					
RSS	.073	.046	.041	.011	.009
R	.190	.591	.646	.922	.936
s	.086	.072	.072	.039	.038
PRESS	.088	.098	.214	.176	17.2
R_L	1	1.01	3.24	3.84	721

Table 4.7(b): Harmonic search results: simple FS procedure, axisymmetric variables, 3 kHz imaginary data.

Variable	Iteration No. 6	7	8	9	10
1,0	1.61 1.30	3.27 1.16	4.19 1.30	4.35 1.61	2.74 1.69
3,0	-9.44 -2.12	-15.9 -1.47	-22.1 -1.57	-22.3 -1.88	-16.9 -2.48
5,0	65.7 2.45	119 1.40	196 1.44	193 1.69	154 2.40
7,0	-260 -2.58	-784 -.989	-1901 -1.12	-1812 -1.26	-1500 -1.90
9,0	-2582 -2.04	2650 .333	1.8×10^5 .818	1.6×10^5 .883	1.4×10^5 1.39
11,0	5×10^4 2.26	5744 .082	-1.5×10^5 -.684	-1.3×10^5 -.714	-1.1×10^5 -1.17
13,0	-	2.3×10^5 .668	8.3×10^5 .950	7.7×10^5 1.05	1.6×10^5 1.71
15.0	-	-	-2330 -.755	2.1×10^4 1.32	-3.1×10^5 -2.25
17.0	-	-	- -1.49	-71.2 2.29	1517
19,0	-	-	-	-	-1.40 -2.40
Statistics					
RSS	.004	.004	.003	.002	2.2×10^{-3}
R	.969	.972	.977	.989	.998
s	.030	.031	.033	.028	.015
PRESS	231	417	271	1.9×10^4	8.1×10^3
R_L	3.2×10^4	5.5×10^5	3.6×10^6	3.3×10^6	3.7×10^6

Table 4.7(b) : Continued.

Variables i	Variables k	r_{ik}
2,0	2,0	1
2,0	4,0	.455
2,0	6,0	.610
2,0	8,0	.733
2,0	10,0	-.114
2,0	12,0	-.463
2,0	14,0	.067
2,0	16,0	.173
2,0	18,0	.173
2,0	20,0	.173
4,0	4,0	1
4,0	6,0	.850
4,0	8,0	.720
4,0	10,0	-.673
4,0	12,0	-.738
4,0	14,0	-.041
4,0	16,0	-.041
4,0	18,0	.123
4,0	20,0	.123
6,0	6,0	1
6,0	8,0	.976
6,0	10,0	-.758
6,0	12,0	-.936
6,0	14,0	-.279
6,0	16,0	-.078
6,0	18,0	-.078
6,0	20,0	-.078
8,0	8,0	1
8,0	10,0	-.643
8,0	12,0	-.898
8,0	14,0	-.314
8,0	16,0	-.122
8,0	18,0	-.122
8,0	20,0	-1.22
10,0	10,0	1
10,0	12,0	.911
10,0	14,0	.189
10,0	16,0	-.006
10,0	18,0	-.006
10,0	20,0	-.006
12,0	12,0	1
12,0	14,0	.278
12,0	16,0	.065
12,0	18,0	.065
12,0	30,0	.065
14,0	14,0	1
14,0	16,0	.976
14,0	18,0	.976
14,0	20,0	.976
16,0	16,0	1
16,0	18,0	1
16,0	20,0	1
18,0	18,0	1
18,0	20,0	1
20,0	20,0	1

Table 4.8(a) Correlation matrix, axisymmetric variables, 3kHz real data

Variables i	Variables k	r_{ik}
1,0	1,0	1
1,0	3,0	-.083
1,0	5,0	-.614
1,0	7,0	.052
1,0	9,0	.404
1,0	11,0	.452
1,0	13,0	-.469
1,0	15,0	-.259
1,0	17,0	-.241
1,0	19,0	-.243
3,0	3,0	1
3,0	3,0	.682
3,0	7,0	.195
3,0	9,0	-.036
3,0	11,0	-.077
3,0	13,0	-.040
3,0	15,0	.237
3,0	17,0	.223
3,0	19,0	.193
5,0	5,0	1
5,0	7,0	.371
5,0	9,0	-.109
5,0	11,0	-.183
5,0	13,0	.600
5,0	15,0	.234
5,0	17,0	.211
5,0	19,0	.188
7,0	7,0	1
7,0	9,0	.872
7,0	11,0	.834
7,0	13,0	.223
7,0	15,0	.027
7,0	17,0	.046
7,0	19,0	.042
9,0	9,0	1
9,0	11,0	.997
9,0	13,0	-.175
9,0	15,0	-.076
9,0	17,0	-.042
9,0	19,0	-.038
11,0	11,0	1
11,0	13,0	-.223
11,0	15,0	-.090
11,0	17,0	-.056
11,0	19,0	-.050
13,0	13,0	1
13,0	15,0	.136
13,0	17,0	.113
13,0	19,0	.104
15,0	15,0	1
15,0	17,0	.998
15,0	19,0	.992
17,0	17,0	1
17,0	19,0	.997
19,0	19,0	-

Table 4.8 (b) Correlation matrix, axisymmetric variables, 3 kHz imaginary data.

Variable	Iteration No. 1	2	3	4	5
2.0	3.34 6.28	3.05 4.58	3.29 6.27	3.26 8.52	3.28 7.96
4,0	-	1.52 .747	-	-	-
6,0	-	-	3.54 1.16	-3.51 -1.08	-3.42 -.984
8,0	-	-	-	-	-
10.0	- -	- -	- -	-1202 -2.98	-1210 -2.81
12.0	-	-	-	-	-
14.0	-	-	-	-	1542 .293
Statistics					
RSS	.537	.506	.468	.222	.219
R	.893	.900	.908	.957	.958
s	.232	.237	.228	.167	.177
PRESS	.583	.697	2.25	1.48	74.9
R_L	1	1.26	1.59	4.68	4.73
F	39.4	19.1	21.1	29.0	19.53

Table 4.9(a): Harmonic search results: REG2, 3 kHz real data. The hopper consisted of the variables (2,0), (4,0), (6,0), (10,0), (14,0).

Variable	Iteration No. 6	7	8	9	10
2.0	3.78 7.39	3.84 8.25	3.90 7.92	3.78 7.39	3.90 7.92
4,0	-2.99 -1.42	-3.37 -1.88	-3.50 -1.87	-2.99 -1.42	-3.50 -1.87
6,0	-1.42 -.419	-	-	-1.42 -.419	-
8,0	-	-	-	-	-
10.0	-1422 -3.46	-1346 -3.86	-1395 -3.77	-1422 -3.46	-1395 -3.77
12.0	-	-	-	-	-
14.0	-	-	2979 .647	-	2979 .647
Statistics					
RSS	.172	.177	.167	.172	.167
R	.967	.966	.968	.967	.968
s.	157	.149	.154	.157	.154
PRESS	3.17	.357	.424	3.17	.424
R_L	5.27	1.95	1.76	5.27	1.76
F	25.2	37.2	26.0	25.2	26.0

Table 4.9(a): Continued. Two more iterations (nos. 11, 12) occurred, which were repeats of iterations 9, 10 respectively.

Variable	Iteration No. 1	2	3	4	5	6
1,0	-.062 -.109	-	-	-	-	-
3,0	-	.691 2.36	.839 1.55	.586 2.05	.870 2.52	.772 3.13
5,0	-	-	-.357 -.332	-	-	-
7,0	-	-	-	4.35 1.71	-2.35 -.427	-
9,0	-	-	-	-	30.56 1.36	21.9 2.32
11,0	-	-	-	-	-	-
13,0	-	-	-	-	-	-
15,0	-	-	-	-	-	-
Statistics						
RSS	0.73	0.47	0.47	0.36	0.29	.030
R	0.34	.599	.605	.718	.779	.773
s	.086	.069	.072	.063	.060	.057
PRESS	.088	.065	.089	.101	1.52	.071
R_L	1	1	1.87	1.04	3.92	1.00
F	.01	5.60	2.59	4.79	4.12	6.68

Table 4.9(b): Harmonic search results: REG2, 3 kHz imaginary data. The hopper consisted of the variables (1,0), (3,0), (5,0), (7,0), (9,0), (13,0), (15,0).

Variable	Iteration No. 7	8	9	10	11	12
1,0	-	-	-.939 -3.27	-1.16 -1.82	-1.16 -2.06	-1.02 -3.27
3,0	.824 3.42	.826 3.21	.974 5.79	1.35 1.39	1.26 1.96	.980 5.66
5,0	-	-	-	-.919 .--.393	-	-
7,0	-	-	-	-	-7.18 -.460	-
9,0	19.7 2.11	19.7 1.98	26.8 4.04	28.9 3.26	57.0 .862	27.2 2.98
11,0	-	-	-	-	-	-
13,0	$-1.3x10^4$ -1.29	$-1.3x10^4$ -1.22	$-2.1x10^4$ -2.96	$-1.4x10^4$ -.681	$-1.0x10^4$ -.411	$-2.1x10^4$ -2.93
15,0	-	228 .172	-	- -	718	-.793
Statistics						
RSS	.024	.024	.010	.009	.009	.009
R	.817	.818	.932	.934	.934	.939
s	.055	.059	.037	.039	.039	.038
PRESS	3.46	4.79	.157	18.0	32.0	4.49
R_L	1.02	1.06	1.25	12.6	48.3	1.25
F	5.35	3.54	11.57	8.20	8.2	8.95

Table 4.9(b): Continued. Three more iterations (nos. 13, 14, 15) occurred, which were repeats of iterations 10, 11, 12 respectively.

CHAPTER FIVE

SUMMARY

This monograph has been a presentation of a new experimental technique for the spatial characterisation of complex, random sound fields. Such fields are encountered, for example, in the study of acoustic fields in ducts, enclosures and in the ocean, and in many other contexts.

The basis of the new technique is the approximation of the wave field with a "free wave" model field, which is spatially homogeneous and composed of uncorrelated plane waves. This model field is completely specified by an angle-dependent plane wave density function, and the book has contained a review of methods by which information about the plane wave density function can be inferred from spectral density measurements. One such method, based on spherical harmonic analysis techniques previously used in the characterisation of the gravitational and magnetic fields of planets, has been developed in detail into a robust, practical algorithm of general applicability.

The analysis method has been validated principally by the application of the technique to data from a duct acoustics experiment. Data with various levels of associated estimation errors were used to study the stability of the analysis results. Much further work remains to be done on this point, however. A useful exercise for future workers would be a numerical study of the degradation of weighting analysis results by the addition of random errors of a known size to synthetic input data.

The value of the new analysis method is shown by the fact that in the practical example studied, the sound field is an acoustic duct, images of the plane wave weighting were obtained at frequencies high enough to allow as many as 500 modes to propagate. It has been shown in this example that the plane wave weighting is intimately linked to the duct field's modal power distribution; thus the new technique has provided an unprecedented glimpse of the structure of the high frequency power distribution in an acoustic duct.

Much work remains to be done on refining and validating the spherical harmonic analysis of the free wave fields. However, it is hoped that just as the new method promises to unlock the secrets of high frequency duct fields, it may also prove a way forward for workers in many areas in which the free wave field idea is applicable.

APPENDIX A: FREE WAVE FIELDS IN ACOUSTIC DUCTS

A1 INTRODUCTION

The purpose of this Appendix is to show, by one example, how a free wave field can approximate to a spatially complex random field, and how the properties of the free wave field are linked to the physical properties of the underlying field.

The example considered is a free wave field in a hard-walled acoustic duct. The main conclusion is that the free wave field plane wave weighting function is closely connected to the modal power distribution of the duct field. The measurement of the modal power distribution at high frequency has been of interest to duct acousticians for many years, and the application of free wave ideas to a practical problem in duct acoustics is described in detail in References (2.27), (2.28), (2.29), (2.30).

A2 THE MODAL ANALYSIS OF DUCT SOUND FIELDS

The proof that a many-mode duct sound field can approach a free wave form is based on a discussion of the properties of complex cross-spectral density (CCSD) in such a field. The first part of the discussion is the derivation of a modal sum expression for CCSD, based on a review of the fundamentals of duct acoustics. Following the lead of studies of rectangular room sound fields (2.13, 2.14), this complicated expression is later reduced by the introduction of simplifying assumptions - principally the neglect of correlation between the modes, and the apprximation of modal sums by integrals. Further manipulation of the resulting CCSD expression results in its final reduction to the free wave integral form of equation (2.14). The proof is given for both rectangular and circular hard-walled ducts.

A2.1 Fundamentals of Duct Acoustics

The discussion here is based on that given by Morse and Ingard (2.2).

Consider the sound field in an infinite, uniform hard-walled duct with cross-section area S. Coordinates are defined in the duct so that the duct's axis is parallel to the Cartesian z-axis. The specific duct shapes to be considered are rectangular, in which case Cartesian coordinates (x, y, z) will be used, with the duct interior being the region $0 \leq x \leq a$, $0 \leq y \leq b$; and circular, in which case cylindrical polar coordinates (s, ϕ, z) will be used, with the duct interior

being the region $0 \leq s \leq a$. (See Figure 2.1). The two coordinate systems are connected by the equations

$$x = s \cos \phi \tag{A1}$$

$$y = s \sin \phi \tag{A2}$$

The Fourier transformed pressure field in such a duct, defined by

$$p(\underline{x}, \omega) = \int_{-\infty}^{\infty} dt\, \tilde{p}(\underline{x}, t) \exp(i\omega t) \tag{A3}$$

satisfies (in the absence of sources) the Fourier transformed wave equation

$$(\nabla^2 + k^2)\, p(\underline{x}, \omega) = 0 \tag{A4}$$

subject to the hardwalled boundary condition

$$\nabla p \cdot \underline{n} = 0 \text{ at duct wall} \tag{A5}$$

where $\underline{n}$ is the normal to the wall. If the duct is rectangular, equation (A5) becomes

$$\partial p/\partial x \big|_{x=0,a} \quad , \quad \partial p/\partial y \big|_{y=0,b} = 0 \tag{A6}$$

if it is circular,

$$\partial p/\partial s \big|_{s=a} = 0 \tag{A7}$$

The frequency is taken to be large, so that $ka \gg 1$.

The wave equation is solved by separating out a solution into a product of functions of each of the three coordinates involved, and then solving an ordinary differential equation for each function. The uniformity of the duct in the z-direction leads to a z-dependence

$$p(\underline{x}, \omega) = \psi(x, y) \exp(ik\tau z) \tag{A8}$$

where the function ψ satisfies

$$(\partial^2/\partial x^2 + \partial^2/\partial y^2 + (\alpha/a)^2)\ \psi(x, y) = 0 \tag{A9}$$

(These equations may be written in terms of cylindrical coordinates.) The separation constants are a dimensionless radial wavenumber α and a dimensionless axial wavenumber τ, which are connected by the equation.

$$(\alpha/a)^2 + (k\tau)^2 = k^2 \tag{A10}$$

α (and hence τ) is determined by the wall boundary conditions. τ may be positive, corresponding to a mode propagating in the positive z-direction (a "positively propagating" mode), or negative, corresponding to a mode propagating in the negative z-direction ("negatively propagating").

Further separation of equation (A9) and the use of the wall boundary conditions yields a set of solutions for the case of rectangular geometry:

$$\psi_{mn}(x, y) = \cos(m\pi x/a) \cos(n\pi y/b) \tag{A11}$$

with

$$(\alpha_{mn}/a)^2 = (m\pi/a)^2 + (n\pi/b)^2 \tag{A12}$$

and for the case of circular geometry:

$$\psi_{mn}(s,\phi) = J_m(\alpha_{mn}\, s/a)\exp(\pm im\phi) \tag{A13}$$

with

$$J_m'(\alpha_{mn}) = 0 \tag{A14}$$

α_{mn} is the n-th turning point of the m-th order ordinary Bessel function J_m. The factor $\exp(\pm im\phi)$ in the circular duct mode function describes modes whose pressure patterns are observed to spin in the positive and negative ϕ-directions respectively ("positively and negatively spinning modes").

For each duct shape, (m, n) can be any pair of positive integrals. Note that for each integral pair there are two rectangular duct modes (positively and negatively propagating) and (unless m = 0) four circular duct modes (positively and negatively propagating and spinning).

The further significance of the radial and axial wavenumbers comes from the fact that it can be shown (section A4) that mode (m, n) can be regarded as a sum or integral of plane waves. The wavenumber vector $\underline{k}$ of each constituent wave will have a radial component α/a, and an axial component k.

The modes are orthogonal in the sense that

$$\iint dxdy\, \psi_{mn}(x, y)\, \psi_{mn}^*(x, y) = \delta_{mm'}\, \delta_{nn'}\, \Lambda_{mn}\, S \tag{A15}$$

with the integral taken over a duct cross-section. $\delta_{mm'}$ is the Kronecker delta:

$$\delta_{mm'} = 1 \text{ if } m = m', = 0 \text{ otherwise} \tag{A16}$$

and Λ_{mn} is a constant for each mode. For the rectangular case,

$$\Lambda_{mn} = 1/\varepsilon_m\varepsilon_n \tag{A17}$$

and for the circular case,

$$\Lambda_{mn} = (1/\varepsilon_m)\ (1 - m^2/\alpha_{mn}^2)\ J_m^2\ (\alpha_{mn}) \qquad (A18)$$

where ε_m is defined by

$$\varepsilon_m = 1 \text{ if } m = 0, = 2 \text{ otherwise} \qquad (A19)$$

A2.2 The (m, n) Plane; Cut-Off

A convenient graphical representation of duct modes is as lattice points in a two-dimensional plane, called the (m, n) plane (see Figure 2.2). There is one lattice point for each (m, n) pair, but each lattice point corresponds to in general more than one mode (as described above). Contours of constant axial wavenumber can be drawn on the plane using equation (A12) or (A14). Different modes corresponding to lattice points on or near such a contour would have the same axial and radial wavenumbers.

An important property of duct modes is the phenomenon of cut-off. From equations (A12, A14) it follows that a mode's radial wavenumber may be arbitrarily large, for large enough (m, n). However equation (A10) predicts that the axial wavenumber τ will be real (and in the range -1 to 1) only if $\alpha \leq ka$, and there are only a finite number of modes for which this is true.

A mode with a real axial wavenumber is called "cut-on" or "propagating", while a mode with a complex axial wavenumber is called "cut-off", and suffers exponential decay as it propagates. At a given frequency there are only a finite number of cut-on modes. These are represented in the (m, n) plane by the lattice points contained within the contour $\tau = 0$ (see Figure (2.2)). In what follows, cut-off modes - which do not contribute to sound power in the duct - will be neglected, and each modal summation will be restricted to cut-on modes only; that is, to a summation over all the lattice points in the cut-on region of the (m, n) plane.

A2.3 Modal Expressions for CCSD and Power

A general duct pressure field may be written as a sum of propagating modes:

$$p(\underline{x}, \omega) = \sum_m \sum_n A_{mn} \psi_{mn}(x, y) \exp(ik\tau_{mn} z) \qquad (A20)$$

The amplitudes A_{mn} are determined by duct termination boundary conditions. The sound field is taken here to be random, so that $\{A_{mn}\}$ are a set of random variables.

For the sake of clarity, modal sums like the above in the following discussion will be taken to include only positively propagating modes, and (for circular geometry) positively spinning modes. Since an assumption of negligible modal correlation will be applied later, it is straightforward to extend results derived using such sums to include contributions from the remaining propagating modes.

Equation (A20) may be used to derive modal sum expressions for various quantities. For example, the total sound power is found by integrating the axial intensity across a duct cross-section:

$$W = \iint dx\, dy\, E\{\tfrac{1}{2} \mathrm{Re}(pV_z^*)\}$$

Using the orthogonality of the modes yields

$$W = \sum_{mn} \sum W_{mn} \qquad (A21)$$

where

$$W_{mn} = \tfrac{1}{2} B_{mn} \Lambda_{mn} \tau_{mn} S/\rho_o c_o \qquad (A22)$$

$B_{mn} = E\{|A_{mn}|^2\}$ is a mode's pressure spectrum. W_{mn} is the power associated with mode (m, n), and the set $\{W_{mn}\}$ is the modal power distribution.

An expression for two-point CCSD follows from the substitution of the modal sum equation (A20) into the defining equation for CCSD:

$$\begin{aligned} CCSD\ (\underline{x}, \underline{x}', \omega) \quad & \sum_m \sum_n \sum_{m'} \sum_{n'} E\ \{A_{mn}\ A^*_{m'n'}\} \\ & x\ \psi_{mn}\ (x, y)\ \psi^*_{m'n'}\ (x', y') \\ & x\ \exp\ (ik\tau_{mn}z - ik\tau_{m'n'}z') \end{aligned} \tag{A23}$$

(x', y', z') are the Cartesian coordinates of position vector $\underline{x}'$. Equation (A23) may be written in terms of cylindrical polars if appropriate.

The free wave field proof depends on the reduction of the discouraging-looking expression on the RHS of equation (A23) to the simple free wave integral form of equation (2.14). This is achieved by the introduction of simplifying approximations, which are described in the next section.

A3 SIMPLIFYING ASSUMPTIONS AND APPROXIMATIONS

A3.1 Conversion of Mode Sums to Integrals

The most important simplifying technique is the replacing of modal sums by integrals. This technique comes from architectural acoustics, where the conversion of sums of modes, represented by points in a three-dimensional lattice, to integrals over a volume has been a much-used technique for many years (2.2).

Elementary introductions to integration show how the area under the graph of a function f(x) can be evaluated by summing the area of N strips of width Δx (see Figure 2.3):

$$A \simeq \sum_{i=0}^{N-1} f(x_i)\, \Delta x \tag{A24}$$

X_{i-1}, x_i are the boundaries of the i-th strip. As N is allowed to increase, the approximation improves, until the limit

$$A = \int dx\ f(x) = \lim_{N\to\infty} \sum f(x_i)\ \Delta x \qquad \text{(A25)}$$

is obtained. Thus a finite summation of N terms could be regarded as an approximation to the final integral.

In the same way, a modal sum such as that for power (equation A21) can be regarded as an approximation of a double integral of a continuous function W(m,n) over continuous versions of the modal coordinates (m,n):

$$W = \sum_{mn}\sum W_{mn} = \sum_{mn}\sum W_{mn}\ \Delta m\ \Delta n$$

$$\simeq \int\int dm\ dn\ W(m,n) \qquad \text{(A26)}$$

(The spacing between the lattice points in the (m,n) plane is $\Delta m, \Delta n = 1$). The integral is taken over the cut-on area of the (m,n) plane (Figure 2.2)).

The assumptions necessary for this approximation are that the modal power distribution $\{W_{mn}\}$ is smooth enough for its approximation by an interpolated continuous function W(m,n) to be meaningful, and that there are enough cut-on modes (enough lattice points in the region of integration) for the error made in replacing the summation by an integration to be negligible.

A3.2 Changing Integration Variables

Because of the shape of the cut-on mode integration region, it is convenient to change the variables in an integral like that in equation (A26). It is useful to choose one new variable related to axial wave-number; it turns out (as discussed later) to be convenient to define a new angle-like variable v' by

$$\cos v' = \tau_{mn} \qquad \text{(A27)}$$

It follows from equation (A10) that

$$\alpha_{mn} = ka \sin v' \qquad \text{(A28)}$$

The range of v' will be from 0 to π, to include both positively and negatively propagating modes.

A second new variable, say another angle-like variable u', is needed to complete the new parametrisation of modal lattice points. For the rectangular duct case, a contour of constant axial wavenumber is an ellipse (see equation (A12)) with axes of length $\alpha\pi$, $\alpha b/\pi a$. u' may thus be simply defined as the polar angle shown in Figure (2.2), so that (m,n) are related to (v',u') by

$$m = (\alpha/\pi)\cos u'$$

$$= (ka/\pi)\sin v' \cos u' \qquad \text{(A29)}$$

$$n = (\alpha b/\pi a)\sin u'$$

$$= (kb/\pi)\sin v' \sin u' \qquad \text{(A30)}$$

These relations are exact and hold throughout the (m,n) plane. The range of u' is 0 to $\pi/2$.

The definition of u' for the circular duct case is less straight-forward. It depends on Debye's large-order asymptotic expansion of Bessel functions (2.31, equation (9.3.3)):

$$J_m(m \sec u') \sim (2/\pi m \tan u')^{\frac{1}{2}} \cos(m \tan u' - mu' - \pi/4) \qquad \text{(A31)}$$

u' varies from 0 to π 2. It can be shown (2.32) that α_{mn}, the n-th turning point of this approximation, occurs when the argument of the cosine term is approximately $(n-1)\pi$. Thus the parametrisation of mode

(m,n) is given by

$$m \sec u' = \alpha_{mn} \qquad \text{(A32)}$$

$$(n-1)\pi = m \tan u' - mu' - \pi/4 \qquad \text{(A33)}$$

That is,

$$m = ka \sin v' \cos u' \tag{A34}$$

$$n = (ka/\pi) \sin v' (\sin u' - u' \cos u') + 3/4 \tag{A35}$$

This approximation has been used by previous workers (2.32, 2.33) to enumerate the modes in cylindrical ducts and rooms. Its main value is that equations (A34, A35), though strictly true only for large m, remain valid over much of the (m,n) plane (2.30).

A3.3 Use and Interpretation of New Variables

When the variables of an integration are changed by such a transformation, a Jacobian factor defined by

$$J = \left|\frac{\partial(m,n)}{\partial(v',u')}\right| = \left|(\partial m/\partial v')\ (\partial n/\partial u') - (\partial m/\partial u')\ (\partial n/\partial v')\right| \tag{A36}$$

must be introduced. This describes the non-uniform density of modal lattice points in the plane of the new variables. For the rectangular duct, the factor is

$$J_R = (k^2\ S/\pi^2)\ \left|\cos v' \sin v'\right| \tag{A37}$$

and for the circular

$$J_C = (k^2\ S/\pi^2)\ \left|\cos v' \sin v' \sin^2 u'\right| \tag{A38}$$

As an example of the use of the new variables, the total number N of modes in a duct whose axcial wavenumbers lie between τ_1 and τ_2 $(0 < \tau_1 < \tau_2)$ can be computed by counting all the (m,n) plane lattice points lying in the band between contours $_1$ and $_2$. The result for a rectangular duct is

$$N \sim \int_0^{\pi/2} du' \int_{\cos v' = \tau_2}^{\cos v' = \tau_1} dv' \, J_R$$

$$= (k^2 S/4\pi) (\tau_2^2 - \tau_1^2) \tag{A39}$$

$$= (k^2 S/2\pi) \tau_1 \Delta\tau \tag{A40}$$

when $\Delta\tau = \tau_2 - \tau_1$ is small. The result for a circular duct is

$$N \sim 2 \int du' \int dv' \, J_C \tag{A41}$$

$$= (k^2 S/4\pi) (\tau_2^2 - \tau_1^2) \tag{A42}$$

(The factor 2 is present in equation (A41) because of the presence of positively and negatively spinning modes for each lattice point). The total number of positively propagating modes at a given frequency is ($\tau_2 = 1$, $\tau_1 = 0$):

$$N \sim k^2 S/4\pi \tag{A43}$$

More exact counts (2.33) show this expression to be the first term in an expansion. The next term in the expansion involves a correction for modes near the perimeter of the integration region; such corrections will be ignored in the following discussion. Equation (A43) is compared in Figure (2.4) with an exact count of the number of modes in a circular duct based on tables (2.34).

The new variables (v',u') are named by analogy with the wavenumber spherical polar angles (v,u). The proof given below that CCSD in a duct field can approach a free wave form depends on the manipulation of modal sums, approximated by integrals, into the form of equation (2.14). The dummy angle-like variables used in the final integrals can then be identified with the wavenumber angles (v,u) used in a free wave integral.

This procedure may seem less like sleight-of-hand if it is noted that the variable v' parametrises the radial and axial wavenumbers of a mode (via equations (A27, A28)). Every plane wave component of the mode will have the same

radial and axial wavenumbers and so will be parametrised by the same polar angle v'.

Some basic modal quantities as functions of (v',u') are as follows:

For the rectangular duct,

$$\Lambda(v',u') = 1/4 \tag{A44}$$

$$W(v',u') = (1/8)\, B(v',u')\, S \cos v' / \rho_o c_o \tag{A45}$$

For the circular duct,

$$\Lambda(v',u') = \sin u' / \pi ka \sin v' \tag{A46}$$

$$W(v',u') = (1/2)\, B(v',u')\, S \cos v' \sin u' / \rho_o c_o\, \pi ka \tag{A47}$$

$B(v',u')$ is the continuous version of the modal pressure spectrum B_{mn}. The range of v' is from 0 to π so that the quantities are defined for modes propagating in both z-directions. The range of u' is 0 to $\pi/2$. Equation (A47) can represent the power of a mode spinning in either ϕ-direction.

In all the equations, the factor ε_m has been replaced by 2 for every mode. The error made is of the same order as the error made in approximating modal sums by integrals, since only modal lattice points at the edge of the (m,n) plane (m or n zero) are affected.

The replacing of modal sums by integrals is an approximation which depends on the requirement that the sound field be high frequency, with many cut-on modes. Other simplifying approximations necessary for the proof are more restrictive, and are discussed in the next subsection.

A3.4 Further Assumptions

It is useful to assume negligible correlation between the modes. This allows the dropping of intermodal contributions to the modal sum expression for CCSD, which

then becomes a sum of decoupled modal contributions.

This assumption clearly depends on the sound field's source mechanism. For example, Dyer (2.1) has shown that uncorrelated modes are generated when a duct is excited by a plane of statistically independent sources.

Modes with different modal coordinates will be assumed uncorrelated, as will two modes with the same coordinates but propagating in different z-directions, and two modes with the same coordinates but spinning in opposite ϕ-directions in a circular duct. These assumptions are justifiable in the absence of a directly reflecting duct termination.

A further simplification is needed for the circular duct proofs: that the modal power distribution in the duct depends only on modal axial wavenumber. This corresponds to an assumption of azimuthal symmetry of the sound field.

There is a body of evidence that this assumption is suitable for the sound field in, for example, jet engine inlet ducts. Rice (2.35) has reported demonstrations that the attenuation effects of a given duct liner on a mode, duct termination reflection of modes, and the far field directivity of modes are all functions only of axial wavenumber.

A4 CCSD EXPRESSIONS IN DUCT SOUND FIELDS

The simplifying approximations described above are the background against which the double modal sum expression for CCSD in a duct sound field, equation (A23), can be reconsidered.

The expression becomes much more manageable on the assumption of zero intermodal correlation, so that the expression collapses to a sum over one set of modal coordinates:

$$CCSD\ (\underline{x},\underline{x}',\omega) = \sum_{mn}\sum B_{mn}\ \psi_{mn}\ (x,y)\ \psi^{*}_{mn}\ (x',y')\ \exp\ (ik_{\tau mn}(z-z')) \quad (A48)$$

It should be recalled that this sum only includes contributions from modes propagating in the positive z-direction, and (in the circular duct case) spinning in the positive ϕ-direction.

The next step is the substitution of particular expressions for modal functions

(equations (A11), (A13)) into equation (A48). The argument for the rectangular case is presented first, followed by the argument for the circular case, beginning again from equation (A48).

A4.1 Rectangular Duct

It is straightforward to show that the expression for CCSD in a rectangular duct field, obtained by substituting equation (A11) into equation (A48), can be converted into a (lengthy) sum of plane wave terms. This depends on the fact that each modal function can be expanded into a sum of waves using the standard results

$$\cos A \cos B = \tfrac{1}{2} \{\cos (A+B) + \cos (A-B)\} \tag{A49}$$

$$\cos A = \tfrac{1}{2} \{\exp (iA) + \exp (-iA)\} \tag{A50}$$

The resulting expression is given in full in Reference (2.30); it includes 16 plane wave terms for each node. It can then be shown that the expression can be simplified by extending the definition of the quantity B_{mn} to negative values of (m,n) by

$$B_{mn} = B_{|m||n|} \text{ for } m,n < 0 \tag{A51}$$

The resulting expression is

$$\text{CCSD}(\underline{x},\underline{x}',\omega) = \sum_{i=1}^{4} \text{CCSD}(\underline{r}_i, \omega) \tag{A52}$$

where

$$\text{CCSD}(\underline{r}_i, \omega) = \sum_{m}\sum_{n} (1/4\, \varepsilon_m \varepsilon_n)\, B_{mn} \exp (i\underline{k}.\underline{r}_i) \tag{A53}$$

with

$$\underline{k} = (m\pi/a,\ n\pi/b,\ k\tau_{mn}) \tag{A54}$$

The vectors $\underline{r}_i$ are given by

$$\underline{r}_1 = (x-x',\ y-y',\ z-z') \tag{A55}$$

$$\underline{r}_2 = (x-x',\ y+y',\ z-z') \tag{A56}$$

$$\underline{r}_3 = (x+x',\ y+y',\ z-z') \tag{A57}$$

$$\underline{r}_4 = (x+x',\ y-y',\ z-z') \tag{A58}$$

$\underline{r}_1$ is the separation vector between the microphone at $\underline{x}$ and the microphone at $\underline{x}'$. $\underline{r}_2$, $\underline{r}_3$, $\underline{r}_4$ are the separation vectors between the microphone at $\underline{x}$ and the images of the other microphone in walls of the duct (see Figure 2.5). The sum of equation (A53) is now taken over modal lattice points in four quadrants of the (m,n) plane (Figure 2.6). The $1/\varepsilon_m\varepsilon_n$ factor in equation (A53) is there to ensure that lattice points with m or no zero are not counted twice in the new form of the sum.

No simplifying assumption (apart from zero intermodal correlation) has yet been introduced; the transformation of the CCSD expression into the wave sum form of equation (A53) has been performed purely by algebraic manipulation. The next step is to approximate the wave sums with integrals, as described in subsection (A3.1). The result is for each i,

$$\mathrm{CCSD}(\underline{r}_i,\ \omega) \sim (1/16) \iint dm\ dn\ B(m,n) \exp(i\underline{k}.\underline{r}_i) \tag{A59}$$

The integral is taken over the cut-on region of the (m,n) plane together with its mirror images (Figure (2.6)). The correction for modes with m or n zero has been dropped; this is consistent with the order of approximation used here.

Changing variables to the angle-like pair (v',u') (equations (A29, A30)) gives

$$\mathrm{CCSD}(\underline{r}_i,\ \omega) \sim (1/16) \iint dv'\ du'\ J_R B(v',u') \exp(i\underline{k}.\underline{r}_i) \tag{A60}$$

with $\underline{k}$ now given in terms of the new variables by

$$\underline{k} = (k \sin v' \cos u', k \sin v' \sin u', k \cos v') \tag{A61}$$

The range of u' is now 0 to 2π to include all four quadrants of the (m,n) plane, and the 0 to π range of v' means that the integral includes contributions from both positively and negatively propagating modes.

The final stage is to substitute modal power into equation (A60) using the results in Section A3.3, giving

$$\begin{aligned} CCSD\ (\underline{r}_i, \omega) \sim\ & (k^2 \rho_o c_o\ 2\pi^2) \iint du'\ dv'\ \sin v'\ W(v',u') \\ & \times \exp\ (i\underline{k}.r_i) \end{aligned} \tag{A62}$$

The CCSD integral has thus been reduced to the desired free wave form, save for the presence of the three image-contributed terms. Following the lead of Lyon and Maidanik's (2.13) analysis of CCSD in a rectangular room, let the (real) microphones be close together and far from the walls of the duct, so that

$$|\underline{r}_1| \ll |\underline{r}_2|, |\underline{r}_3|, |\underline{r}_4| \tag{A63}$$

Then the image-contributed terms will involve a much larger phase shift than the "homogeneous" term, and their contribution to CCSD will be much less coherent, and therefore negligible.

A more quantitative argument can be based on an asymptotic expansion of equation (2.14) (see Chapter 3) which shows that when kr is large (> 10),

$$|C\ (\underline{r}, \omega)| = 0\ (1/kr) \tag{A64}$$

Thus the three image terms may safely be dropped, leaving the final expression

$$CCSD\ (\underline{r},\omega) \sim (k^2 \rho_o c_o / 2\pi^2) \iint du'\ dv'\ \sin v'\ W(v',u')\ \exp(i\underline{k}.\underline{r}) \qquad (A65)$$

A comparison with equation (2.12), and an identification of the dummy variables (v',u') with the wavenumber angles (v,u) gives the plane wave weighting function

$$H(v,u,\omega) = (k^2\ \rho_o c_o / 2\pi^2)\ W/v,u) \qquad (A66)$$

and the normalised plane wave function

$$I(v,u,\omega) = (k^2\ \rho_o c_o / \pi)\ W(v,u)/PSD \qquad (A67)$$

This concludes the desired proof that CCSD in a rectangular hard-walled duct can be represented by a free wave integral, under the assumptions that the modes are uncorrelated, that the frequency is high enough that mode sums can be approximated by integrals, and that the observation points are close together and far from the duct walls.

As can be seen, a simple relation exists between the plane wave weighting function and the modal power distribution. A further interpretation of this result will be given later; first, a proof is given that a similar result holds for the case of a hardwalled circular duct.

A4.2 Circular Duct

The circular duct proof follows a similar pattern to the above rectangular duct proof. An additional assumption - that the modal power distribution is dependent only on axial wavenumber, discussed in subsection (A3.4) - proves to be necessary for the present method of proof. The details of the proof, which is outlined here, are given in Reference (2.30).

Consider again equation (A48) for CCSD in a duct field composed of uncorrelated modes. The first step in its analysis, as for the rectangular duct proof, is to break up the modal functions into plane waves. For the Bessel function circular duct modal function, equation (A13), this is done by using the function's spatial Fourier representation (2.36):

$$\psi_{mn}(s,\phi) = (1/2\pi)\, i^m \int_0^{2\pi} du \exp(imu + i\alpha_{mn}(s/a)\cos(\phi-u)) \qquad (A68)$$

(This expression is for positively spinning modes; its complex conjugate is appropriate for negatively spinning modes.) This representation is more daunting than the simple sum of waves expression for a rectangular duct modal function, but the principle of its use is the same. Note that every wave making up the mode has radial wavenumber α_{mn}/a.

If equation (A68) is substituted into equation (A48), an expression for CCSD in the form of two sums and two integrals is obtained

$$CCSD(\underline{x}, \underline{x}', \omega) = \sum_m \sum_n \int du \int du'' \ldots\ldots \qquad (A69)$$

The modal sum may be converted to an integral over the cut-on region of the (m,n) plane:

$$CCSD(\underline{x}, \underline{x}', \omega) \sim \int dm \int dn \int du \int du'' \ldots. \qquad (A70)$$

and the variables changed to the angle-like pair (v',u'):

$$CCSD(\underline{x},\underline{x}', \omega) \sim \int dv' \int du' J_C \int du \int du'' \ldots \qquad (A71)$$

Both positively and negatively propagating modes are now included in the CCSD, as the range of v' integration is taken from 0 to π. Modal power may now be substituted into equation (A71).

The next simplifying step is to change the order of integration, and to evaluate the u' integral first. It is now necessary to assume that the modal power distribution depends only on axial wavenumber, and so is independent of the modal parameter u'.

It can be shown (2.30) that given this assumption, and if the contributions from both positively and negatively spinning modes are now added in, then the result (of the u' integration is approximately a delta-function, $\delta(u-u'')$, in the range

of v' such that the radial wavenumber α is large. In this range, the u or u'' integration can then easily be performed.

A further approximation to reduce the CCSD expression is to replace the u' integral by the delta-function for every value of v'. This introduces an error since the range of v' extends down to zero, and the use of the delta-function is not valid for small v' (and corresponding small α). However, the approximation can be justified by a consideration of equation (A42) for the number of forward-propagating modes in a band of axial wavenumber. It follows that the ratio

$$\frac{\text{number of modes with } \alpha \text{ in the range } 0 < \alpha < \alpha_o}{\text{total number of modes}}$$

is given by

$$r = (\alpha_o/ka)^2 \tag{A73}$$

So (for example) only 1/4 of the modes have $\alpha_o < ka/2$ (note that ka is a large number). Thus it is plausible that the delta-function approximation is valid for most of the propagating modes.

Evaluation of the u' integral in this way leaves the CCSD expression in the form

$$\begin{aligned} CCSD\ (\underline{x},\underline{x}',\omega) = {} & (k^2 \rho_o c_o/2\pi^2) \int dv' \sin v' \int du \int du'' W(v') \\ & \times \exp(i\underline{k}.\underline{x} - i\underline{k}''.\underline{x}')\ \delta(u-u'') \end{aligned} \tag{A74}$$

where

$$\underline{k}'' = (k \sin v' \cos u'', k \sin v' \sin u'', k \cos v') \tag{A75}$$

$$\underline{k} = (k \sin v' \cos u, k \sin v' \sin u, k \cos v') \tag{A76}$$

giving the final result

$$CCSD\ (\underline{r},\omega) = (k^2 \rho_o c_o/\pi^2) \iint du\, dv' \sin v' W(v') \exp(i\underline{k}.\underline{r}) \tag{A77}$$

This is the desired free wave form. Comparison with equation (2.12) shows that the plane wave weighting function is

$$H(v,\omega) = (k^2 \rho_0 c_0 / 2\pi^2)\, W(v) \qquad \text{(A78)}$$

and the normalised weighting is

$$I(v,\omega) = (k^2 \rho_0 c_0 / \pi)\, W(v)/PSD \qquad \text{(A79)}$$

These results should be compared with the rectangular duct plane wave weighting results, equations (A66, A67). The relation between wave weighting and modal power distribution is essentially the same, providing some justification for the chains of assumptions used to derive the results.

A4.3 Interpretation of plane wave weighting results

This Appendix closes with an interpretation of equations (A66, A67, A78, A79) relating the free wave field plane wave weighting function to modal power distribution.

Suppose that experimental measurements of CCSD have been used to derive an estimate $\hat{I}(v',u',\omega_o)$ of the plane wave weighting in a rectangular duct free wave field, as a function of angle at a particular frequency ω_o. What can be said about the power in a given mode (m,n) at that frequency? The first step in answering this is to compute the wavenumber angles (v',u') associated with the mode from equations (A29, A30). If the mode is forward propagating, v' is taken between 0 and $\pi/2$; otherwise, v' is taken between $\pi/2$ and π. Then an estimate of the power associated with the mode can be obtained from equation (A67):

$$\hat{W}_{mn} \sim W(v',u') \qquad \text{(A80)}$$

If the duct is circular, the power is assumed dependent only on modal axial wavenumber, and the associated plane wave weighting is a function of polar angle v' only. To compute the power associated with mode (m,n) from a given weighting

estimate $\hat{I}(v',\omega_o)$, the mode's radial wavenumber τ_{mn} must first be computed, either from tables or from the approximate equations (A32, A33). A wavenumber angle v' can then be computed for the mode (taking into account its direction of propagation), and an estimate of the mode's power can be obtained from equation (A79):

$$\hat{W}_{mn} \sim W/(v') \qquad (A81)$$

In this case the function $I(v',\omega)$ is proportional to the power of each of the several modes with normalised axial wavenumber given by (approximately) $\tau_{mn} = \cos v'$. The total power in a wavenumber band of width $\Delta\tau$ about a given axial wavenumber τ can be computed by multiplying the function I by the number of modes in the band (equation (A40)).

Some simple normalised plane wave weighting functions are illustrated in Figure (2.7). All the functions represent fields dependent only on axial wavenumber, and are presented as functions of cos v; the area under each graph is 1 (equation (2.16)).

The step function, graph (a), corresponds to an equal power distribution among the modes propagating in the postive z-direction. This weighting is known as "semidiffuse", by analogy with the diffuse field weighting shown as graph (b). The latter graph corresponds to a uniform distribution of power among the modes propagating in both z-directions, in which case the duct is acting like an enclosure and a diffuse field might be expected. The semiduffuse field is perhaps the simplest free wave model of the sound field in a duct with an anechoic termination.

The ramp function, graph (c), is obtained when a positively-propagating mode has a power proportional to its axial wavenumber. A graph of total power at a given axial wavenumber for the equal distribution example (graph (a)) would be a ramp like graph (c), because of the presence of an extra cos v' factor corresponding to the number of modes with a given axial wavenumber (equation (A40)).

A5 CONCLUSION

In this Appendix it has been shown that the sound field in a hard-walled rectangular or circular duct at high frequency can approach a free wave form, and

a relationship has been found between the plane wave weighting function of the free wave field and the duct's modal power distribution.

It is anticipated that similar proofs might be derived in other situations whenever the free wave idea is applicable.

APPENDIX B: CONVERGENCE PROPERTIES OF HARMONIC SERIES

B1 INTRODUCTION

This detailed discussion of the convergence properties of the harmonic series of equations (3.88, 3.89) is summarised in the main text, and is based largely on a series of numerical examples. The emphasis is on the practical consequences of limited convergence of the series for a plane wave weighting analysis method.

The numerical convergence studies concern harmonic representations of CCSD and plane wave weighting for the two parametric field families, strip fields and cosine-power fields, discussed in the main text.

The discussion is restricted to single-strip partially reverberant fields, so every field considered is azimuthally symmetric, and the harmonic series for C,I collapse to

$$I(v) \simeq S_N^I = \sum_{\ell=0}^{N} I_\ell^o Y_\ell^o(v,u) \qquad \text{(B1)}$$

$$C(\underline{r}) \simeq C_N^I = \sum_{\ell=0}^{N} I_\ell^o \, 2i^\ell \, j_\ell(kr) \, Y^o(\theta,\phi) \qquad \text{(B2)}$$

Only square integrable fields are considered (apart from the cosine-power field with $m = -\frac{1}{2}$) so that it is valid to take the summation in equation (B1) up to infinity.

Coefficients for the two types of field may be derived from equation (3.85). For cosine-power weightings (see equation (3.8)),

$$I_\ell^o = (-)^n((4n+1)\pi/4)^{\frac{1}{2}(m+1)} \frac{\Gamma(n-m/2)\Gamma(\frac{1}{2}+m/2)}{\Gamma(-m/2)\Gamma(n+3/2+m/2)} \qquad \text{(B3)}$$

for $\ell = 2n$, and

$$I_\ell^o = (-)^n((4n+3)\pi/4)^{\frac{1}{2}(m+1)} \frac{\Gamma(n+\frac{1}{2}-m/2)\Gamma(1+m/2)}{\Gamma(\frac{1}{2}-m/2)\Gamma(n+2+m/2)} \qquad \text{(B4)}$$

for $\ell = 2n+1$ ($n = 0, 1, 2, \ldots$).

For a partially reverberant field (equation (3.23))

$$I^{o}_{\ell} = (\pi)^{\frac{1}{2}} \quad \text{for } \ell = 0 \tag{B5}$$

for $\ell = 0$, and for $\ell \neq 0$:

$$I^{o}_{\ell} = (\pi/(2\ell+1))^{\frac{1}{2}} (\cos v_1 - \cos v_2)^{-1}$$

$$\times \{P_{\ell+1}(\cos v_1) - P_{\ell+1}(\cos v_2) - P_{\ell-1}(\cos v_1) + P_{\ell-1}(\cos v_2)\} \tag{B6}$$

This result could be extended if desired to general strip fields.

In these equations, $\Gamma(x)$ is the complete gamma function (2.31, chapter 6) and $P_{\ell}(\cos v)$ is the ℓ-th order Legendre polynomial (2.31, chapter 22). (For the derivations of equations (B3-B6), see reference (2.30).

B2 CONVERGENCE OF WEIGHTING SERIES

The qualitative effect on the convergence of the weighting harmonic series of equation (B1) of the presence of singularities and discontinuities in the weighting is illustrated in Figures (3.15-3.18), which are a series of plots of S^{I}_{N} for various cosine-weighting fields, with m ranging from $-\frac{1}{2}$ to 2.

The m = 2 weighting (Figure (3.15)) has a continuous derivative everywhere, and the series converges well after four terms. The m = 1 weighting (Figure 3.16)) has a corner (a discontinuous derivative) at the origin and convergence is less good, especially near the corner. The semidiffuse weighting (Figure (3.17)) is still less well-behaved, with a discontinuity at the origin, and the convergence is considerably poorer. It is worse still for the case $m = -\frac{1}{2}$, which is not even a square integrable weighting (Figure (3.18)). Nevertheless the series still attempts to model the weighting's shape, even close to the singularity at the origin.

A feature of the semidiffuse field weighting case (m = 0) is the presence of fringes to either side of the discontinuity. This is Gibbs' phenomenon, familiar from Fourier series theory, and arises from the fact that a finite number of continuous functions cannot fit the infinite slope at a discontinuity. In trying to fit, the harmonic series overshoots the target function to either side of the discontinuity.

As can be seen from Figure (3.17), as N becomes larger the fringe peaks become narrower and move closer to the discontinuity, but the height of the first peak persists. (Convergence of the series in the mean holds because the area under the narrow fringe peaks eventually becomes vanishingly small.)

This study shows that if a weighting contains discontinuities and singularities, the convergence of the harmonic series is poor, but even when the weighting is not square integrable the series can converge point of point, and attempts to model the shape of the weighting.

B3 CONVERGENCE OF CCSD SERIES

The qualitative behaviour of the convergence of the harmonic series for CCSD (equation (B2)) is illustrated in Figure (3.19), which is a set of modulus and phase plots of S_N^C for various N. The target function is the axial CCSD in a semidiffuse field (equation (3.12)). The main feature of these plots is that convergence is much more rapid in the low-kr range of CCSD.

It can be seen that S_N^C fits well to C in the low-kr region for quite small N; the goodness of fit at larger kr improves as N increases. S_4^C fits the main lobe of the modulus fairly well, and S_6^C begins to pick up the second lobe.

It seems to be generally true that the low-order harmonic coefficients dominate the form of C at low kr. This is consistent with the observations made in subsection (3.3.6) about the domination of low-kr C by low order moments of the plane wave weighting, since each harmonic coefficient is a linear combination of moments.

B4 COMPARISON OF CONVERGENCE OF CCSD, WEIGHTING EXPANSIONS

It is now instructive to compare the overall convergence of the harmonic series for CCSD and weighting. As noted in the main text, a C series is liable to be

"more convergent" than a corresponding I series. This impression is confirmed by the application of simple quantitative measures of the convergence of C,I series to the two families of model free wave fields.

A straightforward measure of the convergence of a harmonic series for a square integrable, azimuthally symmetric plane wave weighting is a normalised version of the minimised mean square error by which the series coefficients are determined (equation (3.84)):

$$\varepsilon_N^I = \left\{ \frac{\int\int dv\, du \sin v \; |I(v) - S_N^I|}{\int\int dv\, du \sin v \; |I(v)|^2} \right\}^{\frac{1}{2}} \qquad \text{(B7)}$$

A similar measure of the convergence of a C series is

$$\varepsilon_N^C = \left\{ \frac{\int_0^\infty dR \int\int d\theta\, d\phi \sin\theta \; |C(\underline{r}) - S_N^C|^2}{\int_0^\infty dR \int\int d\theta\, d\phi \sin\theta \; |C(\underline{r})|^2} \right\}^{\frac{1}{2}} \qquad \text{(B8)}$$

ε_N^C has been made independent of R(= kr) by a simple integration over R. It is a measure of the overall convergence of a C series, and contains no information about the fact that most of a series' convergence errors are made at large R, as noted above. This fact could be reflected by defining an alternative error measure including some weighting dependent on R. ε_N^C is defined as above for its simplicity.

Substitution of equations (B1, B2) into equations (B7, B8) and the use of the orthonormality of the harmonics leads to expressions for ε_N^I, ε_N^C as sums of harmonic coefficients, given the following Bessel function integral result (2.31, chapter 11):

$$\int_0^\infty dt\, j_\ell^2(t) = \pi/(4\ell + 2) \qquad \text{(B9)}$$

The expressions are

$$\varepsilon_N^I = \left\{ \sum_{\ell=N+1}^{\infty} |I_\ell^o|^2 \Big/ \sum_{\ell=0}^{\infty} |I_\ell^o|^2 \right\} \qquad \text{(B10)}$$

$$\varepsilon_N^C = \left\{ \sum_{\ell=N+1}^{\infty} \frac{|I_\ell^o|^2}{2\ell+1} \Big/ \sum_{\ell=0}^{\infty} \frac{|I_\ell^o|^2}{2\ell+1} \right\}^{\frac{1}{2}} \qquad \text{(B11)}$$

In Figure (3.20), ε_N^I is shown for the convergence of series approximations for various cosine-power weightings: m = -0.3, 0, 1. The improvement of convergence with increasing m can be seen; this occurs because the behaviour of the weightings improves with increasing m (finite for $m \geq 0$, continuous for $m > 0$, continuous derivative for $m > 1$). ε_N^I for various partially reverberant field weightings is shown in Figure (3.21). The rough similarity of all the plots suggests that the dominant convergence error source for this type of field is the presence of discontinuities in the weightings.

Figures (3.22, 3.23) show ε_N^C for the two families of weightings. These plots show similar trends but steeper slopes than the corresponding I convergence plots, indicating that the speed of convergence of a given C series is greater than but related to that of the corresponding I series.

The interpretation of this is that although there is a one-to-one correspondence between the terms in the two series, for a given number of terms a harmonic series for a plane wave weighting will be a poorer overall representation of the true function than will the corresponding series for CCSD.

APPENDIX C: HARMONIC SEARCH PROBLEM: REGRESSION ANALYSIS

C1. INTRODUCTION

The purpose of this Appendix is to recast the minimisation problems expressed by equations (4.8, 4.9) into the standard notation of multiple regression analysis (4.1). The Appendix includes a formal discussion of standard regression results, which is summarised in the main text. The Appendix also includes some details of the collinearity argument given in the main text.

C2. REGRESSION ANALYSIS

C2.1 Fundamental definitions

Multiple regression analysis involves the study of equations of the form

$$y = \beta_1 x_1 + \beta_2 x_2 + \cdots \beta_p x_p \qquad (C1)$$

This equation models the prediction by the (real-valued) independent variables x_i, i = 1, p, of the value of the (real-valued) dependent variable y. If n sets of measurements y_j, x_{ij}, j = 1,n, i = 1,p of y,x are made, with p < n, the values of the coefficients may be chosen to minimise the (unweighted) residual sum of squares

$$RSS = \sum_{j=1}^{n} \varepsilon_j^2 \qquad (C2)$$

where the residuals ε_j are given by

$$\varepsilon_j = y_j - (\beta_1 x_{1j} + \beta_2 x_{ij} + \cdots + \beta_p x_{pj}) \qquad (C3)$$

The residuals are regarded as random disturbances, containing no systematic information.

Some versions of equation (C1) include a constant term β_o, independent of x, which is also estimated in the minimisation. However no such constant term is present in equation (4.11); the first term of the real series is determined by the I normalisation and involves no adjustable parameter, and in practice may be subtracted from the data. No constant term is therefore included in equation (C1) for the present discussion.

Each of the two harmonic minimisations, equations (4.8, 4.9), may be cast in the form of equation (C2) as follows. For the real fit, let the independent variables, $\psi^R_1, \psi^R_2, \psi^R_3$ ... and coefficients K^R_1, K^R_2, K^R_3 ... be defined by

$$\psi^R_1 = -2j_2\, Y^o_2 \sin^{\frac{1}{2}}\theta \qquad K^R_1 = I^o_2$$

$$\psi^R_2 = -4j_2\, \mathrm{Re}\, Y^1_2 \sin^{\frac{1}{2}}\theta \qquad K^R_2 = \mathrm{Re}\, I^1_2$$

$$\psi^R_3 = 4\, j_2\, \mathrm{Im}\, Y^1_2 \sin^{\frac{1}{2}}\theta \qquad K^R_3 = \mathrm{Im}\, I^1_2$$

$$\psi^R_4 = -4j_2\, \mathrm{Re}\, Y^2_2 \sin^{\frac{1}{2}}\theta \qquad K^R_4 = \mathrm{Re}\, I^2_2$$

$$\psi^R_5 = 4j_2\, \mathrm{Im}\, Y^2_2 \sin^{\frac{1}{2}}\theta \qquad K^R_5 = \mathrm{Im}\, I^2_2$$

$$\psi^R_6 = 2j_4\, Y^o_4 \sin^{\frac{1}{2}}\theta \qquad K^R_6 = I^o_4 \qquad \text{(C4)}$$

.....

(c.f. main text, equation (4.12).)

Furthermore, let the dependent variable y be defined by

$$y = (\mathrm{Re}\, C - j_o)\sin^{\frac{1}{2}}\theta \qquad \text{(C5)}$$

ψ^R_{ij} is the value of the i-th variable at sampling position $\underline{r}_j$, and y_j is the value of y. Note that the y values depend on the CCSD data, but the ψ values depend only on the array of sampling positions.

With these definitions, the harmonic series for Re C, derived from equation (4.11), can be put into a form equivalent to equation (C1), and the RSS of equation (4.8) can be made equivalent to the RSS of equation (C13). The factor

$\sin^{\frac{1}{2}}\theta$ in the definition of the variables is included so that nc weighting factor is needed in the RSS of equation (C2).

In practice, a p-term harmonic model of the real part of CCSD would not be made up purely of the first p terms in the list above, and the definition of the variables x_1, x_2, in equation (C1) would be made suitably. For example, suppose a model were to be composed of the first three (ℓ even) axisymmetric harmonic terms only, then a suitable definition of x_1, x_2, x_3, β_1, β_2, β_3 would be

$$x_1 = \psi^R \qquad \beta_1 = K^R = I^o$$

$$x_2 = \psi^R_6 \qquad \beta_2 = K^R_6 = I^o_4$$

$$x_3 = \psi^R_{15} \qquad \beta_3 = K^R_{15} = I^o_6 \qquad \text{(C6)}$$

The definitions of equation (C4) give the general principle of labelling a two-index series of harmonics with a single index, with the harmonic terms arranged in order of increasing complexity.

In the following discussion, each of the harmonic terms in equation (C4) will be called a "real harmonic variable".

A similar ordering of "imaginary harmonic variables", contributing to the fit to the imaginary part of the CCSD data, is

$$\psi^I_1 = 2j^o_1 Y_1 \sin^{\frac{1}{2}}\theta \qquad K^I_1 = I^o_1$$

$$\psi^I_2 = 4j_1 \text{ Re } Y^1_1 \sin^{\frac{1}{2}}\theta \qquad K^I_2 = \text{Re } I^1_1$$

$$\psi^I_3 = -4j_1 \text{ Im } Y^1_1 \sin^{\frac{1}{2}}\theta \qquad K^I_3 = \text{Im } I^1_1$$

$$\psi^I_4 = -2j_3 Y^o_3 \sin^{\frac{1}{2}}\theta \qquad K^I_4 = I^o_3$$

$$\psi^I_5 = -4j_3 \text{ Re } Y^1_3 \sin^{\frac{1}{2}}\theta \qquad K^I_5 = \text{Re } I^1_3$$

$$\psi^I_6 = 4j_3 \text{ Im } Y^1_3 \sin^{\frac{1}{2}}\theta \qquad K^I_6 = \text{Im } I^1_3 \qquad \text{(C7)}$$

.....

and the dependent variable y may be defined by

$$y = (\text{Im } C)\ \sin^{\frac{1}{2}}\theta \qquad \text{(C8)}$$

(c.f. equation (4.13).)

This enables the imaginary data minimisation to be cast into the standard form of equations (C1-C3). The notation (ℓ,q - Re), (ℓ,q - Im) described in the main text covers the imaginary harmonic variables as well as the real variables.

C2.2 Matrix Formulation

The discussion of the properties of the two harmonic minimisation problems can now proceed in terms of the standard regression analysis notation of equations (C1-C3). This analysis is usually cast in a matrix formulation, with the data n-vector, the data p x n matrix x, the coefficient p-vector β, and the residual data n-vector ε being defined by

$$Y = \begin{bmatrix} Y_1 \\ Y_2 \\ \cdot \\ \cdot \\ \cdot \\ Y_n \end{bmatrix} \qquad \beta = \begin{bmatrix} \beta_1 \\ \beta_2 \\ \cdot \\ \cdot \\ \cdot \\ \beta_p \end{bmatrix} \qquad \varepsilon = \begin{bmatrix} \varepsilon_1 \\ \varepsilon_2 \\ \cdot \\ \cdot \\ \cdot \\ \varepsilon_n \end{bmatrix}$$

$$x = \begin{bmatrix} x_{11} & \cdot & \cdot & \cdot & x_{p1} \\ \cdot & & & & \cdot \\ \cdot & & & & \cdot \\ \cdot & & & & \cdot \\ x_{1n} & \cdot & \cdot & \cdot & x_{pn} \end{bmatrix} \qquad \text{(C9)}$$

Equations (C2,C3) then become

$$\varepsilon = y - x\beta \qquad \text{(C10)}$$

$$RSS = \varepsilon^T \varepsilon \qquad \text{(C11)}$$

(ϵ^T denotes the transpose of).

It can be shown (4.1) by expanding the residual sum of squares that the coefficient vector estimate b which minimises the sum of squares satisfies the "normal equation":

$$cb = x^T y \tag{C12}$$

where

$$c = x^T x \tag{C13}$$

The solution of the normal equation is

$$b = c^{-1} x^T y \tag{C14}$$

The result leads to the definitionof a further n-vector

$$\hat{y} = xb \tag{C15}$$

which is a prediction of the n data values y_j, j = 1,n. The prediction differs from the data by the observed residual n-vector

$$e = y - \hat{y} \tag{C16}$$

C2.3 Statistical Properties of a Regression

This subsection begins a review of standard statistical results about multiple regressions, including the means by which the statistical quality of a regression maybe assessed (4.1).

A main recommendation of the use of least squares fitting is that the estimates of coefficients and predictions that it yields are unbiased, for unbiased input errors. Assume that the input errors are zero mean and independent so that

$$E[\varepsilon] = 0 \tag{C17}$$

and

$$\text{var}[\varepsilon] = \sigma^2 I_n \tag{C18}$$

say, where I_n is the n x n unit matrix. E denotes expected value. Equation (C18) summarises the equations

$$\begin{aligned} \text{cov}(\varepsilon_j, \varepsilon_n) &= 0 \quad j \neq k \\ \text{var}(\varepsilon_j) &= \sigma^2 \end{aligned} \tag{C19}$$

Then it can be shown that

$$E[b] = \beta \tag{C20}$$

and that

$$E[\hat{y}] = x\beta \tag{C21}$$

Furthermore the variance matrix of the coefficient estimates is

$$\text{var}[b] = \sigma^2 c \tag{C22}$$

An unbiased estimator of σ^2 is

$$s^2 = RSS/(n-p-1) \tag{C23}$$

The ordinary correlation coefficient R^2 is defined by

$$R^2 = 1 - RSS/\sum_{j=1}^{n} y_j^2 \tag{C24}$$

The F-statistic is defined in the main text.

The predicted residual sum of squares (PRESS) is defined by

$$PRESS = \sum_{j=1}^{n} (y_j - \hat{y}_{(j)})^2 \tag{C25}$$

$\hat{y}_{(j)}$ is the predicted value of the j-th data value, made by a predictor function based on a fit to all the data except the j-th value. Thus $y_j - \hat{y}_{(j)}$ is a measure of the deviation of the predictor function from the true value of the "fresh" data y_j.

PRESS has the computational advantage that it can be written in terms of the results of a single regression, based on the full set of n data points:

$$PRESS = \sum_{j=1}^{n} (y_j - \hat{y}_j)^2 / (1 - Q_j)^2 \tag{C26}$$

where

$$Q_j = \sum_{k=1}^{p} \sum_{\ell=1}^{p} x_{kj}\, c_{k\ell}\, x_{\ell j} \tag{C27}$$

The t-statistic (4.1) is the ratio of a coefficient estimate to the estimate's standard error (s.e.), which is defined by

$$s.e. = s\,(c_{ii})^{\frac{1}{2}} \tag{C28}$$

and the t-statistic for the i-th variable is defined by

$$t_i = b_i/s\,(c_{ii})^{\frac{1}{2}} \tag{C29}$$

The t-statistic has a standard probability distribution (the student's t distribution), but its simplest interpretation is as follows. Consider two sets of coefficient estimates made from the same data set: a p-set $\{b_i: i = 1,p\}$ producing a predictor function $\hat{y}$, and a q-set $\{b_i^*: i=1,q\}$ producing a predictor function $\hat{y}^*$, with $p < q$. In general, it can be shown (7.4) that coefficient estimates in the smaller set will suffer from more bias than those in the larger, but their variance will be less. Furthermore, under certain conditions, the mean square error (MSE) of coefficient estimates in the smaller set can be less than the variance of coefficient estimates in the larger set. The MSE is the sum of the variance and the square of the bias. That is, the increase in bias can be offset by the decrease in variance, and the smaller variable set can actually produce a better predictor function than the larger.

The condition for this to be true is that the variables which are deleted from the q-set to yield the p-set should have t-statistics less than one in magnitude: that is, that the size of the coefficient estimates should be less than the associated standard errors.

Such a variable is said to be "insignificant". It can be shown further that the effect of deleting insignificant terms of the final predictor function $\hat{y}$ is also to give it an increase in bias which is offset by a decrease in variance, to yield a predictor with a smaller MSE. In summary, the deletion of insignificant variables from a model improves the quality of a regression.

The collinearity between the independent variables and the dependent variables is measured by the correlation vector r_y, which has elements

$$r_{yi} = S_{iy}/(S_{ii}\,S_{yy})^{\frac{1}{2}},\ i = 1,p \tag{C30}$$

where

$$S_{iy} = \sum_{j=1}^{n} (x_{ij} - \bar{x}_i)(y_j - \bar{y}) \qquad (C31)$$

$$S_{ik} = \sum_{j=1}^{n} (x_{ij} - \bar{x}_i)(x_{kj} - \bar{x}_k) \qquad (C32)$$

$$\bar{x}_i = \sum_{j=1}^{n} x_{ij}/n \qquad (C33)$$

$$\bar{y} = \sum_{j=1}^{n} y_j/n \qquad (C34)$$

The collinearity between the i-th and k-th independent variables is measured by the correlation matrix r, which has elements

$$r_{ik} = S_{ik}/(S_{ii}\, S_{kk})^{\frac{1}{2}} \;,\; i,k = 1,p \qquad (C35)$$

C3 ORIGIN OF COLLINEARITY

This section contains some details of the collinearity origin argument given in the main text.

Consider the sum S_{ik} defined in equation (C32), used in the computation of the correlation between the variables indexed i,k. Suppose first that variable i is high order, and that variable k is low order. Then the term $x_{ij} - \bar{x}_i$ in equation (C32) will be approximately zero for those sampling positions j where x_{ij} is significantly nonzero, and approximately $-\bar{x}_i$ at the others, independently of the positon index j. Thus

$$S_{ik} \cong -\bar{x}_i \sum_{j} (x_{kj} - \bar{x}_k) \qquad (C36)$$

with the j sum taken over those positions where x_{ij} is close to zero. The factor $\bar{x}_i$ is removed when S_{ik} is normalised to give the correlation matrix element r_{ik} (equation (C35)), and so the value of r_{ik} will depend only on the variation of the low order variable, as observed in the correlation matrices described above.

Consider now a variable pair i,k, both high order. Similar arguments to the above demonstrate that

$$S_{ik} \simeq (-\bar{x}_i)(-\bar{x}_k) \tag{C37}$$

so that

$$r_{ik} \simeq 1 \tag{C38}$$

Thus high collinearity among high order variable pairs is predicted, as observed.

At higher frequencies, with increasing kr, a higher order variable will take significantly nonzero values at more sampling positions, and this effect is reduced, as observed.